LINEAR ARRAY STRUCTURES FOR DIRECTION OF ARRIVAL ESTIMATION

by

EDWARD J. VERTATSCHITSCH, B.Sc.

A Thesis
Submitted to the School of Graduate Studies
in Partial Fulfilment of the Requirements
for the Degree
Doctor of Philosophy

McMaster University

LINEAR ARRAY STRUCTURES

To my wife, Michelle,

for all the sacrifices she has made,

and,

my children, Laura, Dale

and those yet unnamed.

DOCTOR OF PHILOSOPHY (1987) McMaster University
(Electrical and Computer Engineering) Hamilton, Canada

TITLE: Linear Array Structures for Direction of Arrival Estimation

AUTHOR: EDWARD J. VERTATSCHITSCH, B.Sc., (McMaster University)

SUPERVISOR: Professor S. Haykin

NUMBER OF PAGES xii, 220

ABSTRACT

The impact of the array geometry, for linear arrays, on the estimation of the direction of arrival of incident plane waves is examined in this thesis. The fundamental result is the establishment of the conditions under which array structures, different from uniformly spaced, may provide improved accuracy or reliability in these estimates. We are primarily concerned with the use of high accuracy estimators, attempting to obtain accuracies well within the classical beamwidth of the array.

Several different criteria for designing thinned array structures are described, with the principal emphasis on redundancy based designs. For a single plane wave incident on the array, the Weiss-Weinstein bound, which is an estimator independent bound, is applied to a variety of array structures and indicates that the thinned arrays will yield greater accuracy, provided the SNR is sufficiently large. The bound allows us to investigate the effects of a priori information on the estimation performance of the different structures considered.

Maximum likelihood estimation is applied to the identical problem and similar tradeoffs are observed. We

propose the concept of outlier probability as a measure for discriminating between array structures and provide models for characterization. Certain algorithms in the literature for the design of nonuniform arrays are shown to be poor under these measures.

The impact of array structure, in a multipath environment consisting a target with a strong specular reflection, is illustrated using exact maximum likelihood estimation. It is shown that the most significant gains to be made for thinned arrays occur when the multipath is such that target and image are well within a beamwidth of the array. Under these conditions, it is found that the nonuniform arrays often outperform uniform arrays consisting of many more elements for all values of SNR and phase differences between the two plane waves.

An experimental, 32-element array was constructed and brought into the field in order to gather multipath data, over water, in a real world environment. For the very closely spaced target and image of this experiment, the nonuniform arrays outperform uniform arrays consisting of even twice as many elements.

ACKNOWLEDGEMENTS

I would like to acknowledge the guidance, support, and the many critical suggestions contributed by Prof. Simon Haykin during the development of this work. His philosophy and enthusiasm, both in and out of the classroom, have enriched my research and being.

Discussions with Prof. John Litva, particularly while with the CRC in Ottawa, Canada, were extremely informative and aided greatly in the development of the experimental apparatus. I am grateful for the suggestions of the other members of my supervisory committee, Profs. D. Taylor, C. Carter and T. Timusk, which helped to make the thesis more coherent and complete.

V. Kezys and T. Greenlay of the CRL, McMaster University, both contributed greatly with many long discussions surrounding the concepts of this thesis and the development of the hardware. Many of my fellow graduate students and colleagues also acted as sounding boards. For their selfless giving of time, I am indeed grateful.

My wife, Michelle, has had to deal with my many emotions, highs and lows, and idiosyncrasies associated with this undertaking. Her patience and comfort have sustained my efforts. For my daughter, Laura, and son, Dale, I can only regret the many long hours spent apart.

Finally, as this work concerns itself with random noise, and simulations play an important role in the characterization, the following passage seems apropos. Guildenstern, reflecting on the nature of tossers of coins (and perhaps researchers using simulations), after having just witnessed 92 consecutive tosses of a coin land 'heads':

> "...The equanimity of your average tosser of coins depends upon a law, or rather a tendency, or let us say a probability, or at any rate a mathematically calculable chance, which ensures that he will not upset himself by losing too much nor upset his opponent by winning too often. This made for a kind of harmony and a kind of confidence. It related the fortuitous and the ordained into a reassuring union which we recognized as nature. ..."[1]

---

[1] Tom Stoppard, Rosencrantz & Guildenstern are Dead, Faber and Faber, London, 1974.

TABLE OF CONTENTS

LIST OF FIGURES

Figure		Page

Figure		Page
4.13a	A priori knowledge on p_o, NR-7	107
4.13b	A priori knowledge on p_o, NR-7	108
4.14	A priori knowledge on MSE, U-7	111
4.15	A priori knowledge on MSE, NR-7	112
5.1	CRLB versus phase in multipath, NR-7	130
5.2	CRLB versus separation, U-7, NR-7	132
5.3	Multipath coarse density, NR7, I	135
5.4	Multipath coarse density, NR7, II	136
5.5	Multipath coarse density, NR7, III	138
5.6	Multipath coarse density, NR7, IV	139
5.7	Multipath coarse density, U7, I	140
5.8	Multipath coarse density, U7, II	141
5.9	Multipath coarse density, U7, III	143
5.10	Multipath coarse density, U7, IV	144
5.11	MLE comparison, separation $2\pi/4$	145
5.12	MLE comparison, separation $2\pi/8$	146
5.13	MLE comparison, separation $2\pi/16$	147
5.14	MLE comparison, separation $2\pi/32$	148
5.15	MLE comparison, separation $2\pi/64$	149
5.16	Smooth surface top transmitter	159

LIST OF TABLES

CHAPTER 1

INTRODUCTION

1.1 General

A linear array structure consists of a finite number of sensors arranged in a single dimension. The outputs of the individual sensors are combined to provide estimates of the parameters which characterize a propagating wave disturbance. Array signal processing, which is the estimation of the parameters of interest, is a continuing area of research in a variety of disciplines. The parameters of interest vary among the different areas, as do the major constraints governing the operation of the array.

Linear and higher-dimensional array structures have been used in radio astronomy, radar, sonar, and geophysics. The most common application is the determination of the location of an object or disturbance relative to the array orientation. The principal interest is the determination of the direction of arrival of the propagating wave impinging on the array structure. In an active system, a signal is sent out and the reflected return carries information about the target and its location. The transmitted signal may be highly directive, thereby concentrating energy in a particular region of space. Passive systems 'listen' to the entire field for signal sources and often operate with significantly lower received signal powers.

When the outputs of the sensors at an instant of time are considered, we refer to this as a snapshot. There is a direct relationship between the estimation of the direction of arrival from a snapshot of a linear array (spatial problem) and frequency estimation from a set of discrete samples in the time domain (temporal problem). Array signal processing techniques are therefore often referred to in the context of spectrum analysis. The 'space-time analogy' [39], is the interchange of temporal dimension (time) with spatial dimension (distance). In the Fourier transform domain, frequency (1/time) is replaced by wavenumber (1/distance). Therefore, the temporal domain signal processing techniques can generally be applied to the array processing problem.

Consider a plane wave (in the far field of the array), as depicted in Figure 1.1, impinging on the structure as in a typical radar environment. We are interested in estimating the elevation angle of the target, measured from boresight, which is taken to be perpendicular to the

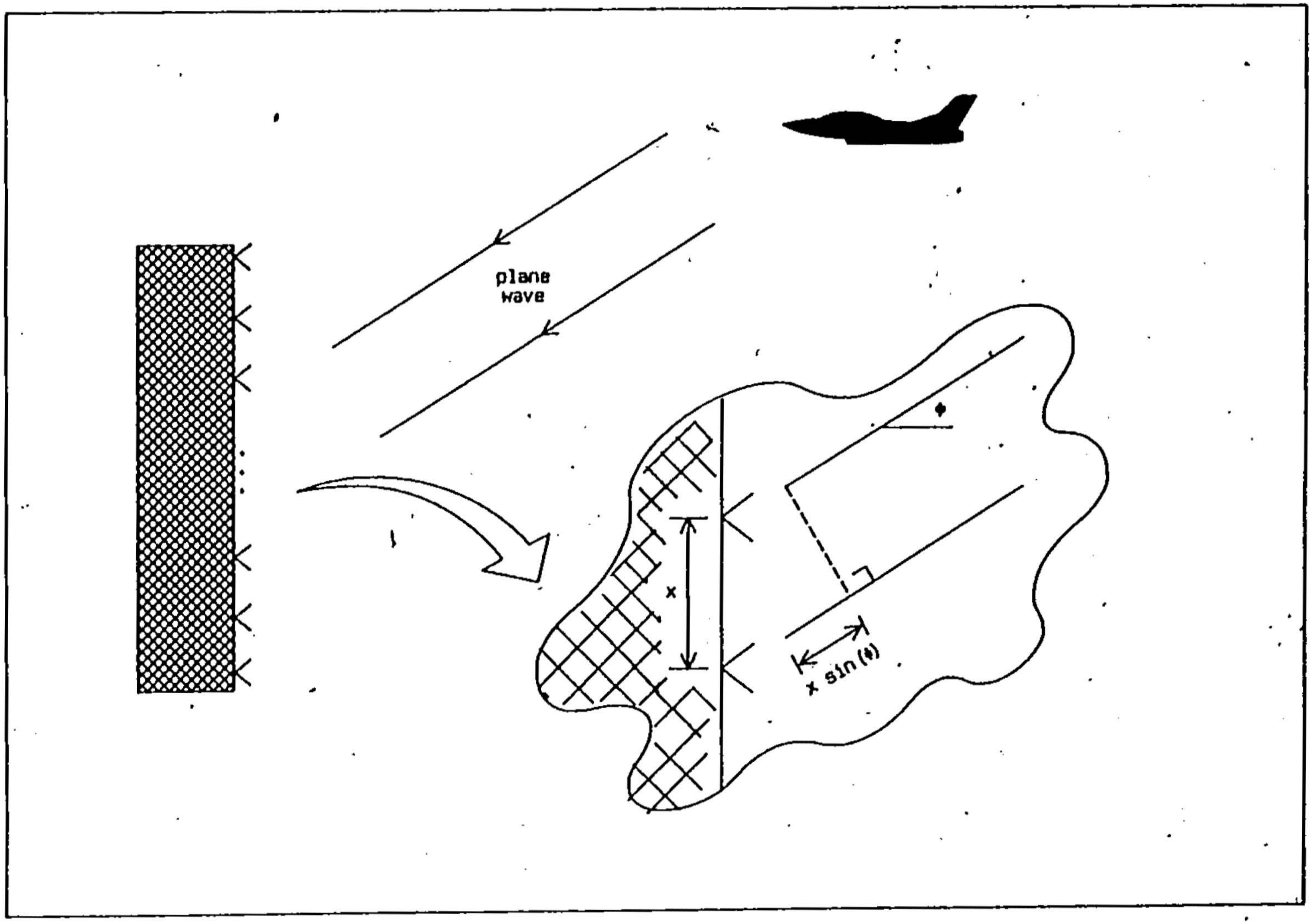

Figure 1.1: Representation of a plane wave impinging upon a linear array.

vertical array. For a narrow band signal, the mathematical model of the complex envelope at the i^{th} sensor is

$$s_i = a \exp\{j(\theta + 2\pi\sin(\phi)x_i/\lambda)\} \tag{1.1}$$

where λ is the radio wavelength,

ϕ is the elevation angle,

a is the amplitude of the signal,

θ is an arbitrary phase shift,

and x_i is the location in space of the i^{th} sensor.

The quantity, $2\pi\sin(\phi)/\lambda$, is referred to as the projected wavenumber, or just simply, wavenumber, and will henceforth be represented by the symbol k. The wavenumber has dimensions of 1/distance. The expression for the signal at the sensor can then be expressed as

$$s_i = a \exp\{j(\theta + kx_i)\} \tag{1.2}$$

The analogy with time domain sampling and frequency estimation is clearly evident from equation (1.2) and virtually all of the same features apply. Consider a set of uniformly spaced time samples. If the sample spacing in the time domain is T seconds, then the unambiguous frequency region is $\pm\pi/T$ radians/second. The aliasing effect has been well documented for time domain sampling [1], and a similar effect exists in the spatial problem. It is impossible to distinguish frequencies outside this interval from those inside this interval.

Another commonly observed phenomenon occurs when samples are taken at a rate very close to twice the bandwidth of the signal, also known as the Nyquist rate. For an infinite number of samples taken with infinite precision, there is no loss of information when the signal is sampled at the Nyquist rate. However, for a finite number of sample points this is not the case. In addition, since our measurements are generally not of infinite precision and are often corrupted by noise, errors are made in determining the parameters of the wave field. This error can be very significant near the edges of the signal spectrum when it has been sampled at the Nyquist rate. Even a small amount of noise may identify a signal having a frequency close to one end of the band as actually being located at the opposite end of the spectral interval. When such an error is critical and must be avoided, the sample rate must be increased well above the Nyquist rate.

For the spatial problem, the wavenumber is restricted to lie in the interval $(-2\pi/\lambda, 2\pi/\lambda)$, since, the target may lie anywhere from -90° to 90°. Therefore, to obtain the total field of view, a sampling distance less than $\lambda/2$ is required. Failing to do so, restricts the field of view and generates what is known as grating lobes. The array structure will respond in exactly the same way to targets in the grating lobes as in the 'true' field of view. For nonuniform arrays a similar restriction applies and the smallest intersensor spacing is normally taken to be no larger than $\lambda/2$.

The problem discussed earlier, when samples are being taken at the Nyquist rate and a complex-valued sinusoid is located at one end of the band, is analogous in the spatial problem of targets near end-fire of the array structure. That is, even a small amount of noise may indicate the target is located in the opposite direction. This would constitute an error of 180° in the target location. For this reason the minimum spacing of an array is normally chosen to be less than the required $\lambda/2$, where λ corresponds to the maximum operating frequency, and so will prevent significant grating lobes.

The beamwidth of a radar, conventional dish or array, is given by λ/A radians of physical space; where A is the length of the aperture and is assumed significantly greater than the wavelength. The wavenumber beamwidth is, therefore, $2\pi/A$. In a conventional radar system, where the aperture consists of one large antenna, the accuracy and/or resolution limit is normally taken to be equal to the beamwidth. In a radar array, each sensor requires a separate receiver. For large numbers of elements, this may become prohibitively expensive. Since the field of view restricts the minimum sampling rate, it may be possible to decrease the beamwidth below that of a uniform array using nonuniform spacing. It is desired to obtain maximum performance from a given, finite number of sensors.

In this thesis, we are primarily concerned with high accuracy estimation. This may be defined as target location accuracies significantly less than a beamwidth. Using optimal estimators we are interested in improving the performance by using a judicious placement of the sensors. The array geometry will impact the estimator performance and the tradeoffs that may be encountered in choosing certain configurations needs to be investigated.

A further complication to the target location/ estimation problem occurs when more than one 'target' is present. This may be due to several independent targets in an area or by reflections of the target echo, for example, from a water surface. The latter effect is known as multipath. It is a particularly difficult problem when the target is at a very low elevation. In this instance, the target and image (specular reflection) may be separated by much less than the beamwidth. The effect of different array structures using optimal estimation procedures needs to be studied and understood.

Since the value λ acts only as a scale factor in the estimation problem, we can develop a normalized system of parameters, which are independent of λ. We measure the sensor locations in units of $\lambda/2$. This implies the smallest spacing in the array must be less than or equal to 1 unit in this normalized system. In turn, this restricts the normalized wavenumber to lie in a range $(-\pi, \pi)$. The majority of the structures discussed in the thesis consist of sensor spacings that are multiples of the minimum spacing. This simplifies the description of many of the structures.

The normalized wavenumber has an alternative interpretation. The value k, is now exactly equal to the observed phase difference (in radians) between two elements which are separated by the minimum spacing of one unit. All of the results may easily be scaled to the actual operating conditions by multiplying spatial distance quantities by $\lambda/2$ and dividing the wavenumber or transform domain locations by $\lambda/2$.

1.2 Background

The literature provides a rich assortment of descriptions for the structures in which the spacing between elements is unequal. Some of the most common are: nonuniform, sparse, thinned, aperiodic, and space-tapered arrays. In addition, many authors simply refer to the structures according to the class construction or array design algorithm. In the 1960's, the advantages of eliminating the restriction of equal spacings became apparent [2]. One of the prime motivations was the reduction of the number of elements required to obtain a desired antenna beam pattern, referred to as thinning. Another common application of nonuniform arrays was the increase in the effective bandwidth through variable spacing, called broadbanding the array.

The 'optimum' array structure is very specific to the particular problem being considered. The formulation of the constraints greatly influences the final solution. In very few of the formulations was a closed form solution found. One such result was obtained when a specific characteristic of the side lobe response was required and the array was constrained to operate with a uniform current excitation [3]. A good summary of the early work is provided in [4]. Beam-shaping, particularly Dolph-Chebyshev patterns, in which the beamwidth is fixed and the side lobe level is minimized, was one of the early incentives of unequally spaced arrays. The advantage being that it was easier to achieve space-weighted than excitation-weighted uniform structures. The disadvantage was the very close spacing of some elements (significantly less than λ/2), and the resultant mutual coupling effects [5].

Another common constraint of many of the designs was a specified aperture for the array structure. The number of possible arrangements of N elements within this aperture may become astronomical. On the other hand, exact solutions for the problem were in many cases not obtainable and dynamic programming approximations were implemented in many of the proposed solutions. An alternative to these procedures was the examination of random arrays. A large number of possible configurations were obtained at random and then the properties of each structure examined, most commonly for the peak side lobe level. A comparison of these results may be found in [6].

Eventually, simultaneous optimization procedures for both space- and excitation-weighted structures were also studied [7, 8]. The latter reference provides a procedure for obtaining the optimum current excitations of the elements for an arbitrary set of spacings in order to obtain a desired beam pattern (in the least squares sense). As mentioned earlier, in many of these studies, optimal solutions could not be found and an assortment of different techniques have been proposed. This line of research still continues and alternative solutions are proposed using a variety of constraints and optimality conditions [9 - 12].

Of principal interest in this thesis are sparse arrays, for which the average spacing between elements is significantly larger than $\lambda/2$. We are also primarily concerned with the high accuracy estimation problem as opposed to the side lobe structure as an entity onto itself.

One of the first studies of the 'redundancy' construction of nonuniform arrays is that of Moffet in the often referenced paper [13], in which a case is made for maximizing the resolution of an array for a given number of sensors. The structures discussed, are actually those proposed by Leech [14], in a mathematical paper whose original intent did not address the array problem. In these constructions we do not impose an aperture length constraint on the array. For a given number of sensors, one or more 'best' arrays are proposed. Although the conceptual solution is straightforward, it is difficult and computationally intensive to implement for large numbers of elements. Therefore, suboptimal ways of extending these structures for very large numbers of elements have also been proposed [15]. Recently, the minimum-redundant arrays cited by Moffet have been obtained from other interpretations as well [16, 17]. There is also considerable work in the region of 2-dimensional arrays, unfortunately, many of the construction algorithms for linear arrays do not extend to higher dimensionality [18 - 22].

An alternative procedure to the minimum redundant sampling was proposed in [23] and is known as a nonredundant construction, although some authors, prior to this paper, referred to those of Moffet as nonredundant. The grid-search method provided a set of arrays that were very nearly the minimum length arrays having zero redundancy. An alternative procedure is developed in this thesis requiring much less numerical computation time, is exhaustive, and indicates an anomaly in the results of [23,34,35].

The problem of interest, in this thesis, is direction of arrival estimation or bearing estimation as it is often referred to in the sonar area. It is difficult to divorce the estimator and array geometry relationship. The actual 'optimum' structure may depend upon the estimator being employed. This poses a difficult problem in defining array performance. An estimator-independent lower bound on the minimum attainable, mean-square wavenumber estimation error is a useful tool for discriminating between the different structures. A comprehensive evaluation of this type has not been found in the literature. One of the few papers which even address the variance bounds and array geometry, does so for a limited set of array structures under high signal-to-noise ratio (SNR) conditions using the Cramér-Rao Lower Bound [24]. The bound used does not indicate any tradeoffs that must exist between the different structures, and neither is it tight at low SNR.

A variety of techniques for bounding the mean-square parameter estimation error are available such as Cramér-Rao, Barankin and Ziv-Zakai bounds. A comparison of these bounding techniques may be found in [25], and a subset has been applied to the wavenumber estimation problem [26]. Some of these techniques are only strictly valid for certain types of estimators and/or may be far from 'tight' in the regions of interest. In many circumstances, there exists a priori information about the location of the target which would have to be taken into account. A recent bounding technique has been found [27], which permits the inclusion of the a priori information and is independent of the estimator. This bound will be shown to possess the desired characteristics for bounding the wavenumber estimation error of a single target in additive, white, Gaussian noise.

In the past, spectral estimation procedures have often been applied to this problem. The location of the peaks of the estimated spectrum are taken to be estimates of the frequency of the sinusoids, or in our case, the target positions. The paper by Kay and Marple, [28], is a good survey of the common spectral estimators. Some of the newer estimators, many of which involve spectral decomposition, have been compiled in a special issue of the Proceedings of the IEEE, September, 1982. This issue describes the work in a variety of disciplines including geophysics, radio astronomy, sonar and radar.

The work of Lang et al, is also significant for being one of the first works implementing high resolution estimation procedures on nonuniform arrays. Since that time, other researchers have also indicated the suitability of nonuniform arrays for direction of arrival estimation and spectral estimation using other techniques [16, 45]. There has been some study, in the sonar area, using cross-sensor beamforming techniques for output SNR performance, resolution, and array gain with nonuniform arrays, principally, the minimum redundant structures of Leech [29-32].

Unfortunately, a detailed study comparing performance of the redundancy based array structures has not been undertaken. Neither have the tradeoffs involved from choosing one of these thinned arrays over a uniform array been demonstrated. Most of the previous works present a single simulation result indicating the possible improvement which may be obtained. The tradeoffs and statistical performance have not been explored. In fact, in 1982, in the Proceedings of the IEEE special issue on spectral estimation, we quote from the conclusions of D.H. Johnson, [33], "The impact of array geometry on spectral estimation procedures is largely unknown." The only references given in this respect are [24] and [23]. It is this impact of array geometry which we wish to explore and, thereby, provide a comprehensive understanding of the behavior of nonuniform arrays for the direction of arrival estimation problem.

1.3 Approach and Scope of the Thesis

While the minimum redundancy arrays, described by Moffet [13], have received a great deal of attention recently in the radar/sonar literature, the description of the nonredundant array has been virtually nonexistent. Chapter 2 builds upon the initial concepts of Lang et al [23], and describes a computational search technique that does not suffer from the limitations of Lang. This allows us to point out an anomalous result quoted in [23] and provides an exhaustive list of these arrays for up to 10 elements, where the previous list ended with 8 elements. These results have already been published in two papers [34, 35]. The limitation in extending the results is the computational effort involved, which grows as N!.

Recently, these array structures have received further attention in the geophysics area. The efforts of Robertson have been presented in an issue of Scientific American [36].

in which these structures are called Golomb rulers. A challenge was proposed to extend the results beyond 13 elements found in 1984. The follow up issue, [37], provides the latest results for a 14 and 15 element array found at the IBM Thomas J. Watson Research Center, again using the same algorithm. Clearly, these structures are now receiving a renewed interest.

In Chapter 3 we examine the single target location problem. Using the very recent bounding technique of Weiss and Weinstein, we are able to obtain useful insights into the performance of linear array structures for direction of arrival estimation. The tradeoffs in performance that may be expected through the use of nonuniform sampling are original concepts of this thesis. To the author's knowledge, these ideas have never been presented in the literature. In fact, the bound itself has never been applied to this problem so that the analytical results and simplified expressions, presented in Appendix A, are also new.

Chapter 4 deals with the identical estimation problem by simulating the maximum likelihood estimation procedure. The results build upon the concepts first described in the now classic paper by Rife and Boorstyn [38]. Their basic discussion of the estimation error dealt exclusively with uniform structures. Those concepts have been extended here to arbitrary array configurations, of which the uniform is a special case. We have also addressed several implementation problems of the maximum likelihood estimator, and have extended the results for both uniform and nonuniform structures.

A tradeoff in performance, similar to that found in Chapter 3, using the different array structures is identified. In addition, we provide an alternative measure of performance for discriminating between the various array structures which may, for certain applications, be more useful to the radar system designer. This, also, has not been addressed in the literature prior to our recent presentation [42].

Chapter 5 describes the results for a typical target location problem in the presence of multipath. The performances of the uniform and nonredundant arrays are compared for the first time. A complete statistical simulation using exact maximum likelihood estimation was implemented. Previous works have, at best, compared performance for a single simulation. We have not only examined the high SNR performance, shown to coincide with the Cramér-Rao Lower Bound, but have also examined threshold effects. The tradeoffs are now significantly more complex owing to the larger number of parameters describing the system. The analysis was also carried out for the best and worst case phase differences between direct and specular echoes.

Finally, an actual 32-element sampled aperture array, operating at X-band, was designed, and field-tested as part of this research program in conjunction with another Ph.D. candidate, V. Kežys. This system provides 'real world' data of a target in a multipath environment. It was then possible to examine the performance of the nonredundant structures using true experimental data. The performance improvements have been clearly established in the final section of Chapter 5. This probes the sensitivity of the nonredundant structure to calibration errors and other performance-limiting error sources which will be present in a working environment. Data of the required accuracy for the examination of high resolution estimators had not been previously available. These results are also original.

We conclude this thesis with a summary of the results obtained in the earlier chapters. The research has provided significant insights on the impact of array geometry on high accuracy estimation procedures and several further areas of investigation have been established. These considerations for future research, both analytical and experimental, are presented in the final chapter.

CHAPTER 2

NONUNIFORM ARRAYS

We have presented a description of the background material initiating the study of nonuniform arrays in Section 1.2 of the previous chapter. Almost all of the recent papers of the 1980's, examining high accuracy direction of arrival estimation, using nonuniform arrays, involve one of the three classes of redundancy-based structures. Since there has not been a detailed assessment made of these structures, we will concentrate on these and the corresponding uniformly spaced arrays in this thesis.

This chapter will discuss the origins of redundancy-based array designs and the differences between the minimum redundant, (restricted and unrestricted,) and the nonredundant structures. The last section will describe the algorithm generated in 1981 to improve the search for the nonredundant arrays and describes the latest results in the search for these structures.

2.1 Origins

In simple terms, an array may be viewed as a grating or compound interferometer. The array is utilized by considering the outputs from all of the possible pairings of elements, with each pair acting as an interferometer. Given N elements, there are N(N-1)/2 possible pairings. In order to determine their spatial-frequency sensitivity, it is necessary to determine the separation between elements of each pair. For a uniform structure having unit spacing (as discussed in Chapter 1, this is generally taken to be $\lambda/2$): there are N-1 pairs having a separation of one unit, N-2 pairs having a separation of two units, etc., ending with one pair of sensors separated by N-1 units.

We can present this type of structural analysis through the use of the coarray. The coarray is described by marking the values of the separations which exist for each pairing of elements as an interferometer. Figure 2.1a presents an example of this type of characterization for the four-element uniform array. Also presented in the figure are the four pairings obtained by considering an element paired with itself. In this context, there are N(N+1)/2 possible pairings. The redundancy concept can readily be seen in Figure 2.1a as there are three pairings separated by one unit compared to only one pair separated by three units.

Array	x	x	x	x
Coarray	x	x	x	x
	x	x	x	
	x	x		
	x			

a)

Array	x	x			x		x
Coarray	x	x	x	x	x	x	x
	x						
	x						
	x						

b)

Figure 2.1: Comparison of 4-element arrays and their associated coarrays (a) uniform, (b) optimum nonredundant.

Reducing the redundancy involves spreading out the coarray, thereby, increasing the number of distinct separations that may be obtained.

An alternate motivation for reducing the redundancy comes from the spectral estimation problem directly. It is well known that the power spectral density is the Fourier transform of the autocorrelation function [1]. A sequence obtained by sampling a process at discrete points is described by an autocorrelation function which is also defined at discrete points. As mentioned in the Introduction, Chapter 1, there exists a direct analogy between temporal sampling and spatial sampling. Therefore, there are abundant references to what was classically associated with the time-frequency transform relationship and is here understood to be applied to the distance-wavenumber transform pair.

In our case, the wavenumber spectrum is the Fourier transform of the autocorrelation function obtained from the sensor outputs. In this discussion, we realize the fundamental difference in using a finite number of sample points versus sampling the entire space, and the arguments are understood to be strictly valid in the latter case alone. Since the wavenumber domain is limited, we can make use of the sampling theorem of Nyquist, [1]. In effect, this states that the wavenumber spectrum may be determined if the autocorrelation function is known at uniform points separated by less than $\lambda/2$. The coarray represents the points at which the autocorrelation function is known. Therefore, it is the coarray, not the initial data sequence, for which uniform sampling is desired. The redundancy-based structures attempt to arrange the sample points such that the coarray is approximately uniformly spaced and is extended beyond the conventional aperture by 'spreading out' the redundant estimates of the correlation function.

Figure 2.1b depicts the four-element nonredundant array. Each spacing of elements provides an estimate of the autocorrelation function at a unique sample point. The coarray contains all positions between zero and six, and only the value at zero is repeated. Comparing the results to the four-element uniform array as described in Figure 2.1a, the increased aperture is immediately apparent. The three redundant estimates of the uniform array effectively have been 'added' to the end of the aperture.

Unfortunately, for N greater than 4, no ideal nonredundant arrays exist. An ideal nonredundant array would be one for which the coarray contains exactly one estimate of a particular autocorrelation sample and the set of samples are contiguous. This would imply an array having an aperture exactly equal to $N(N-1)/2$, since, this is the number of nonzero separations provided by N elements.

As the ideal array does not exist, several 'approximate solutions' have been proposed in the literature. The next section presents the descriptions of these structures.

2.2 Suboptimal Nonuniform Arrays

One of the first works considering redundancy-based structures for direction of arrival was that of Moffet, [13]. His analysis, based upon the interferometer approach, led him to consider a set of structures originally determined by Leech in 1956, [14]. The minimum redundancy arrays are structures for which the redundancy is minimized under the constraint that the structure still provide a coarray that is contiguous.

This definition leads to two further subclasses called restricted and unrestricted. If the coarray is to be strictly filled with no missing values this constitutes a restricted array. If the solution is the one providing a coarray with the greatest number of contiguous estimates, the resultant structure is termed unrestricted (since the entire coarray need not be filled).

This difference is best illustrated by an example for N equal to eight. Figures 2.2a and 2.2b provide a comparison of a restricted and unrestricted solution. The * positions in the coarray are characteristic of more than one pair of

```
Array     xxx        x   x  x  x x

Coarray   ****xxxxxx*xxxxxxxxxx*xx

                           a)

Array     x       x         xx  x x       x       x

Coarray   *xxxxxxx*xxxxxxxxxxxxxxxx       *       x

                           b)
```

Figure 2.2: Comparison of 8-element minimum redundant arrays developed by Leech, [14]. a) restricted, b) unrestricted. * indicates repeated estimate.

sensors. The restricted solution has no missing values although three of the nonzero spacings are repeated in the twenty-three unit aperture (excluding the zero lag). The unrestricted array has a number of missing points in its thirty-nine unit aperture; however, it provides a set of twenty-four contiguous estimates. Leech has compiled a set of solutions for values of N less than or equal to eleven, although not necessarily exhaustive. These results are reproduced here in Table 2.1. For N equal to nine, the unrestricted array was identical to that of the restricted structure.

It was originally proposed that only those pairings which were involved in the uniformly filled portion of the coarray would be used in the estimation procedure [13, 18]. However, as shown in subsequent chapters of this thesis, one can obtain an optimal estimation procedure, based on maximum likelihood estimation, which makes use of all of the information available. Therefore, although there are holes in the unrestricted coarray, it is not necessary to eliminate the information contained in the lags beyond the largest contiguous spacing. This knowledge then leads to an alternative, redundancy-based structure known as the nonredundant array.

Nonredundant arrays, in the most general sense, are defined as arrays in which there is zero redundancy.

Table 2.1

Minimum Redundant Arrays Compiled by Leech, [14]

No. of Sensors	Location										
restricted											
5	0	1	4	7	9						
	0	1	2	6	9						
6	0	1	2	6	10	13					
	0	1	6	9	11	13					
	0	1	4	5	11	13					
7	0	1	2	6	10	14	17				
	0	1	2	3	8	13	17				
	0	1	2	8	12	14	17				
	0	1	2	8	12	15	17				
	0	1	4	10	12	15	17				
	0	1	8	11	13	15	17				
8	0	1	2	11	15	18	21	23			
	0	1	4	10	16	18	21	23			
9	0	1	2	14	18	21	24	27	29		
	0	1	4	10	16	22	24	27	29		
	0	1	3	6	13	20	24	28	29		
10	0	1	3	6	13	20	27	31	35	36	
11	0	1	3	6	13	20	27	34	38	42	43
unrestricted (if different from restricted)											
5	0	3	4	9	11						
	0	4	5	7	13						
6	0	4	5	6	13	16					
	0	6	7	9	11	19					
	0	1	4	10	12	17					
	0	1	8	11	13	17					
7	0	6	9	10	17	22	24				
	0	8	9	12	18	23	25				
	0	14	15	18	24	26	31				
	0	13	14	16	21	25	31				
8	0	8	18	19	22	24	31	39			
10	0	16	17	28	36	42	46	49	51	73	
	0	7	22	27	28	31	39	41	57	64	
11	0	18	19	22	31	42	48	56	58	63	91

Optimum nonredundant arrays are those structures which minimize the number of 'holes' in the coarray under the constraint that they be nonredundant. This should be compared to the restricted arrays which minimize the number of redundant pairings under the constraint that there be no holes in the coarray. The nonredundant arrays would, therefore, provide the densest packing of the coarray of all possible zero-redundancy arrays.

Nonredundant structures were initially developed differently by Lang et al. [23]. Their algorithm for searching was based upon maximizing the minimum separation in the coarray. They define the array to lie on a grid of 400 points with the two exterior elements at the end of the grid. The processing time increases significantly as the grid density increases. They estimate that 400 values would provide enough sensitivity for convergence to a reasonable structure and was computationally feasible, provided the number of elements was not large. Upon convergence, the structure would be normalized such that the minimum spacing is taken to be one unit.

The unnormalized arrays obtained from the previous algorithm, as found in [23], are reproduced in Table 2.2a. When the normalization is applied, such that the smallest spacing is one unit, the resultant description is found in Table 2.2b. We note that the algorithm was never claimed to

Table 2.2

'Nonredundant' Arrays Compiled by Lang et al. [23].

No. of Sensors	Location							
a) unnormalized array locations								
5	0	36	144	328	400			
6	0	23	93	235	281	400		
7	0	16	176	256	304	368	400	
8	0	11	66	211	244	288	378	400
b) normalized to unit minimum spacing (approximate locations)								
5	0.00	1.00	4.00	9.11	11.11			
6	0.00	1.00	4.04	10.22	12.21	17.39		
7	0.00	1.00	11.00	16.00	19.00	23.00	25.00	
8	0.00	1.00	6.00	19.18	22.18	26.18	34.36	36.36

be exhaustive and the final conclusions urge the development of a faster technique for this search. It was this work, [23], which inspired both the development of the algorithm described in Section 2.3, and the need for a systematic comparison of the various structures.

2.3 Nonredundant Arrays

The result of Lang et al. [23], as presented in Table 2.2b, clearly indicates the tendency of the structures to lie on a grid for which the spacing between any two elements is an integer multiple of the minimum spacing. The slight discrepancy is due to the fact that there was finite resolution available and the unnormalized spacings must lie on a 400-point grid. This number was arbitrary, in so far as the structure was concerned, and was only dictated by the processing time.

To improve the processing time in searching for nonredundant arrays a significant improvement results by defining all the spacings as exact multiples of the minimum spacing. There is, therefore, no fixed aperture size associated with this procedure. We can define a minimum aperture from N sensors, since, an array having zero redundancy must be at least N(N-1)/2 units in length.

It is much simpler to deal with the consecutive interelement spacings than the absolute locations themselves. The aperture of the array is equal to the sum of the N-1 spacings. For a given integer length, L, we begin by listing all of the sets of distinct integers which sum to L. If any spacing were repeated; the array could not be nonredundant. For each set, all possible permutations are generated and the coarrays evaluated. If no coarray was found to be nonredundant, the length would be increased to L+1 and the procedure repeated.

Eventually, there will occur a length for which a coarray is found which will possess zero redundancy. At this point, the remaining permutations of the sets of integers which also sum to the current value of L are examined and the search is complete. Every increase in L will necessitate an additional hole in the coarray. Only those arrays having the same value of L as the first zero redundancy array discovered, will have the minimum number of holes as required by the definition for the optimum nonredundant array.

Prior to the examination of a particular permutation of integers, a vector of length L is zeroed, which represents the coarray. As each pairing of elements is found, the corresponding coarray value is examined. If the coarray value was zero, it is incremented; if not, this permutation cannot be nonredundant and no further processing of this permutation is necessary.

To determine all of the possible pairings of elements, the array positions are determined begining at zero, by summing spaces together one at a time, and the corresponding coarray values set to one. From the array positions, the remaining coarray values are determined by indexing through the list and determining the difference in position for each pair of elements. As position zero is set to zero, we begin with position two subtracting position one. The next step begins by choosing position three, subtracting position two and then position one, etc. The last set of values occurs by choosing position N-1 and subtracting in turn positions N-2, N-3, ... , 1. In this way, N(N-1)/2 additions or subtractions are required. The index for which a redundancy occurs also indicates where the next permutation should begin. In this way, all permutations which have any possibility of yielding a nonredundant structure will be examined and the search is exhaustive.

The results of this technique, in searching for optimum nonredundant arrays, are presented in Table 2.3. The arrays agree with most of those presented by [23], as shown in Table 2.2b, to within a small error, easily accounted for by the restriction of using 400 points of resolution. There are a greater number of arrays in Table 2.3 because this technique is exhaustive and because of the increase in

Table 2.3

Nonredundant Arrays

No. of Sensors	Location									
5	0	1	4	9	11					
	0	2	7	8	11					
6	0	1	8	11	13	17				
	0	1	8	12	14	17				
	0	1	4	10	12	17				
	0	1	4	10	15	17				
7	0	1	11	16	19	23	25			
	0	1	7	11	20	23	25			
	0	1	4	10	18	23	25			
	0	2	7	13	21	22	25			
	0	2	3	10	16	21	25			
8	0	1	4	9	15	22	32	34		
9	0	1	5	12	25	27	35	41	44	
10	0	1	6	10	23	26	34	41	53	55

speed, we could examine a larger number of elements.

There is, however, one anomaly in the arrays presented in [23], which is the case for eight elements. In this particular case, the array identified by Lang et al. extends over approximately thirty-six unit spacings, while the array we present, extends over only thirty-four unit spacings. The thirty-six unit array has ten holes in the coarray and the thirty-four unit array has only eight. It is clear that, in this instance, their algorithm did not reduce to an optimum nonredundant array, although the sensors still lie on a grid which is spaced at approximately integer multiples of the smallest spacing. We conclude for the case N equal to eight, the algorithm of Lang et al [23] would have required more than a 400-point grid for convergence to the optimum array and therefore greater computational effort.

Recently, optimum nonredundant arrays have been found by other researchers, such as Robertson, working in Very Long Baseline Interferometry (VLBI), using an algorithm similar to the one just described, [36, 37, 40]. These works denote optimum nonredundant arrays as Golomb Rulers, named by M. Gardner after Dr. Solomon W. Golomb [40]. To date, the longest known Golomb ruler consists of 15 elements and is 151 units in length, [37], found by James B. Shearer of the IBM Thomas J. Watson Research Center. The problem would now seem to be beyond the scope of general purpose computing machines. Dr. Robertson, [41], has pointed out the need for dedicated architectures in furthering the search for these structures.

CHAPTER 3

BOUNDING THE ERROR OF TARGET LOCATION

In this chapter, a model of the direction of arrival estimation problem is formulated. The array structures of the previous chapter are characterized in terms of lower bounds on the mean square error (MSE) of wavenumber estimation. We begin by considering the Cramér-Rao Lower Bound and applying it to a general linear array. While results of practical value are obtained for high elemental signal-to-noise ratios (SNR), the bound is definitely found lacking for lower SNR. This observation lead to the use of a recently proposed lower bound on MSE for random parameters, developed by Weiss and Weinstein [27]. The results of this technique provide some fresh observations on the use of nonuniformly spaced arrays.

3.1 The Estimation Problem

As was shown in the introduction, Chapter 1, angle of arrival estimation is equivalent to the frequency estimation of a complex sinusoid in additive white gaussian noise (AWGN). We formulate the problem specification in this section, and define the terms to be used throughout the remainder of this thesis.

Given the sensor locations $\{ x_1, x_2, \ldots, x_N \}$, the radar operating wavelength λ, the amplitude of the returned signal a, and the angle of the target from boresight ϕ; the signal at the various sensors can be modelled in mathematical terms. We take boresight to be broadside to the array, with positive ϕ being measured toward the axis of increasing x. We further assume that the target is at a sufficient range to model the propagating signal as a plane wave.

With the previous definitions, the signal at sensor position x_i, can be modelled as a complex scalar

$$s_i = a \exp\{j(\theta + 2\pi \sin(\phi) x_i / \lambda)\} \tag{3.1}$$

where θ is an arbitrary unknown phase shift.
We define k, the projected wavenumber, to be $2\pi \sin(\phi)/\lambda$, which may be viewed as a spatial frequency. It is convenient to express all terms in a normalized scale. A useful normalization would be to measure the x_i in units of $\lambda/2$. This, in turn, provides the wavenumber as $\pi \sin(\phi)$.

This convention will be employed, henceforth. For the arrays considered, the minimum spacing is typically to be $\lambda/2$, corresponding, in the normalized scale, to 1 unit. The wavenumber may then range over the interval $(-\pi, \pi)$.

Let $\alpha = (\alpha_1, \alpha_2, \alpha_3)^T = (k, a, \theta)^T$ represent the parameters of the target, where $(\cdot)^T$ denotes transposition. This allows the vector of received data to be written compactly as

$$s(\alpha) = (s_1, s_2, \ldots, s_N)^T.$$

The receiver noise is AWGN, modelled as a complex term, where the real and imaginary components are statistically independent, each of zero mean and variance σ^2. They are also considered independent from sensor to sensor. The vector of sensor outputs is then written as

$$z = s(\alpha) + w \tag{3.2}$$

where w represents the vector of noise terms that are independent from element to element. We define the SNR as the elemental signal-to-noise power ratio, Γ. For the problem just described this corresponds to

$$\Gamma = a^2/(2\sigma^2) \tag{3.3}$$

The problem of interest is to estimate one or more parameters of the target, denoted by the vector α, given the vector of N sensor outputs, z. We consider the receiver noise to be a measurable quantity and therefore known. We are primarily concerned with the estimation of the target wavenumber, which is explicitly related to its direction of arrival.

As remarked earlier, the arrays are all normalized to a minimum spacing of 1 unit. The wavenumber is considered limited to the interval $(-\pi, \pi)$. In general, additional information may be known about the target location. The a priori knowledge may be used to improve the estimation accuracy. For example, if the minimum spacing is actually less than $\lambda/2$, say $\lambda/4$, this translates to a reduced region of wavenumber range, namely $(-\pi/2, \pi/2)$. There are still other ways in which a priori knowledge may be derived. It may be the illumination function is restricted to cover only a portion of the visible region, or the sensors themselves are directive. These forms of a priori knowledge will provide improved estimation of the target location.

If the wavenumber is considered a random parameter, knowledge about the target is specified by the a priori probability density function (PDF). We let k take on any value inside the interval (k_n, k_x) with equal likelihood, that is, the PDF may be considered uniform over this interval. While the nature of the problem may indicate some information about the phase is known, for the radar type problems considered, we will generally assume no a priori knowledge of the phase.

With the problem described, we may now proceed to bound the performance of estimators used to determine the wavenumber from a set of measurements made at a general linear array.

3.2 The Cramér-Rao Lower Bound

The use of the Cramér-Rao Lower Bound (CRLB) to determine the performance limitations of wavenumber estimators is well described in the literature, see for example [38, 25, 43]. The bound has been clearly documented in [44], where its special considerations are described. For these reasons, we will simply state the results of the bound and apply them to our problem. We follow the procedure of [38]. The observations made in the latter reference are here generalized to nonuniform arrays.

The PDF of the received data, z, given the actual parameters, α, is defined by

$$p(z/\alpha) = (2\pi\sigma^2)^{-N}\exp\left\{ - \frac{\| z - s(\alpha) \|^2}{2\sigma^2} \right\} \quad (3.4)$$

where $\|\cdot\|$ denotes the norm of the vector enclosed within. The Fisher information matrix, J , has terms J_{ij} given by

$$J_{ij} = E\left\{ \frac{\partial}{\partial\alpha_i} \ln p(z/\alpha) \frac{\partial}{\partial\alpha_j} \ln p(z/\alpha) \right\} \quad (3.5)$$

where $E\{\cdot\}$ denotes expectation. The CRLB for unbiased estimators can now be written as

$$E\{ (\hat{\alpha}_i - \alpha_i)^2 \} \geq J^{ii} \quad (3.6)$$

where J^{ii} is the i^{th} diagonal element in J^{-1}.

The Fisher Information matrix has a form similar to that given in [38], as shown by

$$J = \begin{bmatrix} 2\Gamma V & 0 & 2\Gamma P \\ 0 & N/\sigma^2 & 0 \\ 2\Gamma P & 0 & 2\Gamma V \end{bmatrix} \quad (3.7)$$

where $P = \Sigma x_i$; $V = \Sigma x_i^2$ and Γ is the elemental SNR. If a parameter is known, rather than one to be estimated, the appropriate row and column are simply removed from the matrix J. The resultant bound on the accuracy of wavenumber estimation for unknown phase becomes

$$E\{ (\hat{k} - k)^2 \} \geq (2\Gamma S)^{-1} \qquad (3.8)$$

where the spread is given by $S = \Sigma (x_i - C)^2$, and C is the centroid given by P/N.

We can now make several observations similar to those made in [38]. First, equation (3.8) is the correct bound whether or not the amplitude is assumed to be known. The fact that knowledge of the amplitude does not improve the bound is quite significant. It indicates that the amplitude need not be considered a random parameter. Also if P = 0, then (3.6) reduces to (3.8) whether or not the phase, θ, is known a priori. That is, the CRLB indicates no change in performance if the phase is known at the centroid of the array. Since S is independent of the absolute location in space of the array, the CRLB is also independent of absolute position.

This bound then provides a technique to compare the performance of two different array structures. For a given specified MSE, we are interested in determining the saving in SNR associated with two different arrays in achieving this specification. Let S_1 and S_2 be the values of S for two different array structures. Then, the saving in SNR can be determined as a ratio given by S_2/S_1. We define the "Sampling Gain", S_G, of an array as the saving in SNR required to achieve the same MSE performance as the corresponding uniform array having the same number of elements. Clearly, the greater S_G, the better the performance. The spread, S, for a uniform array having interelement spacing of 1 is equal to $N(N^2-1)/12$. We may therefore define the Sampling Gain as

$$S_G = \frac{\Sigma(x_i - C)^2}{N(N^2-1)/12} \tag{3.9}$$

It is interesting to observe that it is the "variance" of the element positions and not simply the aperture which governs the performance. In general, we may have an array defined on a larger aperture and yet not achieve the same sampling gain. Consider the 8-element unrestricted array of Leech [14], compared to the 8-element nonredundant array provided in the previous chapter. The unrestricted array spans an aperture from 0 to 39 while the nonredundant array spans only 0 to 34. Yet the sampling gains for the two arrays are 25.0 and 30.4, respectively, (or 14.0 and 14.8 dB). Thus, despite the lower span of the nonredundant array, it offers a sampling gain of about 1 dB in excess of that produced by Leech's unrestricted array.

We observe from (3.8) or (3.9) that the CRLB does not indicate any tradeoff in performance for different array structures. Indeed, the CRLB tells only a portion of the whole story. For instance, doubling the separations between all the elements in a uniform array would clearly increase S. However, this also introduces grating lobes. These lobes correspond to ambiguities in the estimation procedure. Such an effect is not accounted for in the CRLB. Another issue of concern involves knowledge of the phase at the centroid of an array. This can, in fact, provide additional information which would improve the estimation. Consider, for example, a 2-element array (interferometer) operating at high SNR. If the measured data is $(-1\ ,\ 1\ )^T$, being consistent with a wavenumber of $-\pi$ or $+\pi$, that is end-fire, knowledge of the phase at the centroid would clearly indicate which direction is correct. Without this knowledge, either direction is possible; hence, no real decision may be made.

There is another difficulty, namely, the fact that the CRLB requires the estimator to be unbiased. In general, for a nonlinear estimation problem, there may not exist an unbiased estimator. Unfortunately, the CRLB for biased estimators requires knowledge of the bias function; this makes it unsuitable as an estimator-independent bound.

Finally, the addition of a priori information, particularly with uniform PDF's, is essentially invalid, as certain regularity conditions would be violated. The required conditions on the result to be a valid bound are presented in [44]. An important manifestation of this effect is the low SNR region. Since the wavenumber was limited to a finite interval, this 'permits' the use of a sampled aperture. Therefore, any estimator would only search over the interval in which the wavenumber is assumed to lie, for example $(-\pi, \pi)$. For very low SNR, where the estimator may be making random selections, we realize that there is an upper limit to the MSE. The CRLB would, however, approach infinity as $\Gamma \rightarrow 0$. This is a direct consequence of the inability to introduce the search limits (a priori knowledge) into the CRLB.

These limitations in the CRLB require us to search for an alternative bounding technique. We wish to find a bound on the MSE of the parameter that is independent of the estimator, (holding for biased or unbiased estimators). In addition, we would like the bound to be able to make use of any a priori information that is available. It is precisely these considerations that lead us to apply, in the next section, a recently developed bounding technique to the wavenumber estimation problem.

3.3 The Weiss-Weinstein Bound

Recently, a new technique for lower bounding the mean square error of a random parameter estimator has been developed [27]. It does not have the regularity assumption requirements of the Cramér-Rao Lower Bound, nor is the estimator required to be unbiased. In general, however, the bound may become computationally intensive. We will show that for our wavenumber estimation problem, the bound can be implemented with a three-dimensional search, providing a significantly tighter result than the CRLB.

In addition, the Weiss-Weinstein Lower Bound (WWLB) allows us to make use of any a priori information available. We show that the bound lies within 0.5 dB of the achievable MSE at low SNR, and is identical with the CRLB at high SNR.

As the bound is so recent, we repeat the derivation provided in the original paper [27] in Appendix A to verify some of the intermediate steps not included in the correspondence. This will also permit our implementation of the bound to be consistent with the notation used in this thesis. Appendix A also contains the application of the bound to the wavenumber estimation problem since this is initially algebraically tedious.

The wavenumber k and the phase θ are considered random parameters. We assume no knowledge about the phase.

However, we assume that the wavenumber is restricted to lie in an interval (k_n, k_x), a subregion of $(-\pi, \pi)$, with equal likelihood. Then as shown in Appendix A, equation (A.31), the WWLB on wavenumber MSE is given by

$$E\{ (\hat{k}-k)^2 \} \geq h_1^2/Q \qquad (3.10)$$

where $$Q = \frac{H(h_1)\ [\exp\{ 4\Gamma q^2 c(h) \} + \exp\{ 4\Gamma(1-q)^2 c(h) \}]}{H^2(h_1)}$$

$$- \frac{2H(2h_1)\exp\{ 2\Gamma q(1-q)(2c(h)-c(2h)) \}}{H^2(h_1)}. \qquad (3.11)$$

$$c(h) = c(h_1, h_2),$$
$$= N - \sum_{i=1}^{N} \cos(h_1 x_i + h_2), \qquad (3.12)$$

and $$H(\alpha) = \begin{cases} 1 - |\alpha|/(k_x - k_n), & |\alpha| < (k_x - k_n) \\ 0, & \text{elsewhere} \end{cases} \qquad (3.13)$$

The required search regions for the parameters are

$$-\pi \leq k_n \leq k_x \leq \pi \qquad (3.14a)$$

$$0 < h_1 < (k_x - k_n) \qquad (3.14b)$$

$$-\pi \leq h_2 \leq \pi \qquad (3.14c)$$

$$0 < q \leq \tfrac{1}{2} \qquad (3.14d)$$

Equation (3.10) is a bound for any values of h_1, h_2.

and q. The tightest bound of this class is then found by maximizing the right side of (3.10) with respect to the three free parameters, always requiring the three conditions of (3.14) to be satisfied. From (3.10) through (3.14) we notice that the bound is independent of the actual values of k_n or k_x . it is just dependent on the size of the interval they span. Finally, as shown in Appendix A, in the region $(k_x - k_n)/2 < h_1 < (k_x - k_n)$, the maximization with respect to q will always occur at q = ½.

It is also shown in Appendix A.3 that the bounding technique is independent of the absolute array position. Section A.4.1 demonstrates the low SNR results are within 0.5 dB of the attainable performance. We also show that the previously developed CRLB of section 3.2, as applied to our estimation problem, is an asymptotically special case of the WWLB for high SNR.

3.4 A Typical Result and Implications

We display the results of the WWLB in Figure 3.1 and provide the CRLB results for comparison. The configurations used to compute the results are the 8-element uniform and nonredundant arrays described in Table 2.1 and 2.2 of the previous chapter. In both cases, it is assumed that the target lies inside the interval [$-\pi/2$, $\pi/2$] with equal

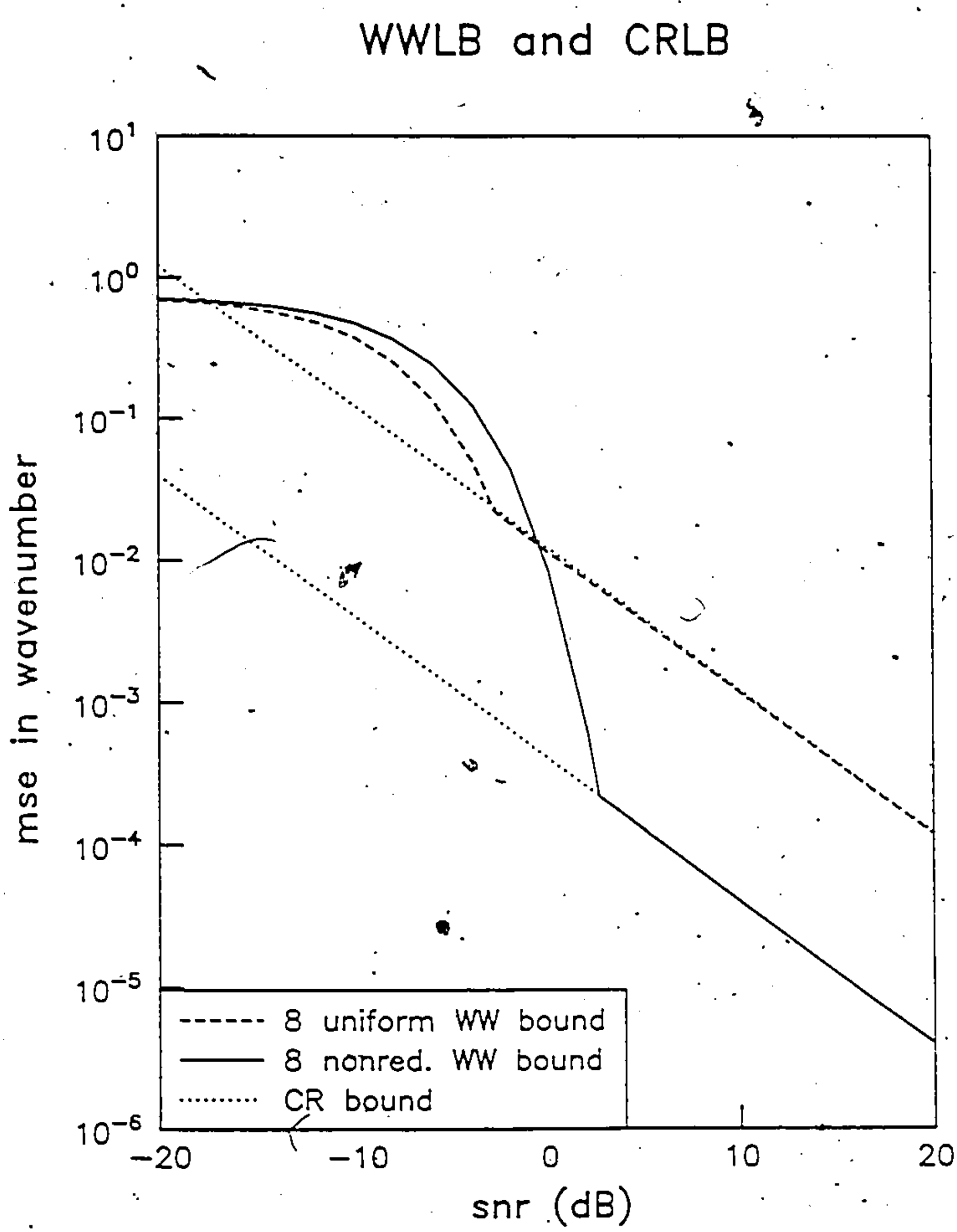

Figure 3.1: Comparison of WWLB and CRLB for 8-element uniform and nonredundant arrays.

probability. We notice that at high SNR, the bound is coincident with the CRLB. At low SNR, the bound accurately reflects the performance of the minimum mean square error estimator (within 0.5 dB), which is identical for both arrays. That is, the estimator that always chooses the midpoint of the interval will in fact have a MSE equal to 0.822 rad^2, while our bound provides 0.73 rad^2.

Perhaps the most significant result of the new bound is the 'threshold' effect. As the SNR decreases the MSE increases inversely with SNR until a critical point is reached after which it rises dramatically, eventually levelling off as the SNR gets very low. This critical point is termed the 'threshold SNR', and is commonly defined as the point for which the MSE has risen 1 dB above the CRLB. The existence of this effect is well known in nonlinear maximum likelihood estimation [25, 38]. To the author's knowledge, the threshold effects for nonuniform arrays have never been evaluated in the literature, nor have any tradeoffs been established. In fact, Figure 3.1 indicates that at high SNR the improved performance of the nonredundant array is penalized by a larger threshold SNR. That is, we require a larger SNR for the system to reach the performance of the CRLB. The crossover point, for which the curves indicate identical performance, lies between the two thresholds.

For low SNR conditions, it is often possible to improve the results by observing the array for longer periods of time. In this way, by observing more than one 'snapshot', the data may be averaged in an appropriate manner to effectively increase the SNR. If the requirement is that to operate on the linear portion of the curve (log scale), then the threshold penalty translates to a larger number of required snapshots. However, once this is achieved, the performance increase may be significant. We will now consider an example using the results from Figure 3.1 to indicate the tradeoff.

The 8-element uniform and nonredundant arrays have respective thresholds of -3.4 and 2.4 dB (from Fig. 3.1). Using L snapshots, and for additive white gaussian receiver noise, independent from one sensor to another, we may consider the SNR to improve by a factor of L. If the receiver were operating below the thresholds of both arrays, then it would require about 4 times the number of snapshots to reach the linear portion with the nonredundant array as compared to the uniform array. However, at this point, the performance would have improved by a factor of 30 in MSE, (the sampling gain S_G of the nonredundant array is 30 or 14.8 dB). Conversely, if the specification were to obtain a certain MSE, which was beyond the thresholds of both arrays, the uniform array would require 30 times as many snapshots to achieve the performance of the nonredundant array.

The preceding discussion reduces to a simple tradeoff based upon the expected or required operating conditions. For the 8-element arrays considered, there is a region of SNR for which the uniform array will outperform the nonredundant array. However, at high SNR (above threshold), or if sufficient averaging (observation) is acceptable, the nonredundant array outperforms the uniform array.

3.5 The Effect of A Priori Information

We now consider the effects of different amounts of a priori knowledge. Using the same arrays as described in the previous section we compare results for which the region of wavenumber, $k \in (-a\pi, a\pi)$, and parameter a varies from 1.00 down to 0.03. These results are presented in Figure 3.2 for the 8-element uniform array and Figure 3.3 for the 8-element nonredundant array.

Except for the case of a = 1, we see that for both arrays the WWLB bound on MSE eventually coincides with the CRLB for a sufficiently high SNR. Therefore, the a priori knowledge effectively varies the threshold point, but not the high SNR performance. If we make the analogy with time-domain sampling, then for the case of a = 1, we are sampling at a rate exactly equal to the Nyquist rate [1].

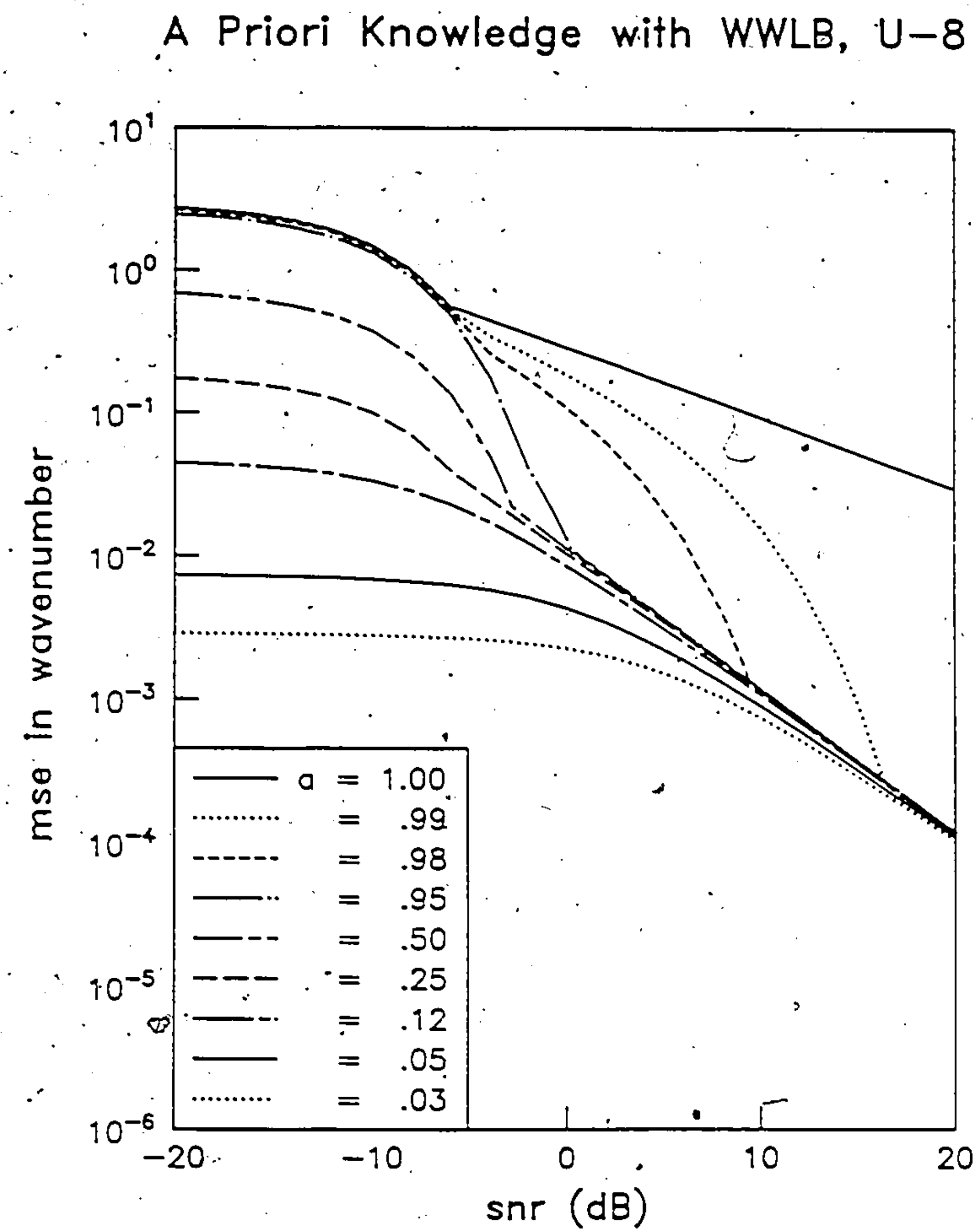

Figure 3.2: Effect of a priori information on the 8-element uniform array based on the WWLB.

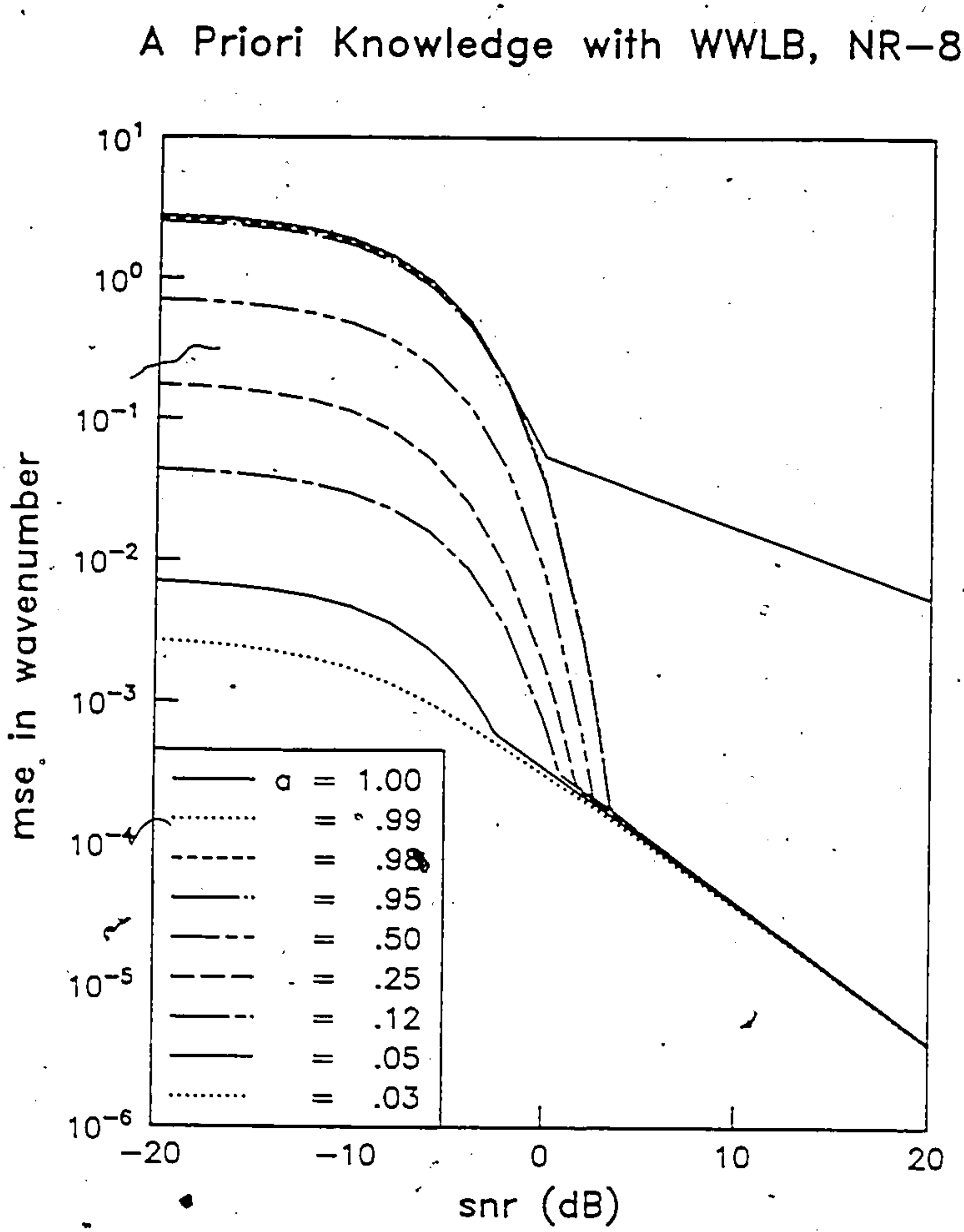

Figure 3.3: Effect of a priori information on the 8-element nonredundant array based on the WWLB.

The sampling theorem normally applies for an infinite number of samples. But, in our case, we are specifically interested in finite numbers of samples. Since the signal is assumed to lie anywhere in the band $(-\pi, \pi)$, there is a distinct problem at the ends. For a restriction on a, such that $a < 1$, there will occur an SNR for which performance will again reach the CRLB.

The reason for the sudden departure as $a \rightarrow 1$, can be understood as an aliasing problem. For infinite SNR, only the values for $k = \pm \pi$ are ambiguous. At sufficiently high but finite SNR, we can consider the CRLB to be representative of the error. The MSE increases proportionally with decrease in SNR. For targets having wavenumbers close to the ends of the interval, at a sufficiently low SNR, the error in estimation may indicate a value just slightly greater than π. This can only be interpreted in our sampled system as a value slightly greater than $-\pi$; the effect is similar to that known as aliasing. This would then translate to an extremely large error, manifesting itself as a tremendous increase in MSE for targets near end-fire (k near $\pm\pi$), whereas targets not near end-fire would have comparatively minute errors.

These results indicate the need to either oversample the field or find some other way of increasing the a priori knowledge. As pointed out in section 3.1, oversampling can be modelled as an increase in a priori knowledge. It is interesting to note that the nonredundant array will require less oversampling than the corresponding uniform array. For example, the 8-element uniform array will operate poorly in terms of MSE for elemental SNR less than 10 dB when the system is pushed to operate out to $\pm 0.98\pi$ (corresponding to oversampling at 1.0204 times the Nyquist rate). The nonredundant array will perform admirably in this condition. While this difference might be considered trivial, as a discriminator between arrays, it is nevertheless an important consideration in an operating environment or when an array is being characterized by simulation experiments.

The WWLB then provides useful insight, quantifying the amount of a priori knowledge required. It also points out that when a system is making consecutive estimates of a target's location, the resultant estimates should probably not be averaged to obtain an improved estimate, but rather a median estimate would be better. If not for all SNR and all values, at least for those conditions for which the WWLB indicates significant performance degradation may result, such as those values near end-fire.

We now turn our attention to the opposite end of the scale for which we have significant amounts of a priori information. The normalized wavenumber beamwidth of the array is defined as $2\pi/A$, where A is the aperture of the array. We notice from Figure 3.2 for the 8-element uniform array that the 'threshold effect' vanishes for those cases for which the target is constrained to lie in an interval less than $(-\pi/8, \pi/8)$ which is approximately the beamwidth definition. That is, if the target location is known a priori to within a ½ beamwidth, there will be no evidence of a threshold SNR. The identical outcome may be observed for the 8-element nonredundant array as shown in Figure 3.3 for which the aperture is 34 units. The threshold vanishes for intervals less than about $(-\pi/33, \pi/33)$.

For constraints greater than a beamwidth and yet not excessively close to the maximum visible range, the threshold varies in a regular manner with the amount of a priori knowledge. For comparison purposes, we do not wish to choose either of the extreme cases; hence, the next section uses the case $a = 0.5$ for evaluation of the different array structures.

3.6 Comparing Some Array Structures

Several different array structures are evaluated for threshold and sampling gain. Ranging from 5 to 10 elements, we choose one representative from each category of uniform (U), minimum redundant (MR) and nonredundant (NR) as described in Chapter 2. Certain unrestricted (UR) arrays are also presented for those element numbers for which neither the minimum redundant nor nonredundant array has the property of the unrestricted array. Table 3.1 describes the particular arrays chosen.

For each of the arrays of Table 3.1, we determine the high SNR performance as predicted by the CRLB. The results, presented in Table 3.2a, are quoted for a 30 dB SNR. The Sampling Gain, S_G , as defined in section 3.2, being relative to the uniform array having the same number of elements is also recorded. The threshold SNR for each array is listed in the final column of Table 3.2a, determined from the WWLB for which the wavenumber was assumed to lie in the interval $(-\pi/2, \pi/2)$. This point was obtained by first generating the bound versus SNR on a curve sampled every 2 dB. Upon approximately locating the threshold, the procedure was repeated with a 0.1 dB step. The threshold point was chosen as the value for which the WWLB exceeded the CRLB by 1 dB. From this set of results, the value providing the closest approximation to the 1 dB threshold was chosen. This will then locate the predicted threshold to a 0.1 dB accuracy in SNR, (or about 2.3%). We have also included the 16- and 32-element uniform arrays for comparison.

It is immediately clear that the uniform arrays have a lower threshold SNR than the other arrays considered. The

Table 3.1

Arrays to be Evaluated

No. of Sensors	Location										Array Property
5	0	1	2	3	4						U
	0	1	4	7	9						MR
	0	2	7	8	11						NR & UR
6	0	1	2	3	4	5					U
	0	1	2	6	10	13					MR
	0	1	4	10	12	17					NR & UR
7	0	1	2	3	4	5	6				U
	0	1	2	6	10	14	17				MR
	0	6	9	10	17	22	24				UR
	0	1	4	10	18	23	25				NR
8	0	1	2	3	4	5	6	7			U
	0	1	2	11	15	18	21	23			MR
	0	8	18	19	22	24	31	39			UR
	0	1	4	9	15	22	32	34			NR
9	0	1	2	3	4	5	6	7	8		U
	0	1	2	14	18	21	24	27	29		MR & UR
	0	1	5	12	25	27	35	41	44		NR
10	0	1	2	3	4	5	6	7	8	9	U
	0	1	3	6	13	20	27	31	35	36	MR
	0	7	22	27	28	31	39	41	57	64	UR
	0	1	6	10	23	26	34	41	53	55	NR

Property Terms from Chapter 2

U Uniform
MR Minimum Redundant
UR Unrestricted
NR Nonredundant

Table 3.2a

Sampling Gain and Threshold Comparison
Using Elemental SNR, Γ

No. of Sensors	Array[1] Type	Aperture Length	Mse (dB)[2] @ Γ=30dB	Sampling Gain (dB)	Threshold[3] SNR (dB)
5	U	4	-43.0	0.0	-4.0
	MR	9	-50.7	7.7	3.3
	NR & UR	11	-52.1	9.1	3.35
6	U	5	-45.4	0.0	-3.5
	MR	13	-54.4	9.0	2.5
	NR & UR	17	-56.6	11.2	3.2
7	U	6	-47.5	0.0	-3.4
	MR	17	-57.3	9.8	2.7
	UR	24	-59.6	12.1	2.5
	NR	25	-61.2	13.7	2.9
8	U	7	-49.2	0.0	-3.4
	MR	23	-60.9	11.7	1.5
	UR	39	-63.2	14.0	2.8
	NR	34	-64.1	14.9	2.4
9	U	8	-50.8	0.0	-3.7
	MR & UR	29	-63.2	12.4	1.3
	NR	44	-66.7	15.9	2.3
10	U	9	-52.2	0.0	-3.9
	MR	36	-65.7	13.5	1.2
	UR	64	-68.5	16.3	1.9
	NR	55	-68.8	16.6	1.6
16	U	15	-58.3	0.0	-5.3
32	U	31	-67.4	0.0	-6.8

[1] Arrays correspond to those listed in Table 3.1

[2] MSE as determined by CRLB @ 30 dB elemental SNR

[3] Threshold elemental SNR determined by WWLB for $k \in (-\pi/2, \pi/2)$

8-, 9- and 10-element arrays have approximately a 5.0 dB lower threshold than the minimum redundant arrays. The improved performance at high SNR of the minimum redundant arrays grows from 11.7 to 13.5 dB over the uniform arrays.

The minimum redundant arrays always had a smaller threshold value, but provided less Sampling Gain than the nonredundant arrays. For element numbers 7 to 10 the minimum redundant placements provided from 0.4 to 1.2 dB lower thresholds. However, for this price, the nonredundant arrays provided from 3.1 to 3.5 dB of increased performance at high SNR.

Therefore, for these arrays we have a tradeoff situation. These results provide the radar system designer with the ability to tradeoff some threshold SNR for improved performance at the higher SNR values. The choice of the appropriate array would now depend upon the particular application being considered.

There was an interesting anomalous behaviour with the unrestricted arrays of length 8 and 10. In both cases, compared to the nonredundant arrays, the unrestricted arrays required an aperture approximately 15% larger, had a poorer threshold by 0.3 and 0.4 dB, and yet provided about 23% and 7% less improvement at high SNR. It seems that in these cases, there does not even exist a tradeoff condition. One can simply state that, the 8- and 10-element unrestricted arrays, considered here, are a poor choice of element placement. In all measured respects, the comparative nonredundant arrays outperformed these unrestricted ones.

We therefore conclude that careful placement of the elements is critical for performance. That is, increased Sampling Gain is not always at the expense of increased threshold SNR.

To compare arrays having different numbers of elements is somewhat more difficult. For the elemental SNR, Γ, the total SNR of the gathered data is $N\Gamma$, hereafter referred to as the array SNR. When arrays comprised of different numbers of elements are compared, the array SNR varies as well as the array structure. Consider, for example, any 5- and 10-element arrays for $\Gamma = 30$ dB. The 5- and 10- element arrays have respective array SNRs of 37 and 40 dB, or in other words, there exists a difference of a factor of 2 in the total received signal SNR. Suppose a 10-element array was created by placing 5 additional elements 'on top of' 5 uniform elements. The array structure would be unchanged and yet the threshold performance would improve when measured by the fixed elemental SNR. The question of the impact of the array structure itself on the performance is then not clearly answered. To separate the effect of increased SNR from the effect of the structure itself, it is useful to compare the results based upon a fixed array SNR.

This exercise is instructive in understanding the effect of the array structure alone.

This also addresses the effect of proportioning the total SNR in different ways including the use of a larger number of elements of perhaps inferior quality. In practice, we can compare systems in which the conversion loss of the first set of mixers may be 3 dB worse (which may be much less expensive), but twice as many elements are used. Similar specifications on low-noise front-end amplifiers could be expressed in this way. The cost analysis may be significantly more complex than this when considering different numbers of elements in a 'real' system, therefore an appreciation of the actual effects of the structure must be obtained.

To facilitate this measurement, we provide Table 3.2b, in which the comparison is made using the array SNR, $N\Gamma$, in place of the elemental SNR. The MSE is compared for a given array SNR and the threshold SNR is also measured in this quantity. If we now consider the MSE for the uniform arrays, we find that it decreases with increasing number of elements. That is, the total SNR has been spread over a larger region and the MSE has been improved. For N large, we see from equation (3.8) that the uniform arrays will improve by 6 dB for every doubling of N for a constant array SNR. For a constant elemental SNR, the improvement is 9 dB

Table 3.2b

Sampling Gain and Threshold Comparison
Using Array SNR, $N\Gamma$

No. of Sensors	Array[1] Type	Aperture Length	Mse (dB)[2] @$N\Gamma$= 40dB	Sampling Gain (dB)	Threshold[3] SNR (dB)
5	U	4	-46.0	0.0	3.0
	MR	9	-53.7	7.7	10.3
	NR & UR	11	-55.1	9.1	10.35
6	U	5	-47.6	0.0	4.3
	MR	13	-56.6	9.0	10.3
	NR & UR	17	-58.8	11.2	11.0
7	U	6	-49.0	0.0	5.1
	MR	17	-58.8	9.8	11.2
	UR	24	-61.1	12.1	11.0
	NR	25	-62.7	13.7	11.4
8	U	7	-50.2	0.0	5.6
	MR	23	-61.9	11.7	10.5
	UR	39	-64.2	14.0	11.8
	NR	34	-65.1	14.9	11.4
9	U	8	-51.3	0.0	5.8
	MR & UR	29	-63.7	12.4	10.8
	NR	44	-67.2	15.9	11.8
10	U	9	-52.2	0.0	6.1
	MR	36	-65.7	13.5	11.2
	UR	64	-68.5	16.3	11.9
	NR	55	-68.8	16.6	11.6
16	U	15	-56.3	0.0	6.7
32	U	31	-62.3	0.0	8.3

[1] Arrays correspond to those listed in Table 3.1

[2] MSE as determined by CRLB @ 20 dB array SNR, $N\Gamma$

[3] Threshold array SNR determined by WWLB for $k \in (-\pi/2, \pi/2)$

for every doubling of N. The majority of the improvement quoted in Table 3.2a, is therefore from the array structure change and not from the increased SNR. Interestingly, the improvement for the nonuniform arrays is even greater than that determined for the uniform arrays. The minimum redundant and nonredundant arrays grow approximately as N^2 in aperture while the uniform arrays grow as N. This accounts for the increase in performance.

The threshold effect does not indicate the same trend as the MSE.. For a given array SNR, the threshold SNR increases with N for the uniform arrays. Therefore, for the uniform structures, the spreading out of the SNR deteriorates the threshold phenomenon. However, for a fixed elemental SNR, the threshold still improves with N. That is, the increased total SNR, overcomes the effect of the larger array geometry, see Table 3.2a. The nonuniform arrays behave similarly in this respect. The minimum redundant and nonredundant structures generally have larger threshold SNR values as N increases. However, for a fixed elemental SNR, the threshold value decreases ~~with~~ increasing N.

CHAPTER 4

SINGLE TARGET MAXIMUM LIKELIHOOD ESTIMATION

Contrasting the bounding approach of the previous chapter, in this chapter we examine the performance of various linear arrays using the maximum likelihood estimator (MLE). We follow a similar approach to that given in [38], where the concepts were developed for uniform arrays. Many of the original ideas are generalized to be made meaningful for arbitrary linear array structures. The implementation of the estimator is examined from a statistical viewpoint. The probability density function of the wavenumber error is examined through computer simulation experiments. Empirical characterization of the error process lends useful insight to the performance of the various arrays. The results of this chapter should provide an accurate and practical guide to performance tradeoffs.

4.1 Maximum Likelihood Estimator Derivation

The estimation problem has been described in section

3.1. where the majority of the terms have been defined. Briefly, the problem is the determination of the wavenumber, k, from noisy data. We assume the amplitude, phase and wavenumber are unknown parameters. The wavenumber is assumed to lie in an interval (k_n, k_x), where

$$-\pi \le k_n < k < k_x \le \pi \tag{4.1}$$

We let α_t be the vector of target parameters, $(k_t, a_t, \theta_t)^T$, and $\hat{\alpha}$ be the maximum likelihood estimate of α_t. We find it convenient to define the vector

$$y(k) = (\exp(jkx_1), \exp(jkx_2), \ldots , \exp(jkx_N))^T \tag{4.2}$$

The vector of received data from the N sensors is

$$\begin{aligned} z &= s(\alpha_t) + \mathbf{w} \\ &= a_t \exp(j\theta_t) y(k_t) + \mathbf{w} \end{aligned} \tag{4.3}$$

where $\mathbf{w}$ is the N-dimensional complex vector of white Gaussian, zero-mean noise, with the real and imaginary components statistically independent. The probability density function (PDF) of the data, given a set of parameters, is

$$p(z/\alpha) = (2\pi\sigma^2)^{-N}\exp\left\{ - \frac{\| z - s(\alpha) \|^2}{2\sigma^2} \right\} \tag{4.4}$$

The ML estimate is the value of α that maximizes the right side of (4.4). In our situation, it is a constrained maximization for $k_n < k < k_x$. Equivalently, we may minimize $\| z - s(\alpha) \|^2$. If we let $c = a \cdot \exp(j\theta)$ be the complex amplitude, then the objective is to minimize

$$\Lambda = \| z - cy(k) \|^2 \tag{4.5}$$

This can be minimized with respect to c (see [46]) by noting that at the minimum, say $\hat{c}$, the projection of the error vector, $z - \hat{c}y$, is normal to the surface cy, as shown by

$$(cy)^H(z-\hat{c}y) = 0 \qquad c \in \mathbb{C} \tag{4.6}$$

Since c is a free parameter, which specifies the surface, we have

$$(y^H z-\hat{c}y^H y) = 0 \tag{4.7}$$

This provides the solution for $\hat{c}$ as

$$\hat{c} = y^H z / N$$
$$= \frac{1}{N} \sum_{i=1}^{N} z_i \exp(-jkx_i) \qquad (4.8)$$

where we make use of the fact that $y^H y = N$. This solution for $\hat{c}$ is then substituted into (4.5), which requires the minimization of the quantity:

$$\Lambda = \| z - yy^H z/N \|^2$$
$$= z^H z - z^H yy^H z/N$$
$$= \|z\|^2 - \|y^H z\|^2/N \qquad (4.9)$$

Equation (4.9) indicates that the minimum of the objective function is realized when $\|y^H z\|^2$ is maximized. The ML estimator reduces to maximizing

$$\Lambda' = \|y^H z\|^2$$
$$= \left| \sum_{i=1}^{N} z_i \exp(-jkx_i) \right|^2 \qquad (4.10)$$

with respect to the wavenumber, k. The other parameters may then be obtained directly from equation (4.8).

When the x_i are uniformly spaced, expression (4.10) can be recognized as the discrete Fourier transform of the received data z; it may therefore be evaluated using the fast Fourier Transform algorithm. If the x_i are not uniformly spaced, but lie on an integer grid, the summation may still be evaluated using the Fast Fourier Transform. Specifically, the received data vector is padded with zeroes wherever a sensor location is 'empty'.

4.2 Implementation of MLE

The maximization of equation (4.10) is a nonlinear problem. We initially search the wavenumber space on a coarse grid, determining the approximate location of the maximum. Upon locating this point, a fine grid search is performed over the coarse intervals on either side. The fine search is repeated in multiple levels until the desired accuracy in estimation is obtained.

The objective of the coarse search is to locate the global maximum. In this way the fine searches are implemented assuming the surface to be convex over the previous search interval. This then necessitates some knowledge of the density required for the coarse search. In an earlier paper [3S], the coarse conclusion was that for uniform arrays of length N, a density of N points in 2π was adequate.

This determination is made from a statistical viewpoint. Given a performance measure to be determined, simulations are conducted, increasing the density of the coarse search at each stage. At the point for which the measure does not change significantly, we say that for practical purposes, the density is adequate. Rife and Boorstyn, [38], view the mean square error as their performance measure. The simulations were performed with the wavenumber at the center of the interval and estimates made at uniform spacings, one of which coincides with the true result.

We will show that nonuniform arrays will, in general, require significantly larger densities than $2\pi/N$. It is of interest to examine the 'beam pattern' of the array structure. The beam pattern, or array power gain pattern, in our notation is defined by

$$G(k) = \left| \frac{1}{N} \sum_{i=1}^{N} \exp(jkx_i) \right|^2 . \qquad (4.11)$$

with k varying over the interval $(-\pi, \pi)$. This result is proportional to that obtained for the objective function of the MLE operating in infinite SNR when the target is at boresight, $k_T = 0$, as given in (4.10). The beam patterns for 7-element uniform and nonredundant arrays, described in

Table 3.1, are presented in Figure 4.1. The pattern for the uniform array is very regular, with side lobes tapering as the distance from boresight increases. The nonredundant array has a somewhat more erratic behaviour, with the peak side lobe being relatively larger than its uniform counterpart. The other principal observation obtained from Figure 4.1 is the reduction in the width of the main lobe for the nonredundant array. The standard beamwidth, in physical space, (measured in radians), for an aperture of size A is defined as λ/A. Translated to the normalized wavenumber space, it becomes $2\pi/A$. This definition is approximately 14% wider than the 3 dB beamwidth definition for uniform arrays.

From equation (4.10) and Figure 4.1, we see that the objective function will have multiple maxima. The coarse search must be dense enough such that the maximum located should correspond to a point on the main lobe. Under 'noisy' conditions, it is difficult to determine the required density which would guarantee this; however, we may use a pragmatic approach. The density will be assumed adequate if the 'average' performance (ie., mean square estimation error, or threshold SNR), is not degraded. We note the result of [38] for uniform arrays, a density of N coarse points for the N element array, is effectively one sample per beamwidth. As an initial starting point, we

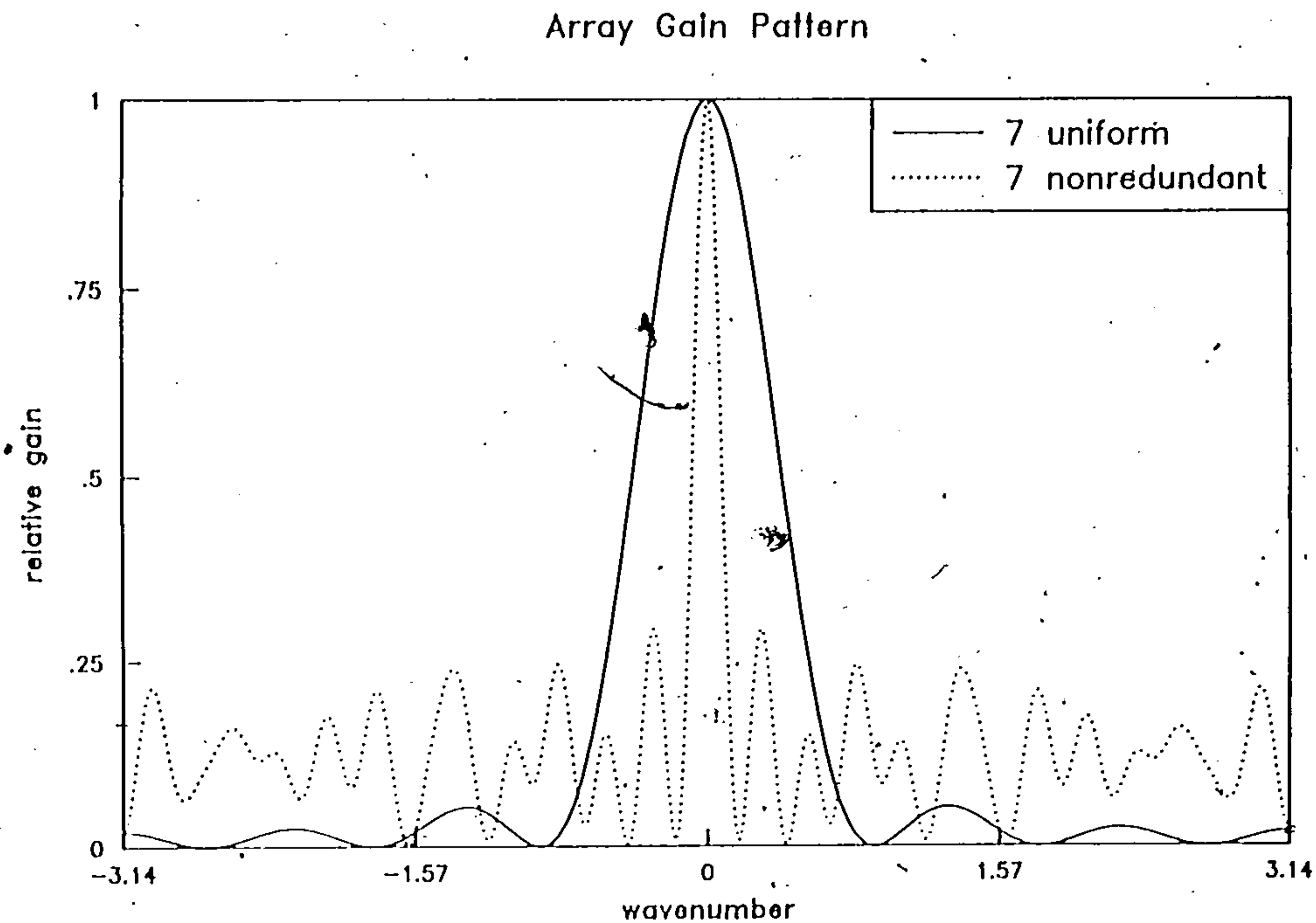

Figure 4.1: Comparison of the standard gain patterns associated with 7-element uniform and nonredundant arrays.

could consider a similar density by using A+1 sample points for the coarse search. We might expect that since the nonredundant arrays have larger side lobe levels, they may require higher densities.

The mean square error (MSE) for the two 7-element arrays is presented in Figure 4.2 for different coarse search densities. The target wavenumber was varied over an interval of $(-\pi/2, \pi/2)$, and the search was carried out over $(-\pi, \pi)$, using 2^{16} (65536) simulations. This variation in wavenumber was used to prevent the true wavenumber always coinciding with one of the coarse sampling points. After locating the coarse maximum position, a fine-grid search was performed extending one interval to either side of the candidate position. The simulations were carried out in the threshold regions.

The results with the 7-element uniform array show a density of 14 points to provide sufficient accuracy in determining the variation of MSE as a function of SNR. For large SNR, 7 points distributed over 2π were found to be sufficient. In the threshold region, the 7-point coarse search provides an error of up to 1 dB in SNR. This would appear to be a contradiction of the results obtained in [38]. Rife and Boorstyn in [38] clearly state, however, that they believe their result to be accurate only if the tone is located at the midpoint of the interval. In their

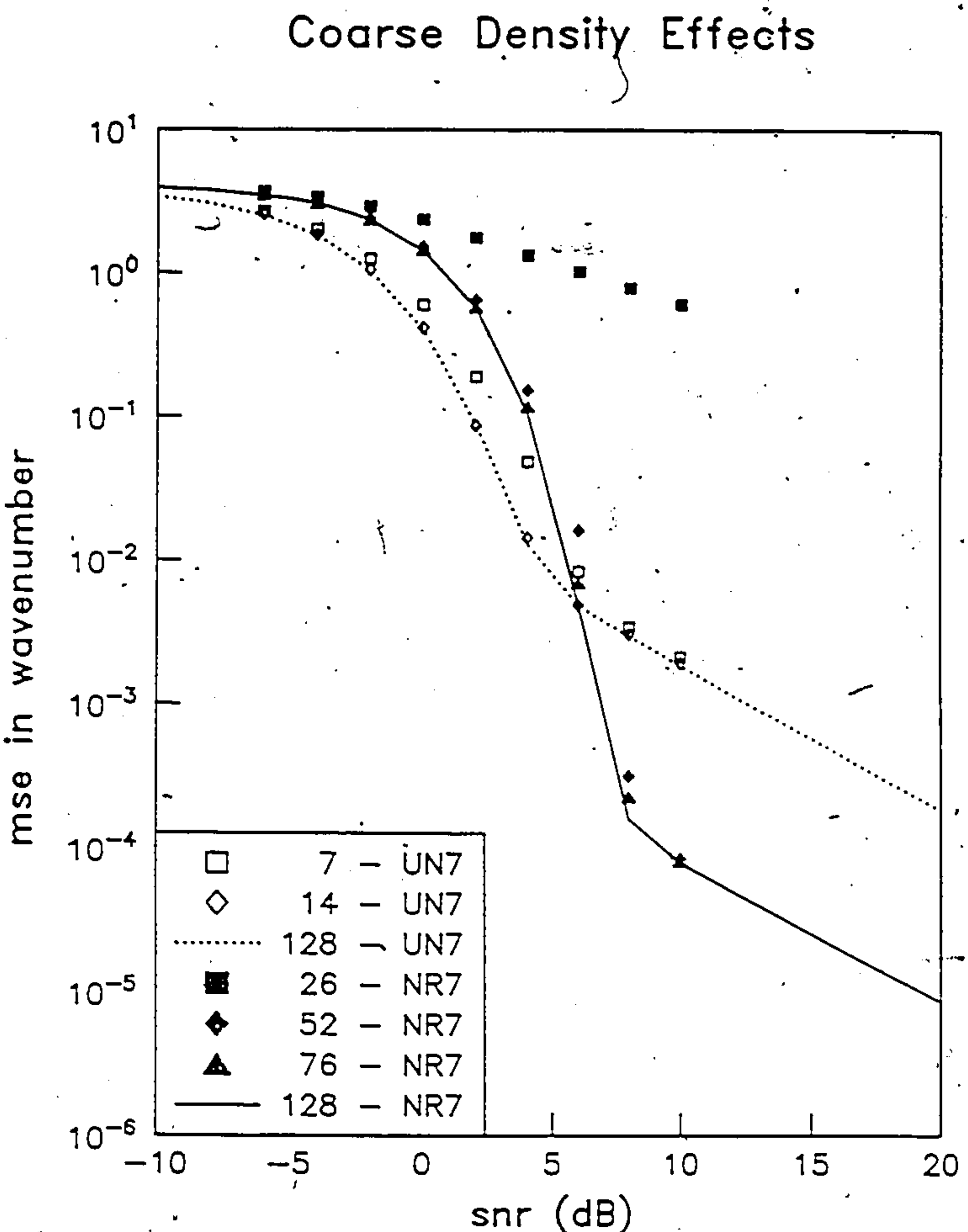

Figure 4.2: Effects of the coarse search density on the performance estimation of 7-element uniform and nonredundant arrays.

simulation, one of the coarse search points always fell at the true value and the others were located at the nulls of the 'beam pattern'. This is obviously a fortuitous circumstance that cannot be expected to occur often. Furthermore, this demonstrates the necessity of using more points in the coarse search for an accurate characterization of performance. The fact that the other sampling points occurred at the nulls of the beam pattern, also permits a simple analytical derivation of performance. This point will be reexamined in a later section of this chapter.

Turning to the nonredundant array, the results indicate that for a coarse search having two points per beamwidth, the threshold region characteristics are in error by approximately ½ dB in SNR. For a density of 3 points per beamwidth, the performance is in agreement with the higher densities within statistical accuracies. This increased density requirement was expected as the peak side lobe levels of the estimator power gain pattern are larger than in the uniform array. It is possible to examine the threshold effect for maximum likelihood estimation in greater detail. This is the focus of the next section.

4.3 Threshold Effect in MLE

The examination of the maximum likelihood estimator in the threshold region provides meaningful insight to the error process. The probability density function of the wavenumber estimation error is gauged from simulation results by generating a histogram of the errors. For each value of SNR, 2^{20} (1048576) estimates of the wavenumber were generated. During each investigation, two histograms were accumulated. The first involved 256 bins covering the region of $(-\pi, \pi)$. The second consisted of 64 bins spread over the 'main beam', covering $(-B/2, B/2)$ where B is the beamwidth defined earlier as $2\pi/A$.

The results shown in Figures 4.3 and 4.4 are for the same two 7-element arrays described earlier, with the target wavenumber restricted to the interval $(-\pi/S, \pi/S)$, and the estimator searching the interval $(-\pi, \pi)$. The experiments were performed at the same SNR values, -2, 1 and 4 dB. For clarity, the +1 dB SNR was not displayed for the nonredundant array in Figure 4.4. Since the significance of the curves cover such a large dynamic range, the natural log (ln) of the histogram bins are displayed. Although each experiment was carried out with the same number of simulations, the histogram was still normalized by dividing by the total number of trials. Similarly, each bin was identical in size for all experiments. The Logarithm of the antenna gain pattern is also presented as the solid curve in each figure.

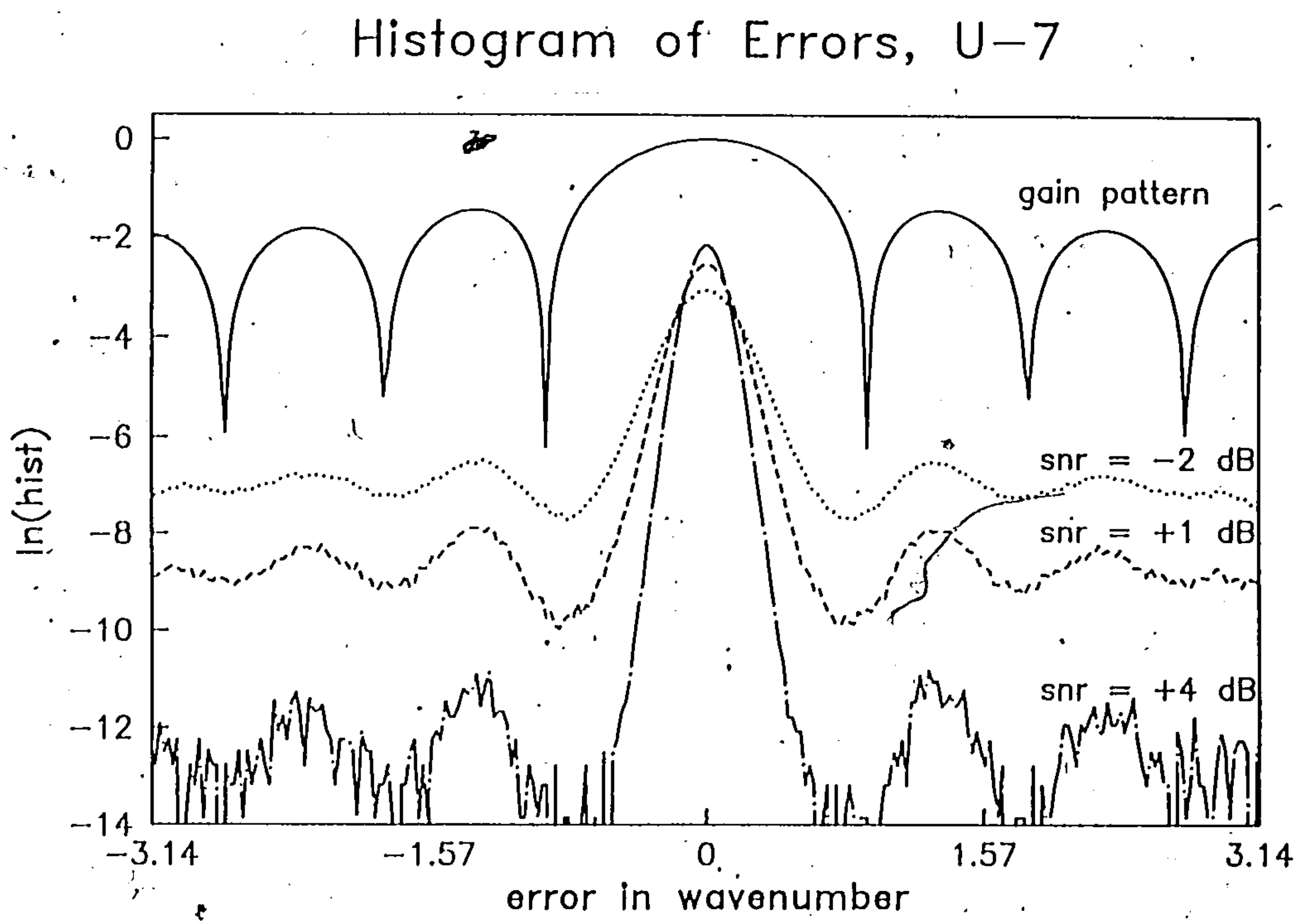

Figure 4.3: Histogram of estimation errors for 3 different values of SNR using a 7-element uniform array. Superimposed is the standard beam pattern.

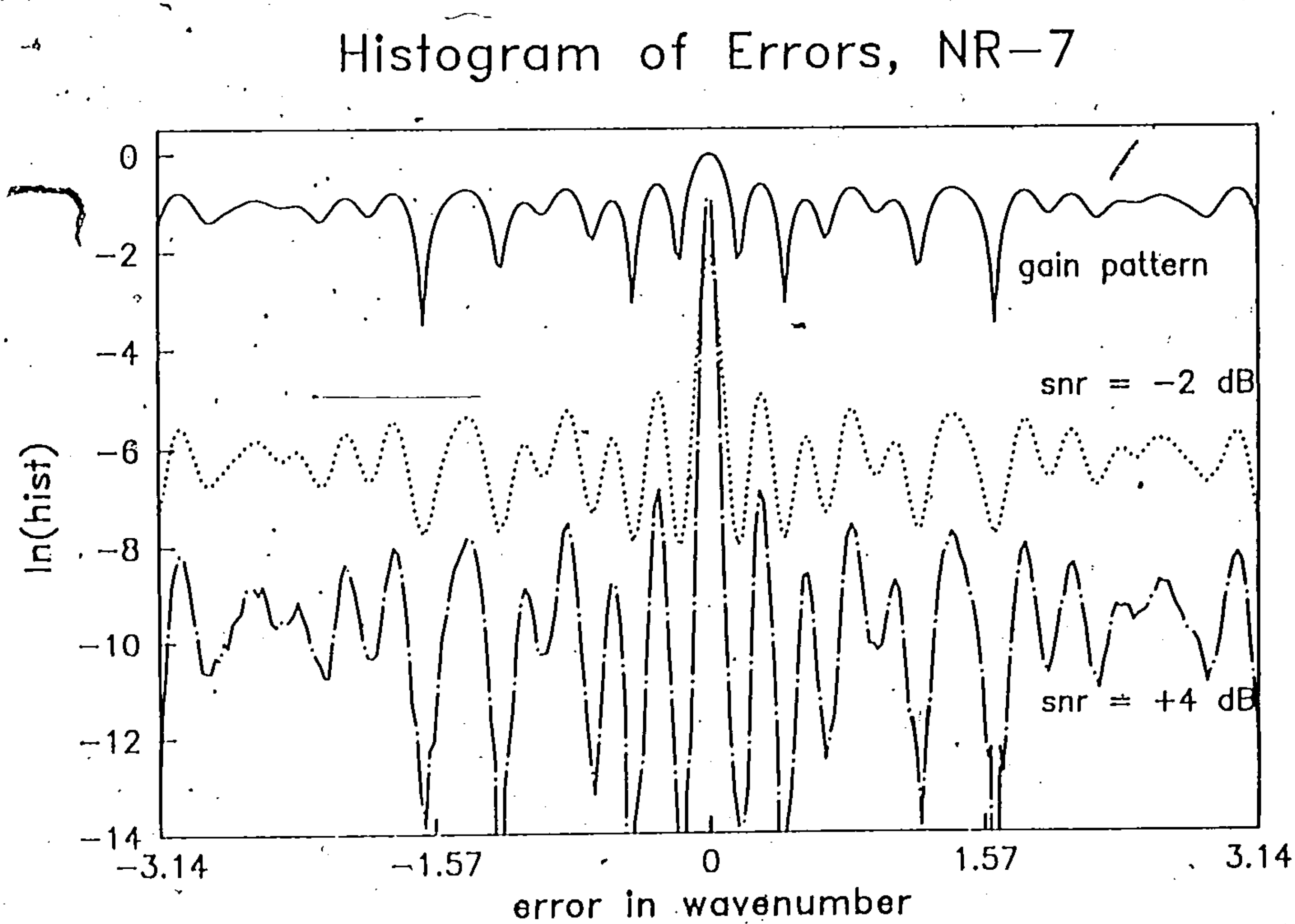

Figure 4.4: Histogram of estimation errors for 2 different values of SNR using a 7-element nonredundant array. Superimposed is the standard beam pattern.

It is clear that the form of the estimator, defined in equation (4.10), is closely related to the gain pattern, defined in equation (4.11). Figures 4.3 and 4.4 both indicate that the probability of an error does not decrease monotonically as the absolute error increases. It is also clear, that when a large error is made, it is more likely to occur near a peak of the side lobe pattern than at the null. In other words, noise increases the likelihood of one of the 'side lobes' being greater than the area surrounding the main beam. When this occurs, the error is termed an outlier [38]. The probability of an outlier is defined as the probability that the error in wavenumber falls outside the beamwidth of the array.

For errors within the beamwidth of the array, the performance is more conventional. Figures 4.5 and 4.6 present the normalized histograms covering the beamwidth. For each value of SNR, the solid curve represents the predicted performance based upon a Gaussian distribution of zero mean and variance given by the Cramér-Rao Lower Bound of section 3.2. These predictions were compensated for the probability of outlier value measured, p_o. The adjustment is only necessary for the lower SNR values. For +4 dB, p_o was such that the prediction requires less than a .3% adjustment in scale for the nonredundant array, and less than 0.1% adjustment for the uniform array. We note that

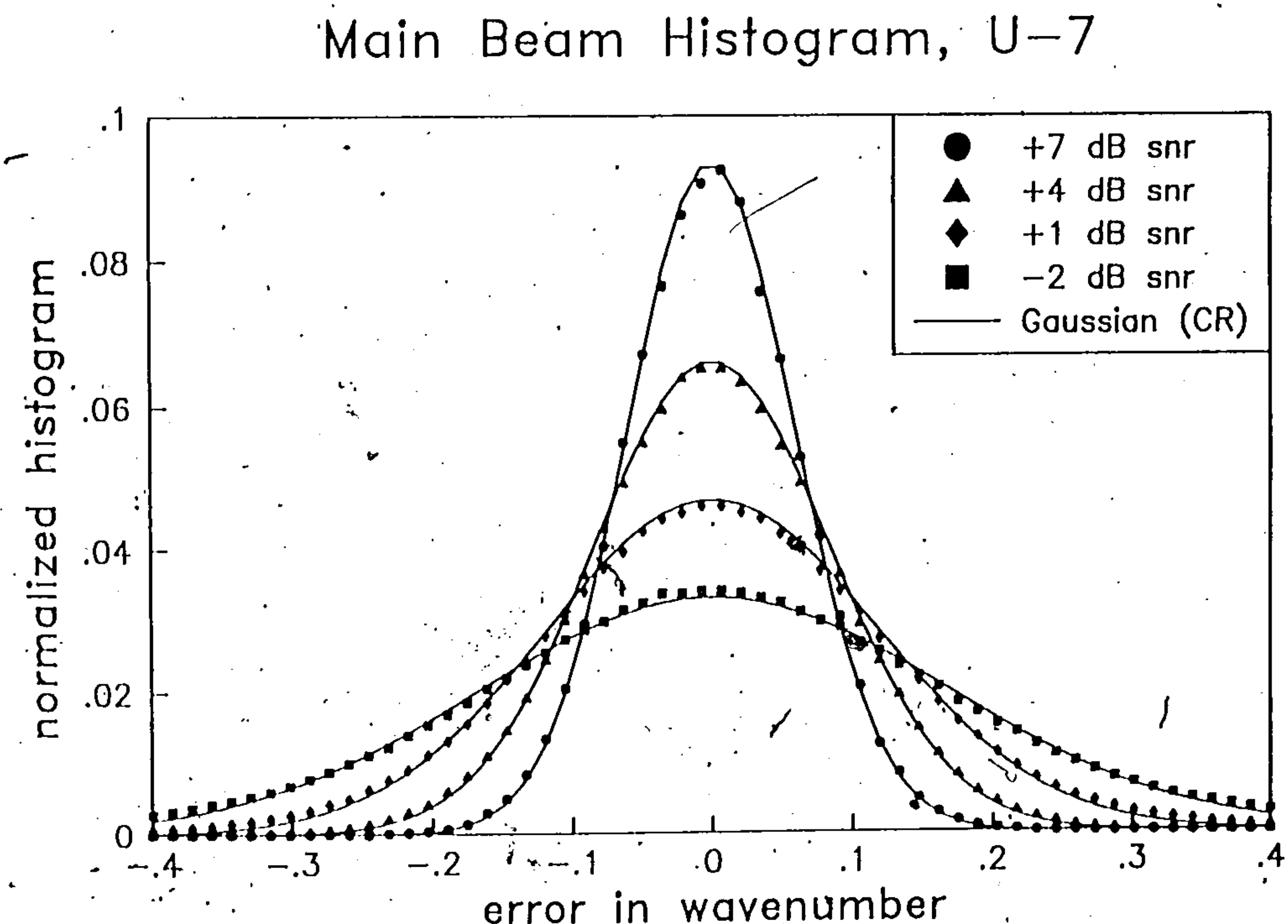

Figure 4.5: Expanded histogram of the region associated with the main lobe of the gain pattern for a 7-element uniform array. Included is the equivalent gaussian probability distribution.

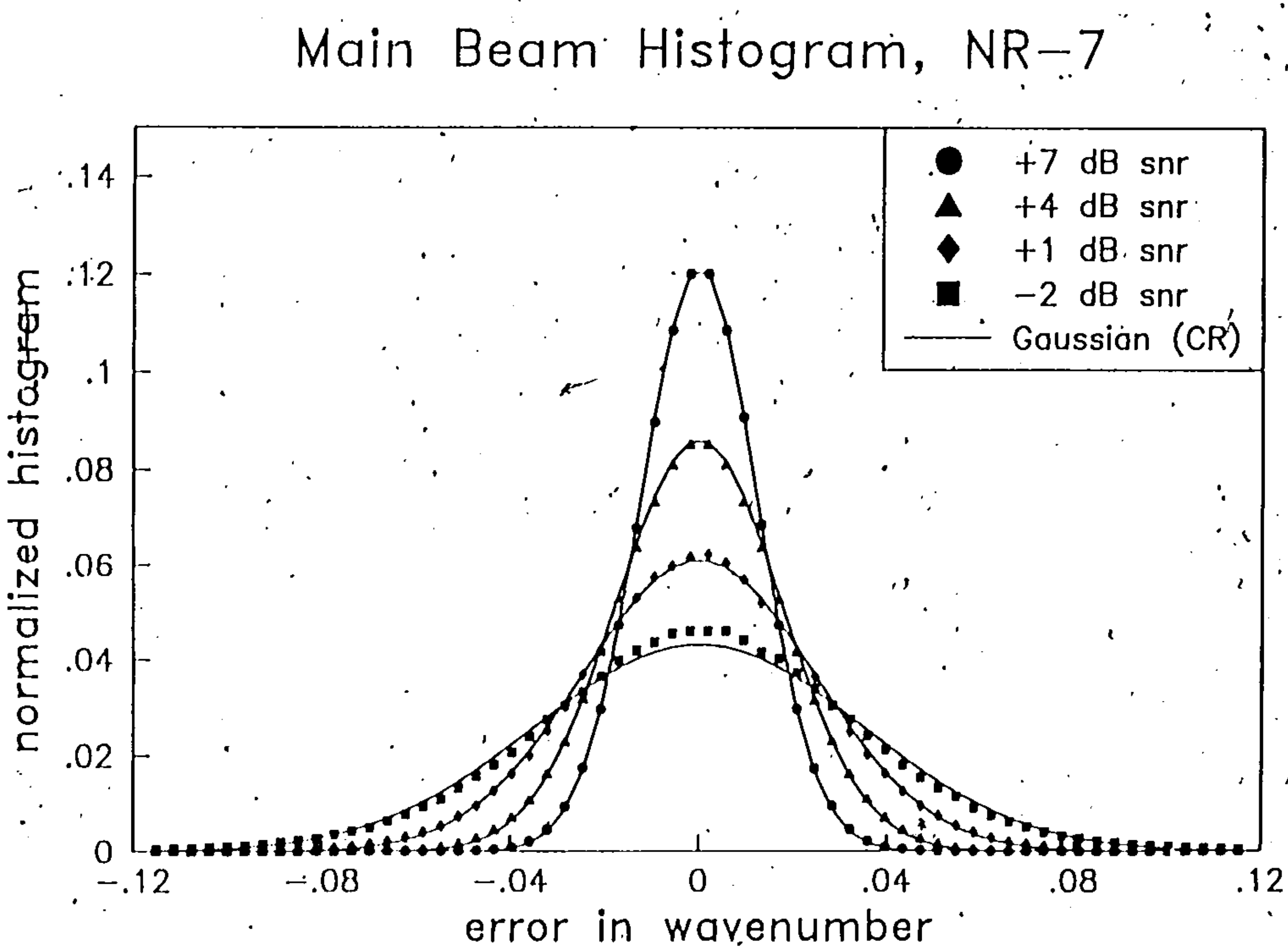

Figure 4.6: Expanded histogram of the region associated with the main lobe of the gain pattern for a 7-element uniform array. Included is the equivalent gaussian probability distribution.

for lower SNR values, the Gaussian distribution is not as good an approximation as for the higher SNR. As the SNR is decreased, the width of the Gaussian eventually becomes comparable to the beamwidth, at which point the gain pattern of the array becomes significant.

While the mean square error is certainly an important measure of performance, it is not the only consideration. We can view the errors as coming from one of two distributions. With probability p_o (a function of SNR), it is an outlier, and with probability $(1-p_o)$ it is Gaussian distributed with variance given by the CRLB. The threshold SNR is determined to be the minimum SNR at which the system should be operated. Rather than choose the point for which MSE is 1 dB greater than the CRLB, a radar design engineer may require a certain maximum probability of outlier occurrence. When an outlier occurs, it is almost as likely to make extremely large errors, near π, as it is to make those just outside a beamwidth. In this region the probability does not fall off as a Gaussian would, and the existence of very large errors may be critical to the design engineer.

We return to the model used by Rife and Boorstyn [38], for which an N-point coarse search was implemented on an N-element uniform array. Provided one of the coarse search points falls on the true target location, their definition of outlier is the event for which one of the incorrect values of the coarse search would provide a greater maximum than the one corresponding to the true location.

These assumptions allow the probability of outlier to be calculated analytically. This result has been determined by Rife and Boorstyn [38, eq.60], and is reproduced here (using our notation) as

$$p_o = \frac{1}{N} \sum_{m=2}^{N} \frac{N!\ (-1)^m}{(N-m)!\ m!} \exp\left\{ -N\Gamma \frac{(m-1)}{m} \right\} \qquad (4.12)$$

For high SNR, the equation is dominated by the term m=2.

$$p_o \cong \frac{N-1}{2} \exp(-N\Gamma/2) \qquad (4.13)$$

or taking logarithms,

$$\ln(p_o) \cong -\frac{N}{2}\Gamma + \ln\left(\frac{N-1}{2} \right) \qquad (4.14)$$

The probability of outlier given by (4.12) and the approximation given by (4.13) are plotted for various values of N in Figure 4.7. We see that the approximation is poor for small values of Γ, where p_o is near 1; however, for $p_o < 0.01$, the approximation is adequate for use in the determination of SNR.

Unfortunately this definition of an outlier is specific to a particular set of parameter circumstances. In general, the target will not coincide with one of N points in the

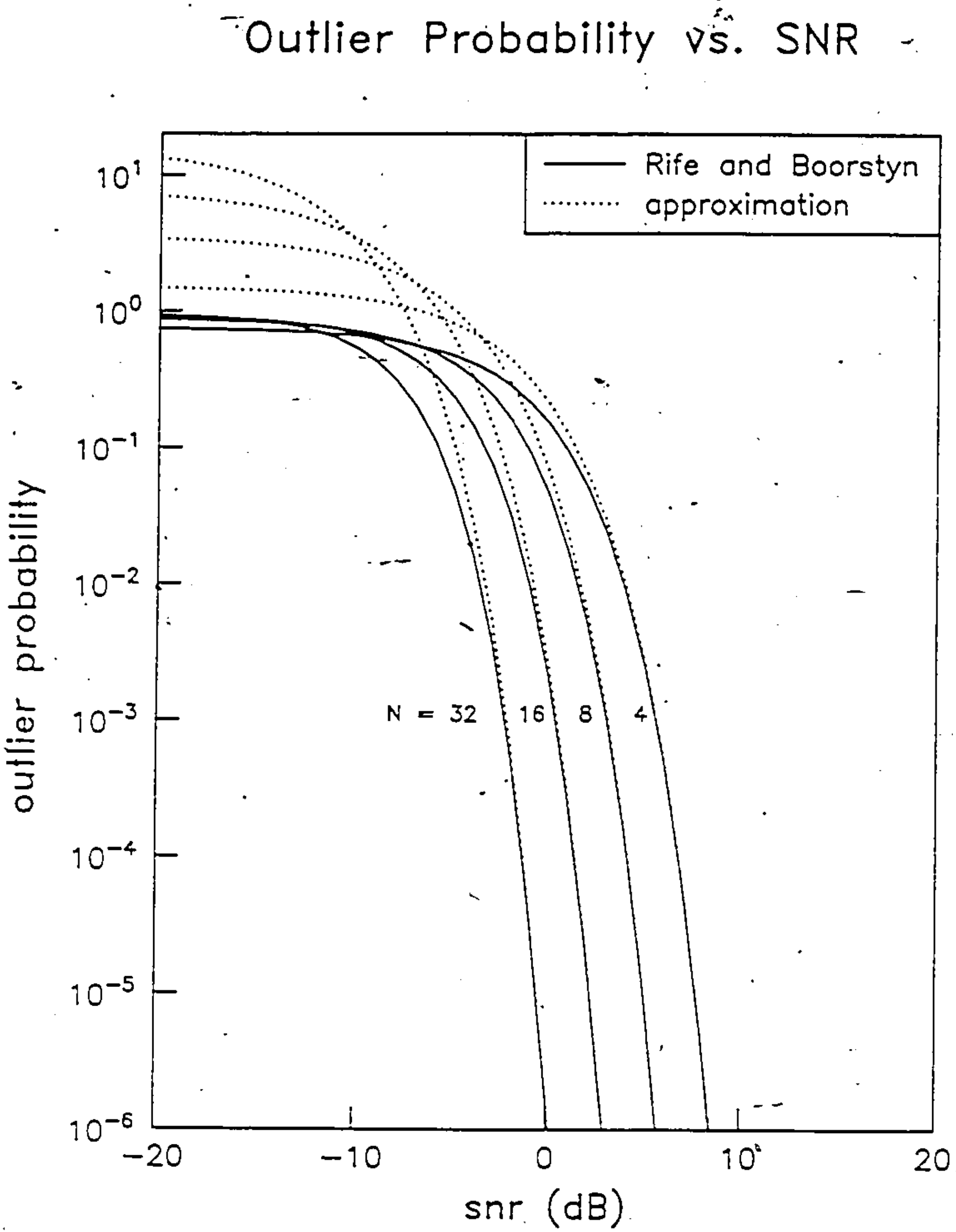

Figure 4.7: Outlier probability distribution for uniform arrays as defined by the Rife and Boorstyn [38] and the high SNR approximation.

coarse search region, and therefore we find an increased number of points are required in the initial grid search. Finally, it is also not suitable for extensions to nonuniform arrays.

We will now show, however, that the trend indicated by equation (4.13) is nevertheless accurate. That is, for $p_o < .01$, we show empirically that the probability of outlier decreases as a simple exponential in SNR. We begin by considering the result for uniform arrays. We position the target at boresight, and using a proper search implementation, indicate the measured probability of outlier versus SNR. To validate the estimator and previous expressions, we also implement the search described in [38]. The results are presented in Figure 4.8 for the 8-element uniform array, for which we plot p_o (on a logarithmic scale) versus Γ (on a linear scale). The error bars shown are the estimates of the standard deviation of the value of $\log(p_o)$, determined statistically.

The solid curve is a plot of equation (4.12) which fits the 8-point coarse search quite well. The 'true' performance is indicated through the use of a 128-point coarse search. For $p_o < 0.01$, we fit the $\ln(p_o)$ to a linear curve in Γ. The results of the calculation are displayed as the 'empirical fit' in Figure 4.8. The fitting was performed as a weighted least-squares fit using orthogonal

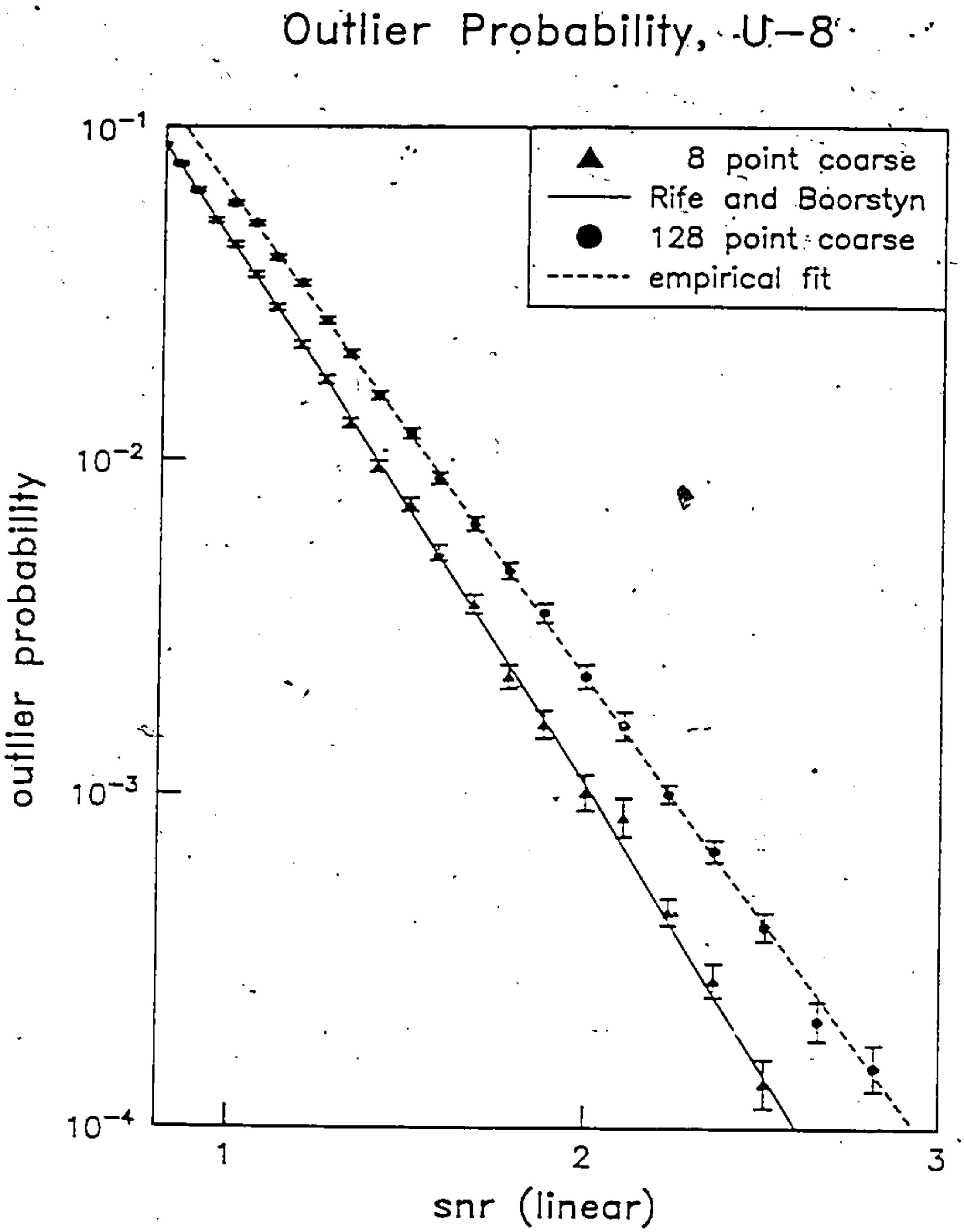

Figure 4.8: Probability of outlier for an 8-element uniform array showing the overly optimistic results obtained in [38], 'true' performance is indicated by the '128 point coarse' search.

polynomials. The entire statistical analysis is described in Appendix B, including the goodness of fit criterion used, namely, the reduced chi-squared test.

The probabilities of outlier were found in two stages, initially using 2^{14} point simulations which would provide reasonably accurate estimates of the probabilities in the larger regions of p_o. The region having lower values of p_o were then simulated again with a greater number of simulations. The fitting process used those data points for which $p_o < 0.01$ and at least 25 outliers occurred (corresponding to a relative accuracy of 20% in the estimate of p_o). Clearly, if only 1 or 2 events are observed, the statistical validity of the estimate of p_o must be suspect. The 25 outlier requirement, then restricts the p_o range to values above $25/N_S$, where N_S is the number of simulations. Typically, for N_S equal to 2^{16}, this translates to fitting values of p_o in the region $4x10^{-4} < p < 10^{-2}$. (if N_S equals 2^{20}, the effective range for p_o is $2.5x10^{-5} < p < 10^{-2}$).

The error bars plotted are the estimate of the standard deviation of the measured quantity. This corresponds to, approximately, the 68% confidence limit. In other words, for a valid model, in the range of p_o for which the fitting was performed, one would expect about 1/3 of the points to lie off the curve (that is, the vertical error bar does not intersect the curve).

For the data in Figure ~~4.8,~~ we find 11 points in the range for p_o (the maximum value of N_S was 2^{18}). Therefore, there are 9 degrees of freedom, producing the reduced chi-squared value of 0.35, as described in Appendix B. The probability that a value greater than this would occur with 9 degrees of freedom if the model was accurate would be about 0.95. This indicates that the model is quite reasonable, and that we were fortunate in this experiment to obtain this low a value for the reduced chi-squared. (see Appendix B). A very low probability would have been indicative of an incorrect model selection, and we expect 0.5 to be typical.

We note from Figure 4.8 that although the values of $p_o > 10^{-2}$ were not chosen for the fitting, they still lie very close to the estimated curve for values up to 0.1. Finally, we observe the Rife and Boorstyn simulations were optimistic, both in the probability of outlier and the rate at which it falls off. The Rife and Boorstyn result predicted a curve in this region of SNR to be of the shape

$$p_{RB} \cong 3.5 \exp(-4\Gamma)$$

$$\cong \exp(1.25 - 4.000\Gamma) \qquad (4.15)$$

The fit (we performed) indicates the true behaviour to be

$$P_o = \exp(a + b(\Gamma-\beta))$$
$$\cong \exp(0.53 - 3.318\Gamma) \tag{4.16}$$

where

$$a = -5.83 \pm 0.02 \tag{4.17a}$$
$$b = -3.318 \pm 0.062 \tag{4.17b}$$
$$\beta = 1.9150 \tag{4.17c}$$

Therefore,
$$a-b\beta = 0.53 \pm 0.12 \tag{4.18}$$

Figure 4.9 presents the probability of outlier simulation results and straight line fits for 4-, 8- and 16-element uniform arrays. We discuss the goodness of fit in more detail following the analysis of a large selection of arrays below.

We now use this technique to examine the same performance in nonuniform arrays. Simulations similar to those described earlier are repeated for the 7-element uniform and nonredundant arrays. The estimated probability of outlier and the straight line fit are presented in Figure 4.10. The reduced chi-squared values were 1.24 and 1.07 for the uniform and nonredundant arrays, respectively, providing associated probabilities of 30% and 40%. Again the model would be justified within the statistical errors.

Figure 4.10 clearly shows the increased probability of

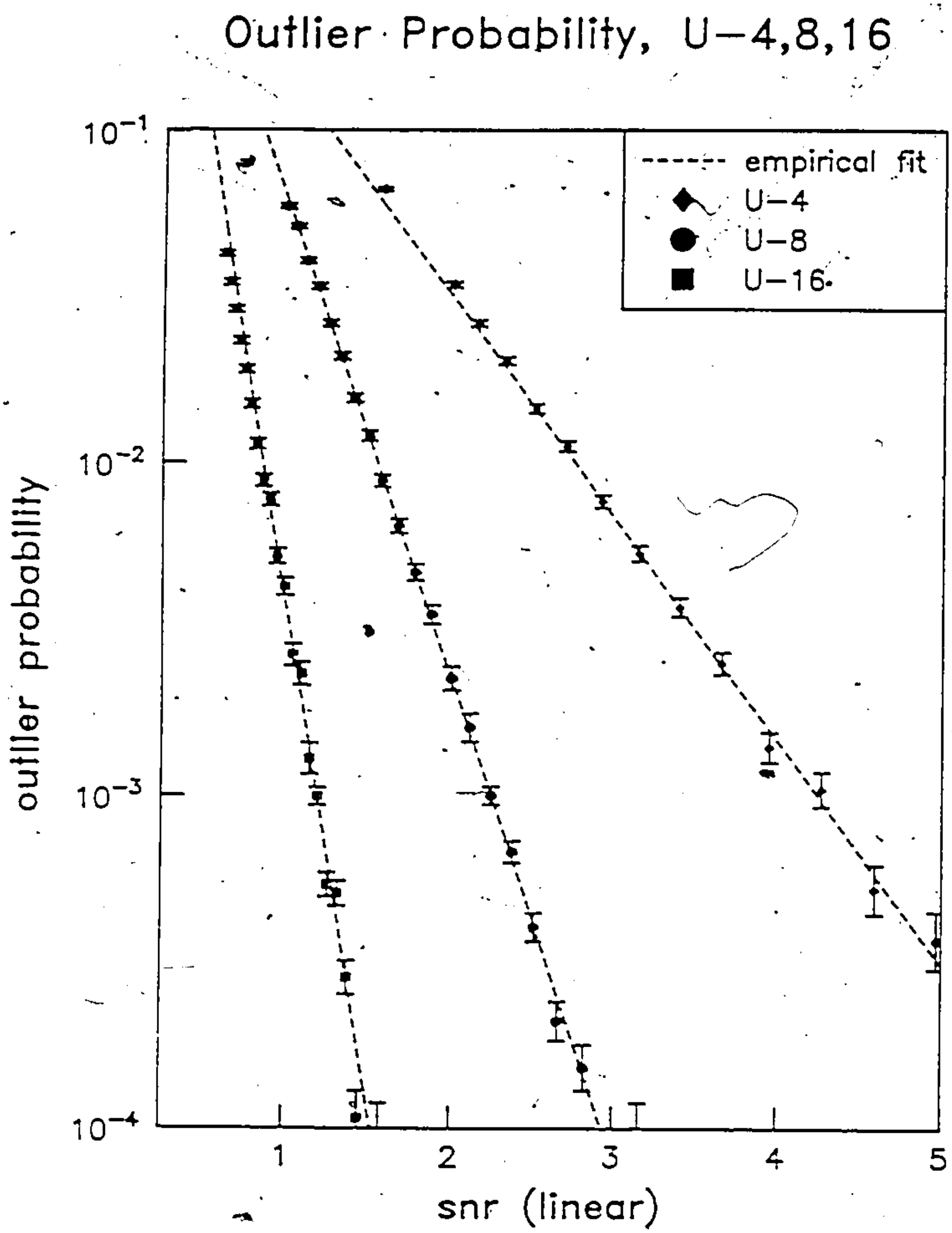

Figure 4.9: Empirical fitting of the outlier probability determined by simulation for 4-, 8- and 16-element uniform arrays.

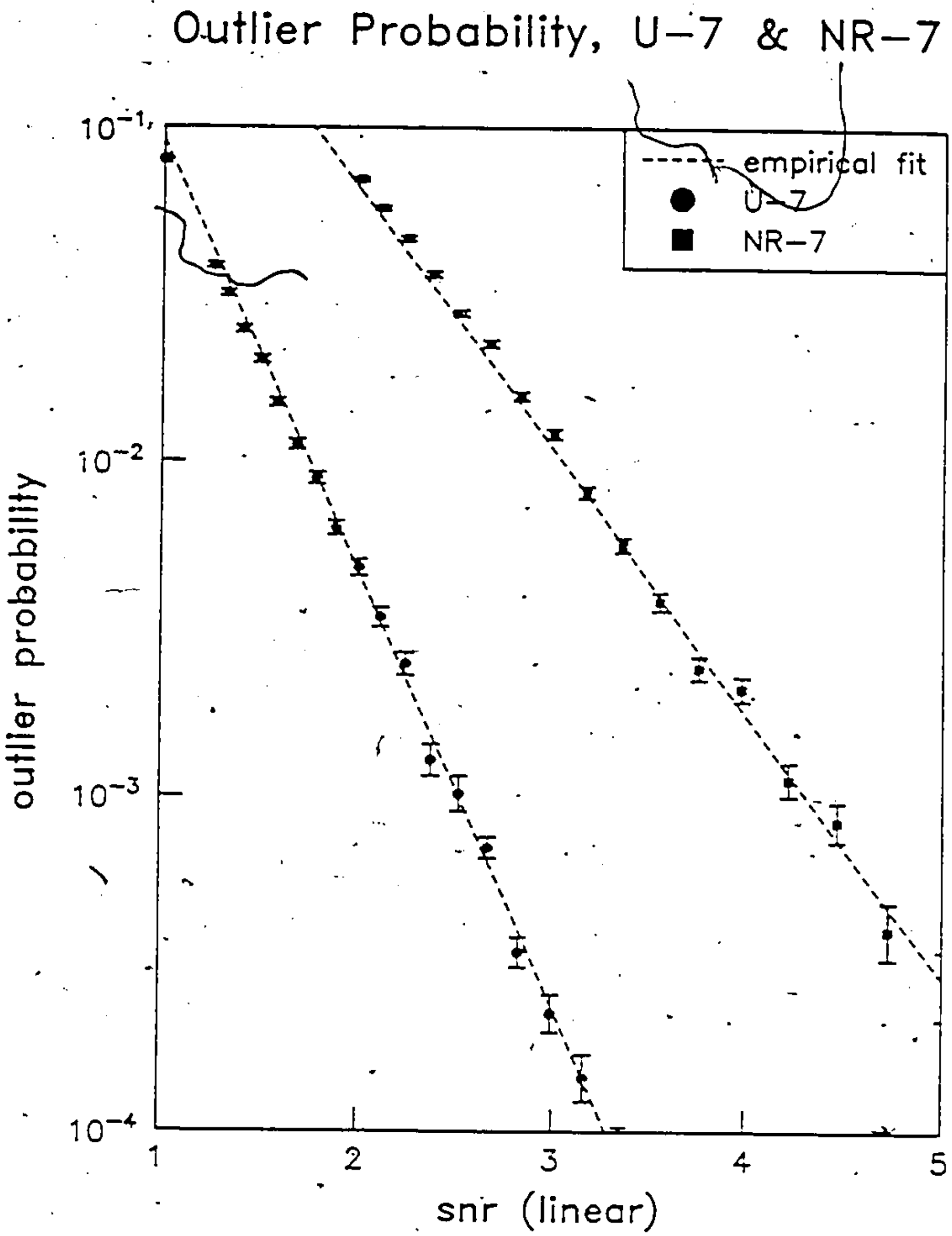

Figure 4.10: Empirical fitting of the outlier probability determined by simulation for 7-element uniform and nonredundant arrays.

outlier for the nonredundant array. Not only is it larger, but it also falls off at a slower rate with SNR than it does for the uniform array. Therefore, we can define a new critical SNR, which is the point at which the probability of outlier reaches a required specification. Using the fit results, we can invert the function to find the expected SNR corresponding to the required p_o. Since orthogonal polynomials were used, the coefficients are independent and a proper error can be assigned to the SNR. For values of p_o within the fitting range, this will be an interpolation with very accurate results. However, we may now extrapolate to much lower values of p_o, using the inverse as well. For these results, the estimated error of extrapolation grows as the value of p_o decreases. The advantages of this technique for moderate extrapolations will be a reasonable estimate of SNR, for which the outlier probability may be impractical to simulate. It also provides an estimate of the required SNR, and once a designer has narrowed down the array configurations to be considered, a more accurate simulation may be performed. For example, for a 20% reliability in probability of outlier at $p_o = 10^{-6}$, it would require some 25 million trials. Clearly, we would like to have an approximate idea of the required SNR, so that experiments of this magnitude are not wasted.

The selected arrays described in chapter 3, Table 3.1, are examined for this probability of outlier variation with SNR. If we consider each array to be an independent test of the goodness of fit, we can compile some statistical results. Let $P(\chi^2, \upsilon)$ be the probability of exceeding χ^2 with υ degrees of freedom (see Appendix B and [47]). We expect approximately 50% of our arrays to provide values of $P(\chi^2, \upsilon)$ greater than 0.5, and 50% less than 0.5. Of the 24 arrays examined, 13 produced a value greater than 50%. In terms of the spread, we expect 50% of the arrays to provide values of $P(\chi^2, \upsilon)$ between 25% and 75%. For this statistic, 13 of 24 arrays indeed fell in this category. There did not appear to be any correlation with the number of elements or with the array structure. From these figures, we feel justified in proposing the single exponential fit for probability of outlier versus SNR for sufficiently low values of p_o. In fact, for the arrays up to 9 elements, the fit agreed with the simulated values of p_o, up to 0.10, within statistical errors. For 32-elements, the fit was in error by about 0.25 dB at $p_o \cong 0.10$. For larger numbers of elements, it would be suggested that the upper limit on p_o used be reduced below 0.01, although this will require increased computational effort for the same degree of accuracy.

For each array, the interpolated/extrapolated SNR corresponding to values of p_o equal to 10^{-3} and 10^{-6} are determined from the fit, along with the accuracy of the estimate. The SNR values are measured in dB, as is the error. For all arrays, the accuracy of the fit at $p_o = 10^{-6}$ is better than 0.1 dB, while at 10^{-3} it was accurate to better than 0.05 dB. The results are presented in Table 4.1a, where the Sampling Gain is quoted from the previous Table 3.2a. In order to compare the different arrays, we also measure the quantities in terms of the array SNR, defined as $N\Gamma$. Table 4.1b repeats the data of Table 4.1a, using this measure. The results for maximum likelihood estimation can now be further reduced.

We obtain the significant result that, for all uniform arrays measured, for $p_o = 10^{-6}$, the required array SNR is 15.4 dB ± 0.1 dB; this includes 5- to 32-element uniform arrays. In this region, the required array SNR is virtually independent of the number of elements. We find it is also possible to make similar statements about the nonuniform arrays. All minimum redundant arrays, labelled MR, required 17.2 ± 0.1 dB of array SNR, again well within the measurement accuracy. The nonredundant arrays required 17.3 dB ± 0.3 dB in all cases. We note that these arrays extend from 11 to 55 units of length. Since each individual value has an error standard deviation of 0.1 dB, these results may be considered constant to within statistical errors. In fact, in 4 of 6 cases, the nonredundant arrays were equal to

Table 4.1a

Sampling Gain and Threshold Comparison
Using Elemental SNR, Γ

No. of Sensors	Array[1] Type	Sampling Gain(dB)	p=10^{-3} @ SNR (dB)[2]	p=10^{-6} @ SNR (dB)[2]	Threshold[3] SNR (dB)
5	U	0.0	5.4	8.4	5.6
	MR	7.7	7.4	10.3	8.7
	NR & UR	9.1	7.5	10.3	9.0
6	U	0.0	4.6	7.7	4.9
	MR	9.0	6.6	9.3	8.1
	NR & UR	11.2	6.8	9.6	8.5
7	U	0.0	4.0	6.8	4.5
	MR	9.8	6.0	8.8	5.7
	UR	12.1	6.1	8.8	7.9
	NR	13.7	6.3	9.1	8.5
8	U	0.0	3.5	6.4	4.2
	MR	11.7	5.5	8.2	7.4
	UR	14.0	5.6	8.3	7.7
	NR	14.9	5.6	8.1	7.6
9	U	0.0	3.1	5.9	3.8
	MR & UR	11.7	5.0	7.7	7.0
	NR	15.9	5.0	7.6	7.2
10	U	0.0	2.6	5.5	3.5
	MR	13.5	4.4	7.1	6.6
	UR	16.3	4.5	7.0	6.8
	NR	16.6	4.5	7.0	6.7
16	U	0.0	0.8	3.4	2.0
32	U	0.0	-2.0	0.4	- .4

[1] Arrays correspond to those listed in Table 3.1
[2] Elemental SNR, Γ, required to obtain specified probability of outlier determined from empirical fit.
[3] Threshold elemental SNR determined by MLE for target at boresight and search over $(-\pi, \pi)$. Mse greater than CRLB by 1 dB.

Table 4.1b

Sampling Gain and Threshold Comparison
Using Array SNR, $N\Gamma$

No. of Sensors	Array[1] Type	Sampling Gain(dB)	$p=10^{-3}$ @ SNR (dB)[2]	$p=10^{-6}$ @ SNR (dB)[2]	Threshold[3] SNR (dB)
5	U	0.0	12.4	15.4	12.6
	MR	7.7	14.4	17.3	15.7
	NR & UR	9.1	14.5	17.3	16.0
6	U	0.0	12.4	15.5	12.7
	MR	9.0	14.4	17.1	15.9
	NR & UR	11.2	14.6	17.4	16.3
7	U	0.0	12.5	15.3	13.0
	MR	9.8	14.5	17.3	14.2
	UR	12.1	14.6	17.3	16.4
	NR	13.7	14.8	17.6	17.0
8	U	0.0	12.5	15.4	13.2
	MR	11.7	14.5	17.2	16.4
	UR	14.0	14.6	17.3	16.7
	NR	14.9	14.6	17.1	16.6
9	U	0.0	12.6	15.4	13.3
	MR & UR	11.7	14.5	17.2	16.5
	NR	15.9	14.5	17.1	16.7
10	U	0.0	12.6	15.5	13.5
	MR	13.5	14.4	17.1	16.6
	UR	16.3	14.5	17.0	16.8
	NR	16.6	14.5	17.0	16.7
16	U	0.0	12.8	15.4	14.0
32	U	0.0	13.0	15.4	14.6

[1] Arrays correspond to those listed in Table 3.1
[2] Array SNR, $N\Gamma$, required to obtain specified probability of outlier, determined from empirical fit.
[3] Threshold array SNR determined by MLE for target at boresight and search over $(-\pi, \pi)$.

or better than the minimum redundant value of SNR for $p_o = 10^{-6}$, although the difference was always within one standard deviation of the statistical error.

These results provide an extremely accurate and yet very simple design guideline in choosing amongst the different array structures, provided the maximum likelihood estimator is employed.

We will now compare the estimate of the mean square error to that observed in the simulations. Using a similar approach to [38], with the appropriate modifications, we consider the total MSE to be a weighted sum of the values obtained with and without outlier occurrence as

$$\widehat{MSE} = p_o(\text{MSE given an outlier}) + (1-p_o)\,\sigma^2_{CR} \qquad (4.19)$$

where σ^2_{CR} is the Cramér-Rao Lower Bound variance, and p_o is derived from the empirical models. To simplify the calculation, we assume the error to be uniformly distributed outside the beamwidth, B, given an outlier has occurred. The MSE, given an outlier has occurred, is then given by

$$\text{MSE given outlier} \cong \frac{(2\pi)^2 + 2\pi B + B^2}{12} \qquad (4.20)$$

We also put an upper limit on p_o (for low SNR), to be

$(2\pi - B)/2\pi$, and we acknowledge that the fitting is not accurate in this region. Also, since σ^2_{CR} increases indefinitely with decreasing SNR, we hard limit the MSE estimate to that obtained by random guesses over the interval. Hence, we do not allow the MSE to go above $(2\pi)^2/12$. These restrictions are actually cosmetic, since we are only critically interested in performance at SNR values increasing from just below threshold, and, it is in these regions we require a 'good' fit.

Figure 4.11 demonstrates the quality of the MSE estimate described above. For the uniform array, the simulated points fall on the predicted curve throughout the threshold region. Of course at high SNR, the curve follows the Cramér-Rao Lower Bound values. For low SNR values, the curve overestimates the MSE since the value of p_o is overestimated in this region.

For the nonredundant array the performance for most of the threshold region is accurately described by (4.19). At the threshold point itself, there are a few points which do not lie on the predicted curve. Upon closer inspection, we determine that the predicted value of p_o in that region is close to 10^{-5}, for which the simulations are simply not very accurate. Our results, in fitting the probability of outlier for such a modest extrapolation, lead us to believe the predicted curve is in fact a better representation of

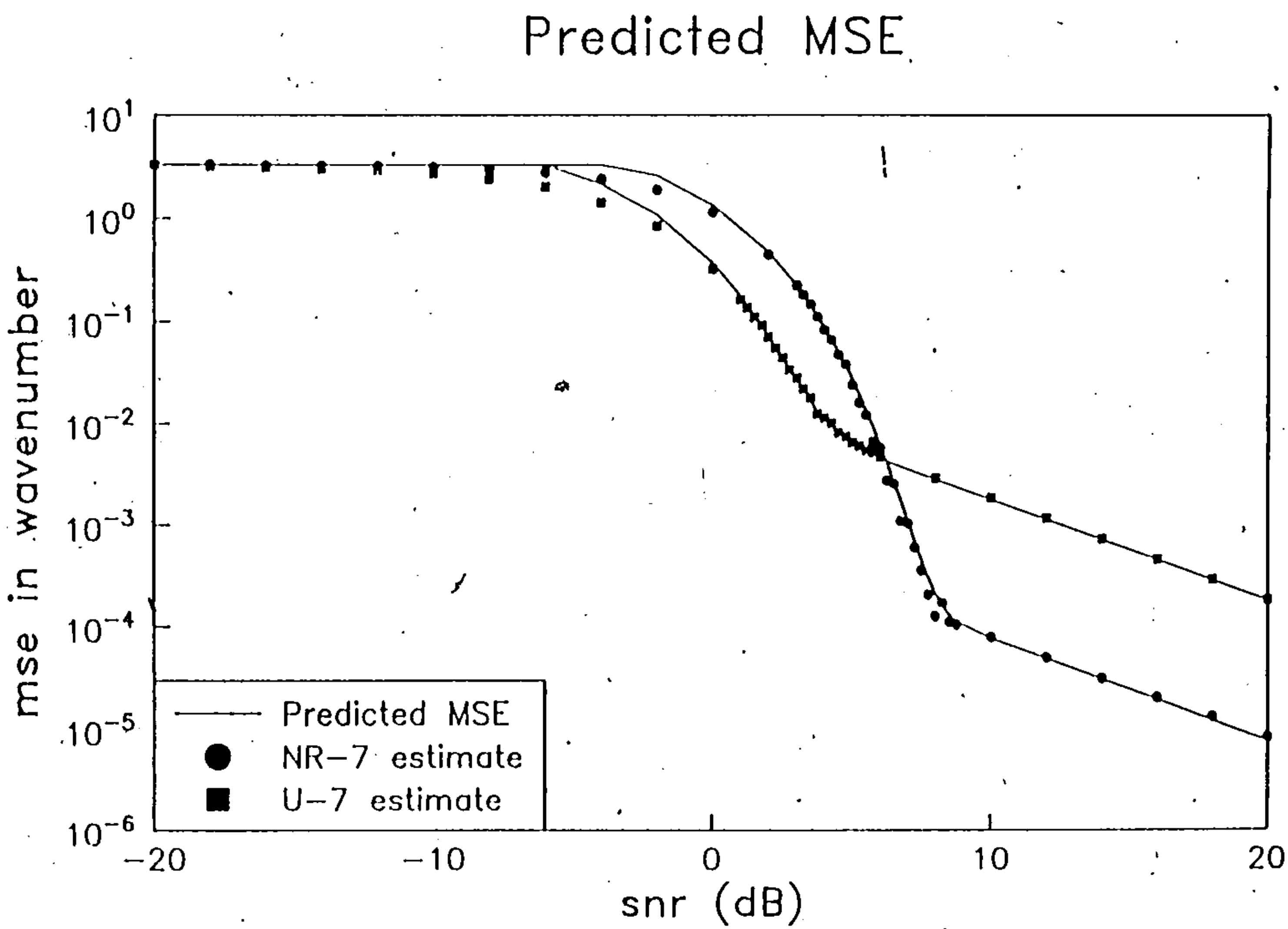

Figure 4.11: MSE for 7-element uniform and nonredundant arrays as well as the predicted values based upon the CRLB and outlier probability analysis.

the MSE in this region than the simulations could be. The result is significant for the nonredundant array since the deviation from the CRLB occurs for a much lower probability of outlier than the uniform array. That is, the improved MSE, (sampling gain is 13.7 dB), will deteriorate earlier for even a small number of outlier occurrences. This effect will become more important as the number of elements increases. Therefore, we use the predicted MSE given by (4.19) to estimate the 1 dB threshold point and provide these results in the last columns of Table 4.1a and Table 4.1b.

Many researchers evaluate the 1 dB threshold (see for example [25, 3S]), although in this author's opinion, when maximum likelihood estimation is employed, the probability of outlier specification would appear to provide the better measure for comparison purposes. These results should not be compared with the Weiss-Weinstein Lower Bound results of Chapter 3, since no account has been taken of a priori information. The next section will focus on the effects of having a target which may lie anywhere in a specified interval and the maximum likelihood performance.

4.4 MLE and A Priori Knowledge

We will now examine the effects of a priori knowledge on the performance of maximum likelihood estimation of the target wavenumber. The modelling of the a priori knowledge of the target location has been dealt with in detail in Section 3.1 of the previous chapter. The basic assumption consists of restricting the target to be located in a given interval (k_n, k_x), a subset of the visible region. We assume the target is equally likely to occur at any point in this interval.

The implications of this knowledge on the probability of outlier , the threshold SNR, and the high SNR MSE will be investigated. This determination will be made by simulating the MLE with the target taking random positions over the interval from trial to trial. The target is uniformly distributed over the interval ($-a\pi$, $a\pi$), where $a<1$. The maximum likelihood estimator is then constrained to operate on the same interval.

We begin with an analysis of the probability of outlier. The 7-element uniform array evaluated using various values of a with the probability of outlier characterized as in Section 4.2. The simulation results are presented in Figure 4.12a with the error bars omitted for clarity. For large values of a, very close to 1, the values of p_Q are clearly not distributed linearly. The reduced chi-squared values for a = 0.98 and a = 0.95 are 4.43 and 3.02, respectively, with corresponding values of $P(\chi^2, \upsilon)$ of

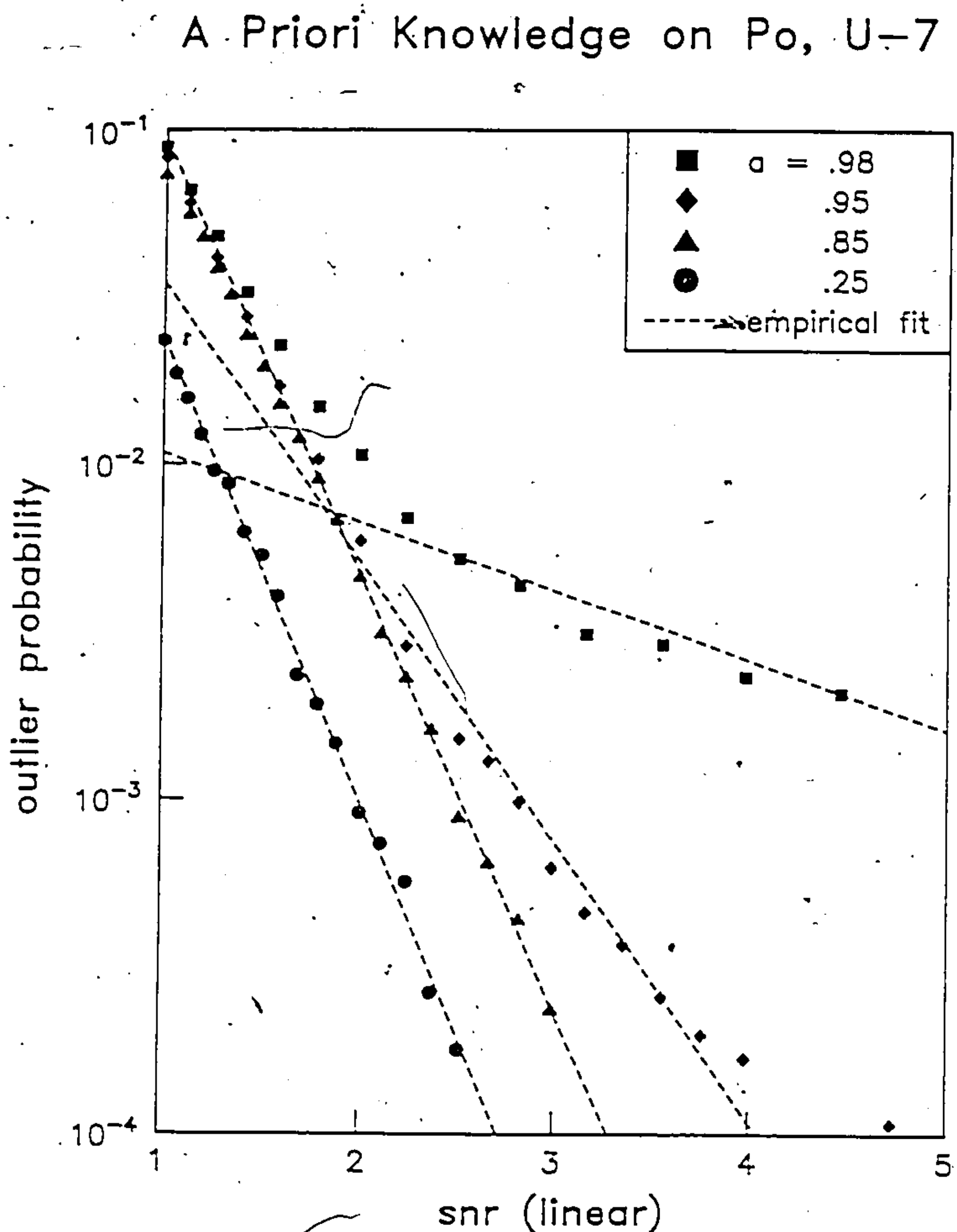

Figure 4.12a: Outlier probability compared for varying amounts of a priori knowledge for the 7-element uniform array.

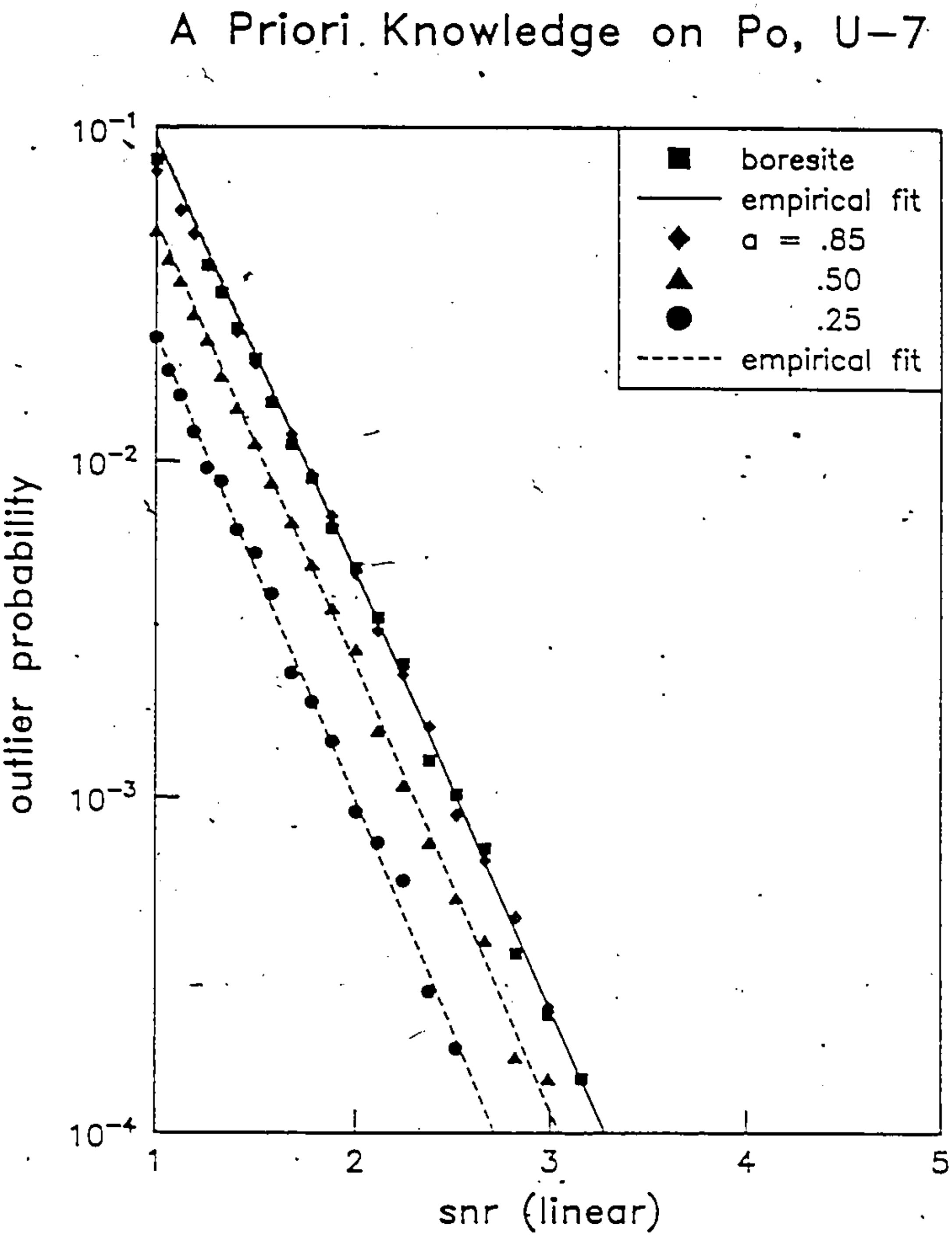

Figure 4.12b: Selected outlier probabilities compared for varying amounts of a priori knowledge for the 7-element uniform array and the result of Figure 4.10

less than 0.001 in both cases. This indicates the model chosen, a linear curve, is very likely incorrect. However, for $a = 0.85$ down to 0.25 the reduced chi-squared values were close to 1. Examination of the figure would also reinforce this knowledge, where the linear curves provide reasonable models of the values of $\ln(p_o)$ versus elemental SNR. To emphasize this, we plot the results of the previous chapter, where the target was kept at boresight and the estimation performed over the full interval $(-\pi, \pi)$, in Figure 4.12b along with these a priori curves.

The interval $(-0.85\pi, 0.85\pi)$ restricts the target to a region more than a half beamwidth from either end of the visible region. If the target was located at 0.85π, the error required to estimate the target at -0.85π would be at least one beamwidth. For $a = 0.85$, the curve is indistinguishable from the 'boresight' curve. We also notice that the curves all have nearly identical slopes. The error analysis indicates values of -3.00 ± 0.06, -3.04 ± 0.05, -3.18 ± 0.07 for the values of $a = 0.85$, 0.50, and 0.25, respectively. The 'boresight' slope was -3.00 ± 0.07 for which one can say that all of these values are equivalent within statistical errors with 95% confidence. Further, the probability of outlier decreases approximately proportionally with a. For example, at 4.0 dB SNR, p_o was $(1.00 \pm 0.15)\times10^{-3}$ for the boresight curve. While for

$a = 0.50$ and 0.25, the values were $(0.52 \pm 0.07) \times 10^{-3}$ and $(0.21 \pm 0.03) \times 10^{-3}$, respectively.

As the search region is narrowed, side lobes of the antenna gain pattern are eliminated. If each side lobe is assumed to exert approximately the same influence on the error, then reducing the number of side lobes should reduce the probability of outlier. The side lobes for uniform arrays are essentially equally spaced. Of course, this is only an approximation, and clearly larger side lobes may have a more significant effect on p_o than the smaller ones.

The same procedure is repeated for the nonredundant, 7-element array, and the results are presented in Figures 4.13a and 4.13b. The beamwidth of this array is approximately 0.08π, and therefore the interval $(-0.95\pi, 0.95\pi)$ provides a full beamwidth of buffer. For $0.08 < a < 0.95$, the maximum value of the reduced chi-squared was 1.15, and we feel the linear model was justified. The comparison with the nonredundant simulations at boresight of the previous section are displayed in Figure 4.13b. The curves for $a = 0.95$ and the boresight results are almost identical. The slopes are also in agreement for $a = 0.95$ down to 0.08 within statistical errors. The value of the slope at boresight was -1.80 ± 0.03, while for $a = 0.95$, 0.50 and 0.08 it was -1.81 ± 0.03, -1.86 ± 0.04 and -1.87 ± 0.06, respectively. The probability of outlier

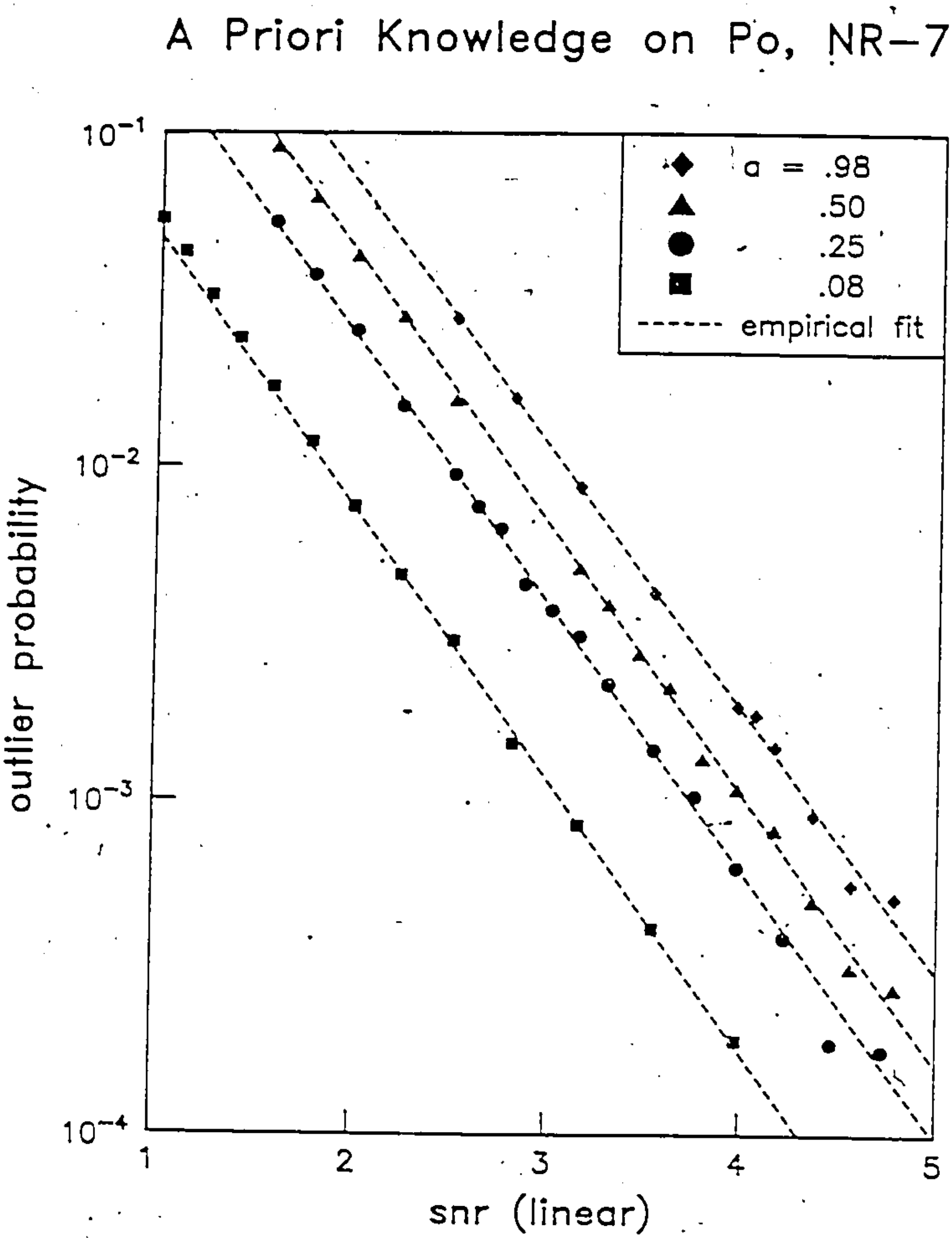

Figure 4.13a: Outlier probability compared for varying amounts of a priori knowledge for the 7-element nonredundant array.

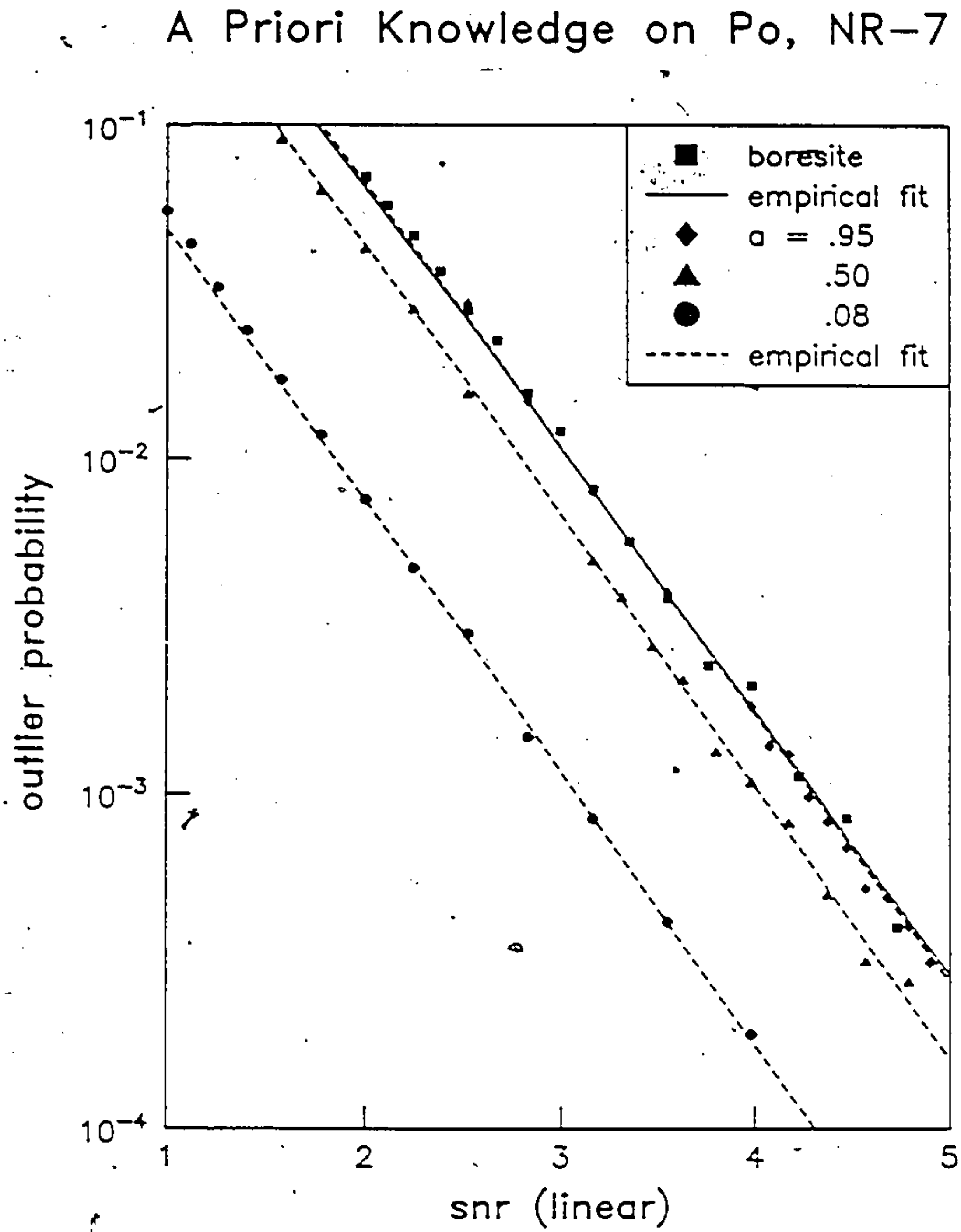

Figure 4.13b: Selected outlier probabilities compared for varying amounts of a priori knowledge for the 7-element uniform array and the result of Figure 4.10

also varies approximately proportionally with a: for a = 0.95, the probability of outlier at 6.0 dB was $(1.93 \pm 0.21) \times 10^{-3}$, while for a = 0.08, the value was $(0.18 \pm 0.04) \times 10^{-3}$.

In both cases, we see the results of positioning the target at boresight may be viewed as the limiting case for $a \rightarrow 1$. The deviation for cases in which $a > 0.98$ from the other values was anticipated from the use of the Weiss-Weinstein bound, and was discussed in great detail in Section 3.5. For wavenumbers near the edges of the visible region, we may expect the target to be estimated at the opposite end of the interval in noisy data. We find that for maximum likelihood estimation the target should be no closer than 1 beamwidth from the edge of the visible region for the trends in probability of outlier discussed so far to hold. Failing this restriction, we require extremely large values of SNR for reasonable accuracy in target location.

At the lower end, it is clear that if the interval of the target location is known to much better than a beamwidth, it restricts the occurrence of outliers. As the interval gets below about 2 beamwidths, the probability of outlier is significantly reduced. This is due to the elimination of even the first side lobe, and depends significantly on the location of the target. For a ½ beamwidth interval, no outliers may occur according to our definition, regardless of the target wavenumber.

Figures 4.14 and 4.15 display the simulation results of the mean square error of wavenumber estimation for various values of a. We observe trends very similar to the results of Section 3.5, using the bounding technique of Weiss and Weinstein. For targets located within one beamwidth of the visible region, the MSE curves indicate extremely poor performance. There is a great deal of difficulty in simulating this region, since even a single outlier will produce a very large error. For these figures, the simulation was performed with 2^{15} trials in the threshold regions. For large enough SNR, the curves all coincide with the Cramér-Rao Lower Bound.

As the interval is reduced, the performance is somewhat more stable, allowing a reasonable estimate of the threshold SNR. However, for values of a such that the interval was less than ½ of a beamwidth, the threshold effect disappears. This is coincident with the disappearance of the outliers discussed earlier. For this region, performance is always below the CRLB and approaches it from below. This effect was predicted by the WWLB, albeit for a larger value of a.

The set of representative arrays, of Table 3.1, will be compared for threshold performance for the case where a = 0.5. The results of the WWLB are compared with the MLE simulations. The threshold results are accurate to

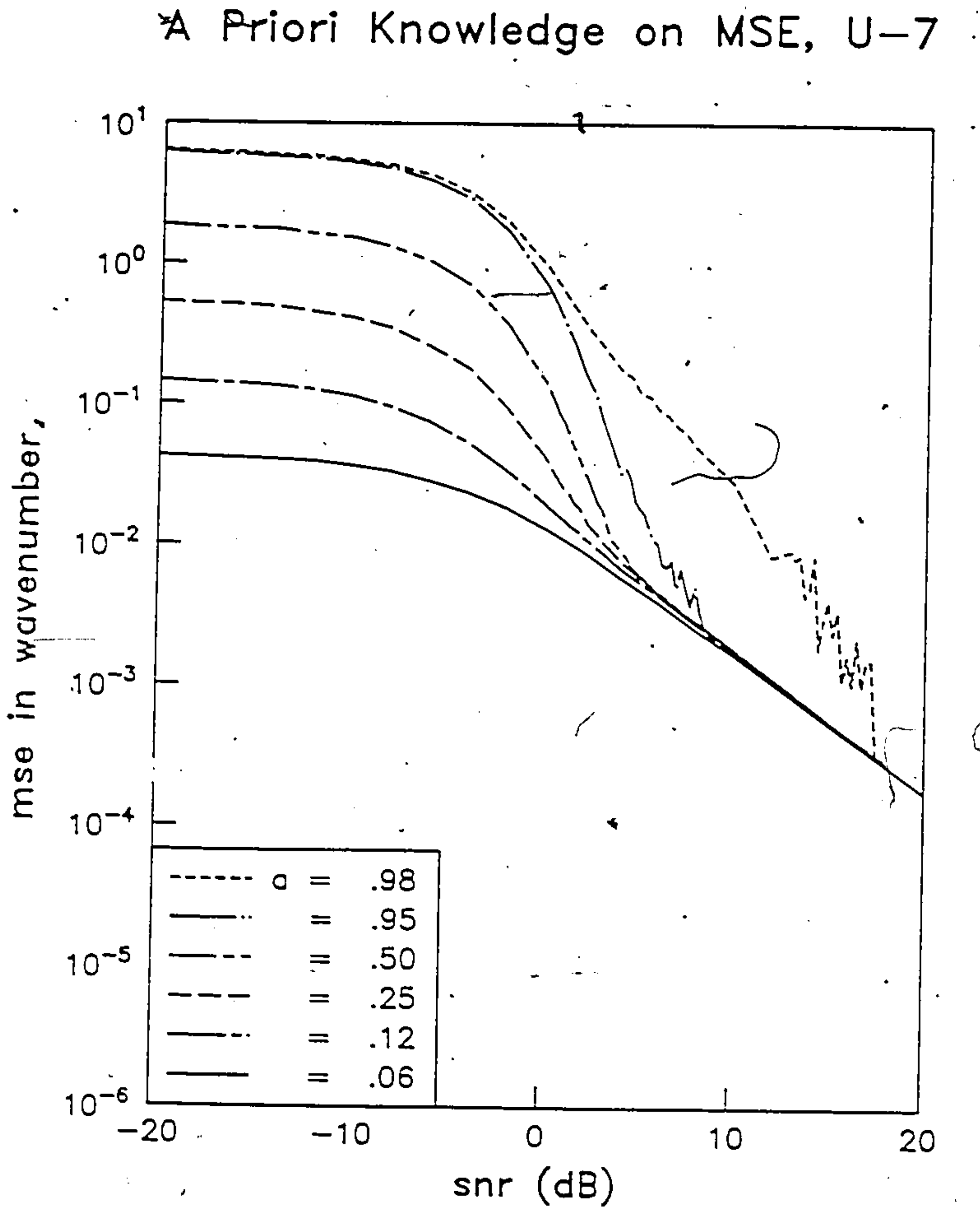

Figure 4.14: Effects of a priori information on the MSE for the 7-element uniform array.

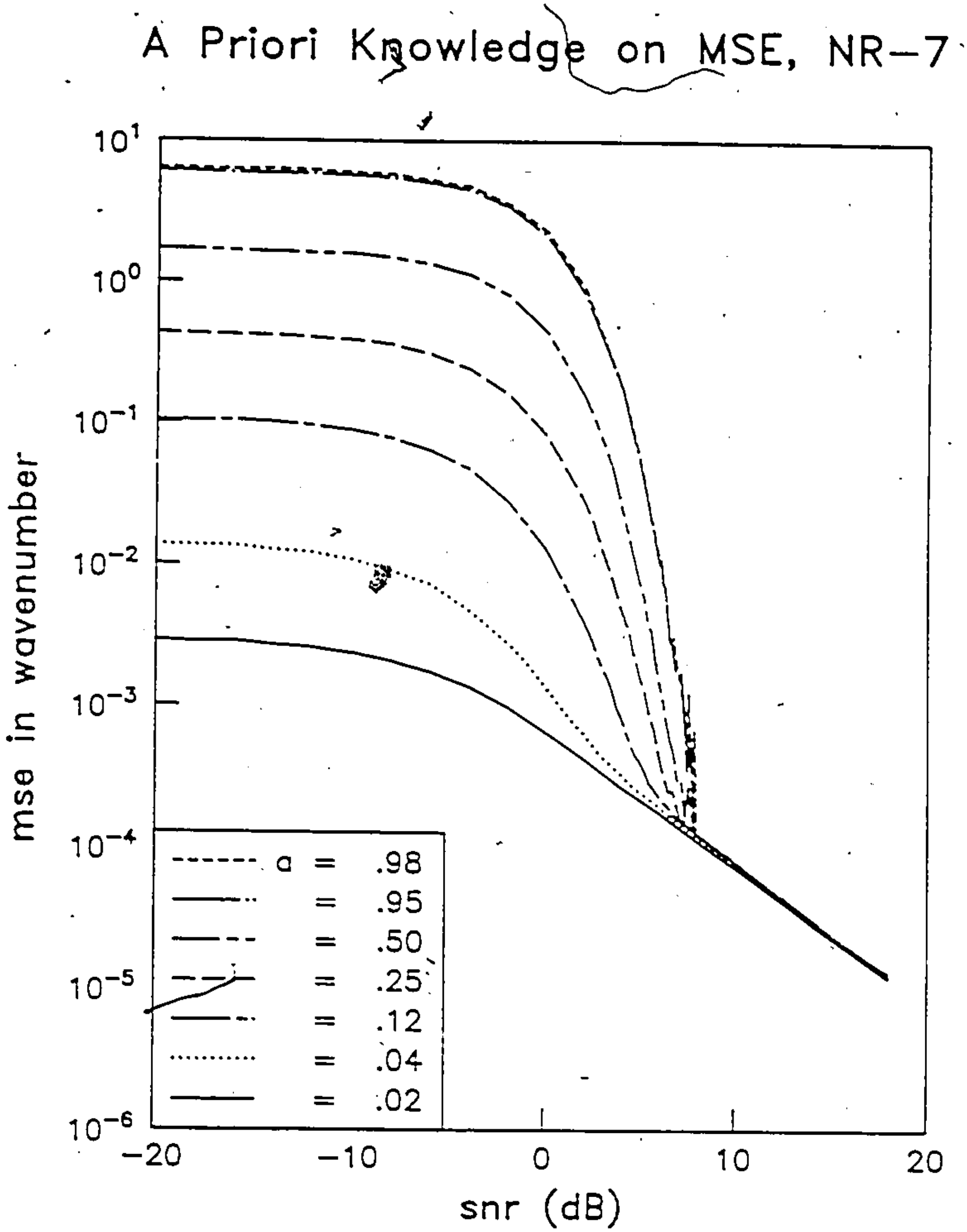

Figure 4.15: Effects of a priori information on the MSE for the 7-element nonredundant array.

approximately 0.3 dB with 99% confidence; they are presented in Tables 4.2a and Table 4.2b. The comparison is done for elemental SNR, Γ, and for total array SNR, $N\Gamma$ respectively.

The MLE was found to approach the WWLB performance for high SNR. As predicted by the WWLB, the threshold array SNR increases with the number of elements as displayed in Table 4.2b and discussed in Chapter 3. At low SNR, the WWLB predicts the qualitative behaviour demonstrated by the MLE; however, the actual location of the threshold points indicates a gap of 9 dB for the 5-element uniform array and 6 dB for the 32-element uniform array. The gap is slightly less than 5 dB for the nonredundant arrays composed of 5 to 10 elements, inclusive.

This gap in performance estimation may be explained a number of ways. It may be that even the WWLB is not tight enough in the threshold region, in which case improved bounds must be sought. It must be remembered that the WWLB is a bound on any estimator. There are bounding techniques which claim to provide performance within 2 dB for the threshold region for MLE type estimators, see [25]. On the other hand, it may be that the maximum likelihood estimator is not the minimum mean square error estimator in the threshold region. This is certainly true for very low SNR, for which the mean square error is $2(2a)^2/12$ and yet the biased estimator, which chooses the midpoint of the interval

Table 4.2a

Sampling Gain and Threshold Comparison
Using Elemental SNR, Γ

No. of Sensors	Array[1] Type	Sampling Gain (dB)	Threshold[2] MLE (dB)	Threshold[3] WWLB (dB)
5	U	0.0	5.0	-4.0
	MR	7.7	8.2	3.3
	NR & UR	9.1	8.5	3.3
6	U	0.0	4.5	-3.5
	MR	9.0	7.8	2.5
	NR & UR	11.2	8.0	3.2
7	U	0.0	4.0	3.4
	MR	9.8	7.2	2.7
	UR	12.1	7.5	2.5
	NR	13.7	7.7	2.9
8	U	0.0	3.5	-3.4
	MR	11.7	7.0	1.5
	UR	14.0	7.5	2.8
	NR	14.9	7.3	2.4
9	U	0.0	3.2	-3.7
	MR & UR	12.4	6.7	1.3
	NR	15.9	7.0	2.3
10	U	0.0	2.9	-3.9
	MR	13.5	6.3	1.2
	UR	16.3	6.7	1.9
	NR	16.6	6.5	1.6
16	U	0.0	1.6	-5.3
32	U	0.0	-.6	-6.8

[1] Arrays correspond to those listed in Table 3.1

[2] Threshold elemental SNR from MLE simulation $k \in (-\pi/2, \pi/2)$

[3] Threshold SNR determined by WWLB for $k \in (-\pi/2, \pi/2)$

Table 4.2b

<u>Sampling Gain and Threshold Comparison</u>
<u>Using Array SNR, $N\Gamma$</u>

No. of Sensors	Array[1] Type	Sampling Gain (dB)	Threshold[2] MLE (dB)	Threshold[3] WWLB (dB)
5	U	0.0	12.0	3.0
	MR	7.7	15.2	10.3
	NR & UR	9.1	15.5	10.3
6	U	0.0	12.3	4.3
	MR	9.0	15.6	10.3
	NR & UR	11.2	15.8	11.0
7	U	0.0	12.5	5.1
	MR	9.8	15.7	11.2
	UR	12.1	16.0	11.0
	NR	13.7	16.2	11.4
8	U	0.0	12.5	5.6
	MR	11.7	16.0	10.5
	UR	14.0	16.5	11.8
	NR	14.9	16.3	11.4
9	U	0.0	12.7	5.8
	MR & UR	12.4	16.2	10.8
	NR	15.9	16.5	11.8
10	U	0.0	12.9	6.1
	MR	13.5	16.3	11.2
	UR	16.3	16.7	11.9
	NR	16.6	16.5	11.6
16	U	0.0	13.6	6.7
32	U	0.0	14.5	8.3

[1] Arrays correspond to those listed in Table 3.1

[2] Threshold array SNR from MLE simulation $k \in (-\pi/2, \pi/2)$

[3] Threshold SNR determined by WWLB for $k \in (-\pi/2, \pi/2)$

$\hat{k} = 0$, will only have an error of $(2a)^2/12$. In fact, the WWLB actually accommodates this estimator. This leads us to believe that there may well be other estimators, which may have better threshold characteristics; although they may not have the equivalent high SNR performance of the MLE.

As discussed earlier, the MLE is closely related to the antenna gain pattern. Although not pursued in this work, the use of windows to suppress the side lobes (although generally increasing the width of the main lobe), may have different characteristics than the MLE. It has been pointed out that windows may increase the MSE at high SNR [48], and as such involve additional tradeoffs for the radar design engineer.

The anomalous behaviour, predicted by the WWLB for the 8- and 10-element unrestricted arrays was also observed using the MLE. They required larger apertures, provided less sampling gain and had poorer threshold SNR values than the equivalent nonredundant arrays. Therefore, we conclude that there is no advantage to choosing these arrays over the nonredundant ones.

The nonredundant arrays generally had threshold performance not larger than 0.3 dB of the minimum redundant arrays and yet provide up to an additional 3 dB of MSE reduction (for N=10). Generally, we would expect that the nonredundant arrays would be preferred over the other nonuniform arrays considered. In terms of probability of outlier, the results are similar. The primary tradeoff is for the uniform arrays versus the nonredundant ones. We summarize the simulations to obtain the result that the nonredundant arrays require approximately a 2 dB larger elemental SNR to provide the same probability of outlier as the uniform arrays. The benefit is an improved MSE at the higher SNR values of 9.1 dB for the case N=5, to 16.6 dB for N = 10. That is, provided the data can be averaged for the additional time, or the SNR is above the critical point for one snapshot, the 10-element nonredundant array will provide a mean square estimation error 45 times smaller than the 10-element uniform array.

CHAPTER 5

MULTIPATH

5.1 Some Preliminaries

In this chapter we consider a direction of arrival estimation problem that is different from the one studied in the previous two chapters. The situation now involves two coherent plane waves. Of particular interest is the case of a single target flying close to the water surface such that the radar receives both the direct target as well as an image reflected from the water surface. This reflection may have all the characteristics of a second target at the radar. When reflections or multiple signals are received from a single target, the phenomenon is known as multipath.

For radars in the gigahertz region, and low flying targets, the reflection from the water surface is highly specular. That is, the image appears at the radar with an amplitude almost equal to the direct signal but with a fixed and unknown phase difference. It is of great concern when the separation between the two signals is less than a beamwidth. Many high-resolution estimation schemes have been proposed for precisely these conditions. A good survey of the earlier techniques may be found in [28] which are based upon spectral estimation. Recently, several new techniques have also been studied which use an eigenvalue decomposition of the autocorrelation matrix of received data, [43,49]. Throughout this time, the maximum likelihood estimator has also been studied, [55, 56], and many of the previous works compare performance to the MLE. The primary advantage of the other estimators occurs for large numbers of targets, for which the estimation schemes often require only a minor increase in computation. In all cases, the goal is to achieve maximum likelihood performance with less computational effort. The maximum likelihood estimator, as it is proposed here, requires a nonlinear search over K dimensional space for K targets. A recent paper, [50], provides a useful overview of these new methods and compares them to the MLE.

For two targets, or one target with a direct and specular image, we find the maximum likelihood estimator to be well suited for the direction of arrival estimation problem. It will be derived for use with an arbitrary linear array geometry and studied for threshold effects as well as high SNR performance. We find that performance may be significantly affected both by the separation between image and target, as well as by the phase difference between them. Therefore, it would be unsuitable to model any of these parameters as random variables. In this sense random parameter estimation bounds such as the Weiss-Weinstein bound are not applicable. The literature does not contain reference to any other nonrandom parameter bounds which might be applied in the multiple target environment. At any rate, we find the Cramér-Rao Lower Bound (for nonrandom parameters) to be a useful indicator of the MLE performance at high SNR.

Early in the research, it was proposed to build a sampled-aperture radar with sufficient accuracy to examine the performance of high-resolution estimation algorithms. The specifications of the hardware may be found in Appendix C, with the pertinent details and experiment description outlined in the body of this chapter.

Finally, we examine the performance of the seven-element nonredundant array and compare it to various uniform arrays. This is a 'real-world' demonstration of the practicality of the new array structures for use in direction of arrival estimation in multipath. The performance is compared using data that has all of the characteristics associated with real data including calibration and placement accuracy limitations, as well as possible modelling limitations.

5.2 MLE Derivation

We follow the technique of [49], in the development of the maximum likelihood estimator for two plane waves, with a straightforward extension to nonuniform arrays. The derivation is similar to that used in Chapter 4, Section 4. Let the target and image be described by the parameter vectors as follows, respectively,

$$\alpha_t = (k_t , a_t , \theta_t)^T \tag{5.1a}$$

and

$$\alpha_i = (k_i , a_i , \theta_i)^T \tag{5.1b}$$

Using the conventions described in Chapter 4, we obtain

$$\begin{aligned} z &= s(\alpha_t) + s(\alpha_i) + w \\ &= c_t y(k_t) + c_i y(k_i) + w \end{aligned} \tag{5.2}$$

for the received data from each sensor, where $y(k)$ is defined by equation (4.2) and c_t , c_i are the complex amplitudes. As before, the noise is assumed white, Gaussian of zero mean and variance σ^2 with the real and imaginary portions independent. It is convenient to use a matrix notation for this problem, and so we require the definition of two new symbols. We define the matrix

$$Y = [\, y(k_1) \,\vdots\, y(k_2) \,] \tag{5.3}$$

and a complex-valued vector as

$$c = (\, c_1 \,.\, c_2 \,)^T \tag{5.4}$$

We can now write the probability density function of the received data given the parameter sets, as

$$p(z/\alpha_1 . \alpha_2) = (2\pi\sigma^2)^{-N} \exp\left\{- \frac{\| z - Yc \|^2}{2\sigma^2}\right\} \tag{5.5}$$

The maximum likelihood estimates are those values for which

$$\Lambda = \| z - Yc \|^2 \tag{5.6}$$

is a minimum. As in Section 4.1, this linear least squares problem can be solved for c (see [46]), by noting that at the minimum, say $\hat{c}$, $z-Y\hat{c}$ is orthogonal to the surface Yc. We therefore have

$$(Yc)^H (z-Y\hat{c}) = 0 \tag{5.7}$$

Since c is a free parameter, we may also write

$$Y^H z - Y^H Y\hat{c} = 0 \tag{5.8}$$

Making use of the pseudo-inverse, we obtain

$$\hat{c} = (Y^H Y)^{-1} Y^H z \tag{5.9}$$

Substitution of this result into equation (5.6) yields

$$\Lambda = \| z - Y(Y^HY)^{-1}Y^Hz \|^2$$
$$= z^Hz - z^HY(Y^HY)^{-1}Y^Hz \qquad (5.10)$$

Therefore the maximization now reduces to minimizing the scalar

$$\Lambda' = z^HY(Y^HY)^{-1}Y^Hz \qquad (5.11)$$

Define the scalars D_m and ρ as follows:

$$D_m = y^H(k_m)z \qquad (5.12)$$

and $$\rho = y^H(k_1)y(k_2) \qquad (5.13)$$

The previous equation (5.11) can then be simplified further since,

$$Y^Hz = (D_1 \ . \ D_2)^T \qquad (5.14)$$

and $$(Y^HY)^{-1} = \begin{bmatrix} N & \rho \\ \rho^* & N \end{bmatrix}^{-1}$$

$$= (N^2 - \rho\rho^*)^{-1} \begin{bmatrix} N & -\rho \\ -\rho^* & N \end{bmatrix} \qquad (5.15)$$

The expression thus reduces to maximizing the new scalar

$$\Lambda'' = \frac{|D_1|^2 + |D_2|^2 - 2\,\mathrm{Re}\{ \rho D_1^* D_2/N \}}{N^2 - |\rho|^2} \qquad (5.16)$$

The maximum likelihood estimate is found by performing a 2-dimensional search in wavenumber for pairs of values k_1, k_2.

The maximization will be performed by first implementing a coarse grid search. The values of ρ, which are independent of the data, may be precalculated for all pairs of k_1, k_2 used in the coarse search.

Before presenting the simulation results, we will derive the Cramér-Rao Lower Bound for this problem. In this way the simulation performance may be compared to the bounding results.

5.3 CRLB for the Multipath Problem

The CRLB has been derived for the multipath problem by other authors, for example [51] and [48], and as such, we present only a brief derivation here. For greater detail, we refer the interested reader to [44]. The procedure is similar to that of [48], where it was initially derived for an arbitrary linear array; however, the majority of their results were obtained assuming a uniformly spaced array. Although the extensions are straightforward, we wish to stress those properties which will hold for the nonuniform array structures considered in this work.

We require the determination of the Fisher Information matrix J, whose terms are defined by

$$J_{im} = - E\left\{ \frac{\partial^2}{\partial\alpha_i \ \partial\alpha_m} \ln\left[p(z/\alpha)\right] \right\} \tag{5.17}$$

The parameter set is defined as

$$\alpha_{3i-2} = k_i \tag{5.18a}$$

$$\alpha_{3i-1} = a_i \tag{5.18b}$$

$$\alpha_{3i} = \theta_i \qquad i=1,2 \tag{5.18c}$$

The terms of equation (5.17) can now be rewritten as

$$J_{3i-2,3m-2}$$

$$= \mathrm{Re}\left\{a_i a_m \exp\{j(\theta_i-\theta_m)\} \sum_n x_n^2 \exp\{j(k_i-k_m)x_n\}\right\} / \sigma^2$$

$$J_{3i-2,3m-1} = \mathrm{Re}\left\{ja_i e^{j(\theta_i-\theta_m)} \sum_n x_n e^{j(k_i-k_m)x_n}\right\} / \sigma^2$$

$$J_{3i-2,3m} = \mathrm{Re}\left\{a_i a_m e^{j(\theta_i-\theta_m)} \sum_n x_n e^{j(k_i-k_m)x_n}\right\} / \sigma^2$$

$$J_{3i-1,3m-2} = \mathrm{Re}\left\{-ja_m e^{j(\theta_i-\theta_m)} \sum_n x_n e^{j(k_i-k_m)x_n}\right\} / \sigma^2$$

$$J_{3i-1,3m-1} = \mathrm{Re}\left\{e^{j(\theta_i-\theta_m)} \sum_n e^{j(k_i-k_m)x_n}\right\} / \sigma^2$$

$$J_{3i-1,3m} = \mathrm{Re}\left\{-ja_m e^{j(\theta_i-\theta_m)} \sum_n e^{j(k_i-k_m)x_n}\right\} / \sigma^2$$

$$J_{3i,3m-2} = \mathrm{Re}\left\{a_i a_m e^{j(\theta_i-\theta_m)} \sum_n x_n e^{j(k_i-k_m)x_n}\right\} / \sigma^2$$

$$J_{3i,3m-1} = \mathrm{Re}\left\{ja_i e^{j(\theta_i-\theta_m)} \sum_n e^{j(k_i-k_m)x_n}\right\} / \sigma^2$$

$$J_{3i,3m} = \mathrm{Re}\left\{a_i a_m e^{j(\theta_i-\theta_m)} \sum_n e^{j(k_i-k_m)x_n}\right\} / \sigma^2$$

(5.19a-i)

The bound on the wavenumber becomes

$$E\{\ (\hat{k}_1 - k_1)^2\ \} \geq J^{11} \tag{5.20}$$

where J^{11} is the first diagonal element in J^{-1}. It can be shown that

$$J^{11} = Q^{11}/\Gamma \tag{5.21}$$

where Γ equals $a_1/2\sigma^2$, and Q^{11} is independent of a_1, a_2 and σ^2, [48]. Therefore, the CRLB is again inversely proportional to SNR and is independent of the amplitude of the interfering signal.

At this point, the work of [48] assumes uniform spacing of the array. We will use a similar technique without restricting the samples to be uniformly spaced and show that similar properties hold for the nonuniform arrays discussed in this work.

From equation (5.19a-i), it is clear that the Fisher Information matrix, and hence the bound, is only dependent upon the difference in phase and wavenumber of the two targets and not on the absolute value of either of these parameters.

The CRLB is periodic in phase θ_1 or θ_2 with period π. This property requires a simple proof as follows.

Consider the submatrix

$$M_{im} = \begin{bmatrix} J_{3i-2,3m-2} & J_{3i-2,3m-1} & J_{3i-2,3m} \\ J_{3i-1,3m-2} & J_{3i-1,3m-1} & J_{3i-1,3m} \\ J_{3i,3m-2} & J_{3i,3m-1} & J_{3i,3m} \end{bmatrix} \tag{5.22}$$

Then the Fisher matrix can be written as

$$J = \begin{bmatrix} M_{11} & M_{12} \\ M_{21} & M_{22} \end{bmatrix} \tag{5.23}$$

where M_{11} and M_{22} are independent of wavenumber and phase. Now let $\theta_1' = \theta_1 + \pi$. From (5.19) we find that $M_{12}' = -M_{12}$, $M_{21}' = -M_{21}$, $M_{11}' = M_{11}$ and $M_{22}' = M_{22}$. Therefore

$$J' = \begin{bmatrix} M_{11} & -M_{12} \\ -M_{21} & M_{22} \end{bmatrix}$$

$$= \begin{bmatrix} I_3 & O_3 \\ O_3 & -I_3 \end{bmatrix} J \begin{bmatrix} I_3 & O_3 \\ O_3 & -I_3 \end{bmatrix} \tag{5.24}$$

where I_3 is the 3x3 identity matrix and O_3 is the 3x3 zero matrix. The inverse of the primed Fisher matrix is

$$(J')^{-1} = \begin{bmatrix} I_3 & O_3 \\ O_3 & -I_3 \end{bmatrix} J^{-1} \begin{bmatrix} I_3 & O_3 \\ O_3 & -I_3 \end{bmatrix} \tag{5.25}$$

which leaves the diagonal submatrices equal to those of J^{-1}. Therefore the diagonal elements of $(J')^{-1}$ are identical to the diagonal elements of J^{-1} and the CRLB is unchanged. This shows that the CRLB is periodic in θ_1. Clearly, the same argument can be made with respect to θ_2, thereby completing the proof.

We note that the structures being examined have element positions which may be written as integer multiples of the minimum spacing, in our case normalized to be 1 unit. It follows from inspection of (5.19a-i) that the matrix, J, is periodic in the normalized wavenumber with value 2π, since the x_n are all integers. In general, if the x_n are all integer multiples of d, not necessarily uniform, then the CRLB is periodic in wavenumber with period $2\pi/d$.

For the remainder of this section, we will examine the CRLB when the amplitudes of the two targets are equal. We expect to use the estimator under conditions in which there will be a strong specular reflection. For the case in which the amplitudes are equal and the phase difference is 0° or 180°, the worst case conditions result. This can also be thought of as the opposite condition to that examined in Chapter 4. In this framework, the single target case might be considered to correspond to the case in which the image amplitude is 0.. Other conditions would lie somewhere between the zero amplitude image and the equal amplitude image.

When we speak of the phase, or phase difference, we understand this to be measured at the midpoint of the array. Further, since the CRLB for the MSE of wavenumber estimation is inversely proportional to the elemental SNR, Γ, we evaluate it for $\Gamma = 0$ dB. The value for any other SNR is then simply obtained by subtracting from the quoted value the desired operating SNR determined in dB..

Using a 7-element nonredundant array, (see Table 3.1), Figure 5.1 demonstrates the variation of the CRLB with phase difference, θ, for various wavenumber separations. The range of separation extends from a third of a beamwidth to approximately six beamwidths, where one beamwidth equals $2\pi/25$ in normalized wavenumber. The dependence on phase may, in certain instances be quite severe, particularly for separations less than a beamwidth. The curves do in fact have a period of π. Although the plots seem to be even about the worst-case phase point, they are not exactly symmetrical. In addition, the worst-case phase point varies with separation. In general a search is required to accurately determine this point. For the case in which $k_1-k_2 = 2\pi/6$, the worst-case phase point occurs at approximately 16°, and the minimum CRLB phase is 106°. It was observed that as the separation gets well below a beamwidth, the maximum CRLB phase difference tends to 0° when measured at the midpoint of the array. The best phase

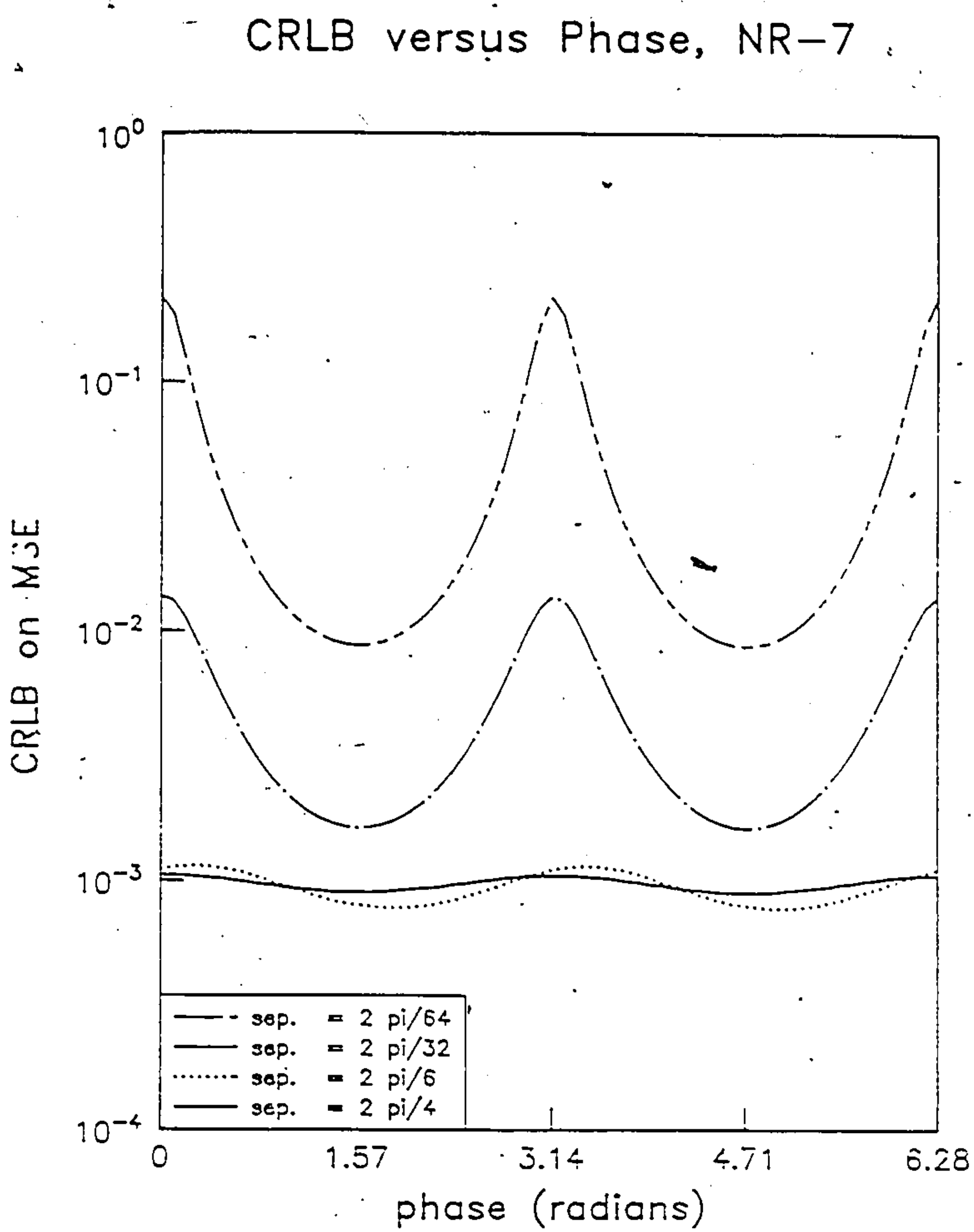

Figure 5.1: Variation of the CRLB with phase difference for several target/reflection separations for the 7-element nonredundant array.

difference tends to 90° under the same conditions.

Given this variation with phase difference, it becomes instructive to examine the CRLB versus separation for the worst and best-case phase differences. This is evaluated for the 7-element uniform and nonredundant arrays and presented in Figure 5.2. Also shown in the figure are the bounds for a single target at the same SNR (0 dB), which appear as horizontal lines in the plot. This gives an idea of the variation that can be expected with phase for the two array structures.

The 7-element uniform array is significantly more sensitive to phase difference at the smaller separations. For a single target, the 7-element nonredundant array has a performance improvement of 13.7 dB. For small separations, this improvement may be much greater.

5.4 MLE Simulation Results

In this section we examine the implementation of the maximum likelihood estimator as it will be used for the multipath problem. It is to be used for the estimation of target position when that target is low over the water surface. It is instructive to examine the performance using simulated data to analyze the required coarse search density, and threshold effects, as well as the high SNR performance.

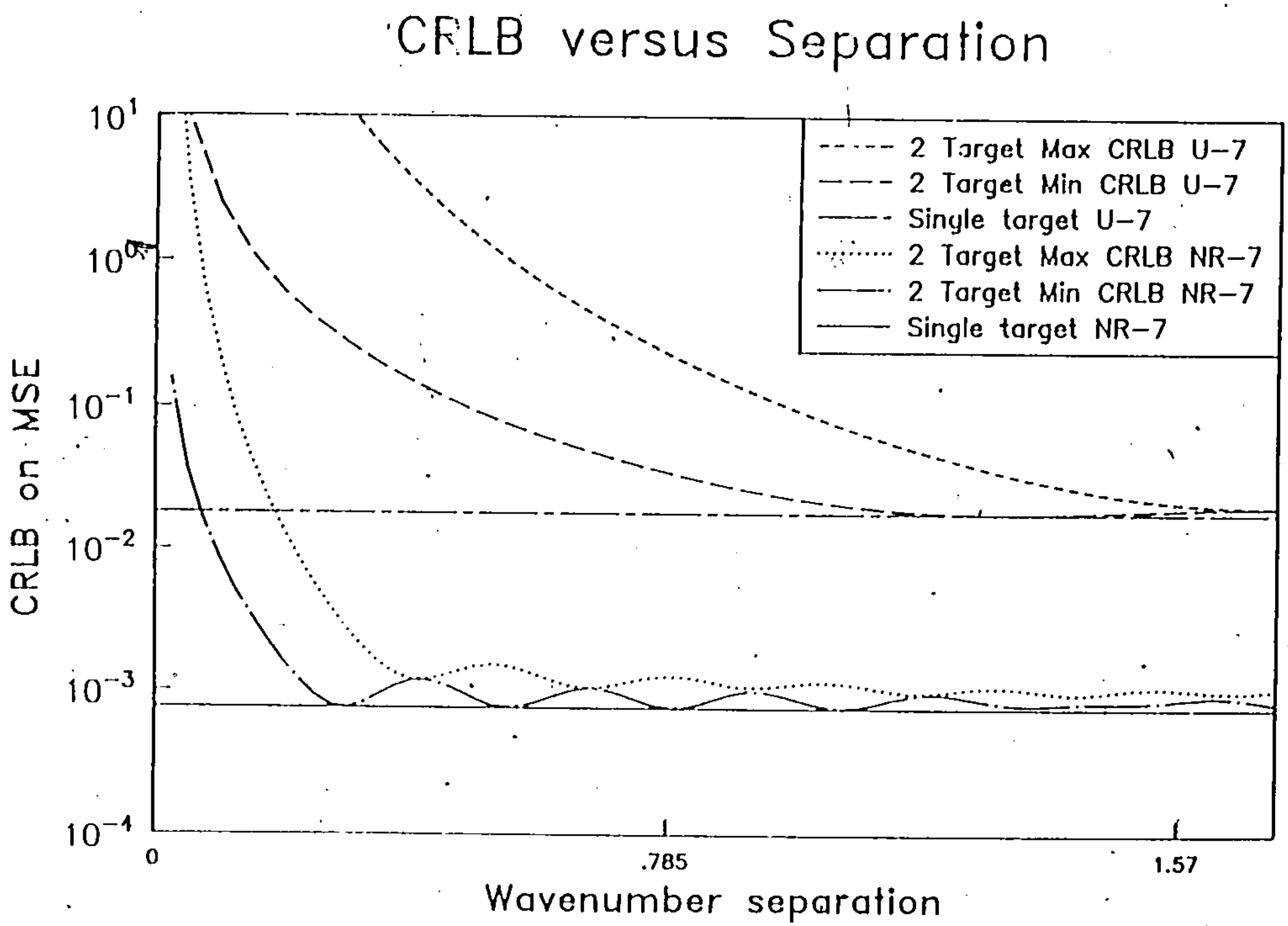

Figure 5.2: Comparison of best- and worst-case phase impact for CRLB versus separation for 7-element uniform and nonredundant arrays and the single target CRLB is provided for reference.

Since we expect to use the estimator under conditions with a strong specular reflection, the simulated data was generated using equal amplitude target and image. Of course, the estimator makes no assumptions about the relative strengths of the targets. It is assumed that the height of the array above the water surface is known. The horizon angle for the structure may then be calculated. We search for a target above the horizon and for an image below the horizon, corresponding to a reflection from the water surface.

The maximum likelihood estimator then chooses pairs of candidates (D_1, D_2), D_1 from the target domain, D_2 from the reflected image domain according to (5.12) and evaluates the objective function (5.16). The pair of values which maximize the objective function are then considered to be the estimates of the target and image wavenumber. In all of our simulations, we measure the mean square error of the target estimate from the 'true' target position.

For the simulations we simply set the horizon to be at $k = 0$, with the target having a positive wavenumber and the image wavenumber negative. The set of N_c 'steering' vectors, $y(k)$, used in the coarse search are generated prior to any estimation from equation (4.2). This requires $2N_cN$ floating-point numbers to be stored. In addition, we also evaluate the set of corresponding values of ρ, and $(N^2-|\rho|^2)$

using equation (5.13) which require $3N_c^2$ floating-point storage locations.

The fine search consists of iterative evaluations of the objective function, surrounding the previous level estimate. The number of levels is calculated to provide the desired accuracy in wavenumber. This technique is almost entirely limited in terms of computation time, by the coarse search density, which requires $(N_c/2)^2$ objective function evaluations. There are in fact $(N_c/2)$ in each of the target and image domains.

The first priority is the determination of a suitable coarse density. As was done earlier, we establish the required density from a statistical viewpoint. We will tolerate a 2 dB error in SNR in the threshold region and anticipate the threshold may vary with phase; therefore, the analysis will require several cases.

For large separations in wavenumber, it is reasonable to assume a value equivalent to that obtained from the single target estimation of Chapter 4 would be sufficient. We examine the performance for various coarse search densities with a 7-element nonredundant array which has a beamwidth of $2\pi/25$. The target and image are simulated with equal amplitudes and are located at $\pm\ \pi/4$. The CRLB is a minimum at 91° and a maximum at 1°. Figures 5.3 and 5.4 present the results of these simulations consisting of 1024

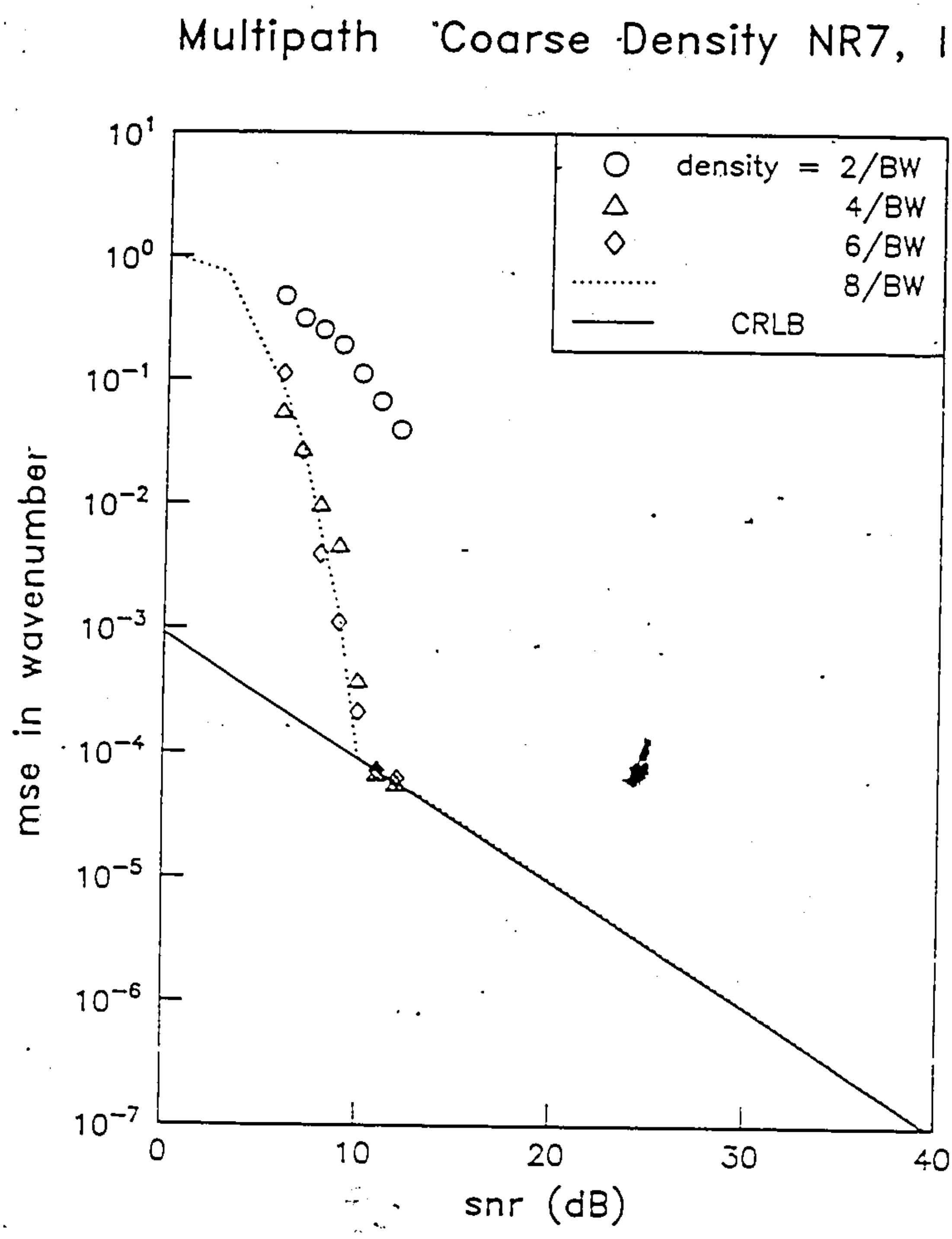

Figure 5.3: Effects of the coarse search density on the best-case phase difference for the 7-element nonredundant array when target separation is $2\pi/4$.

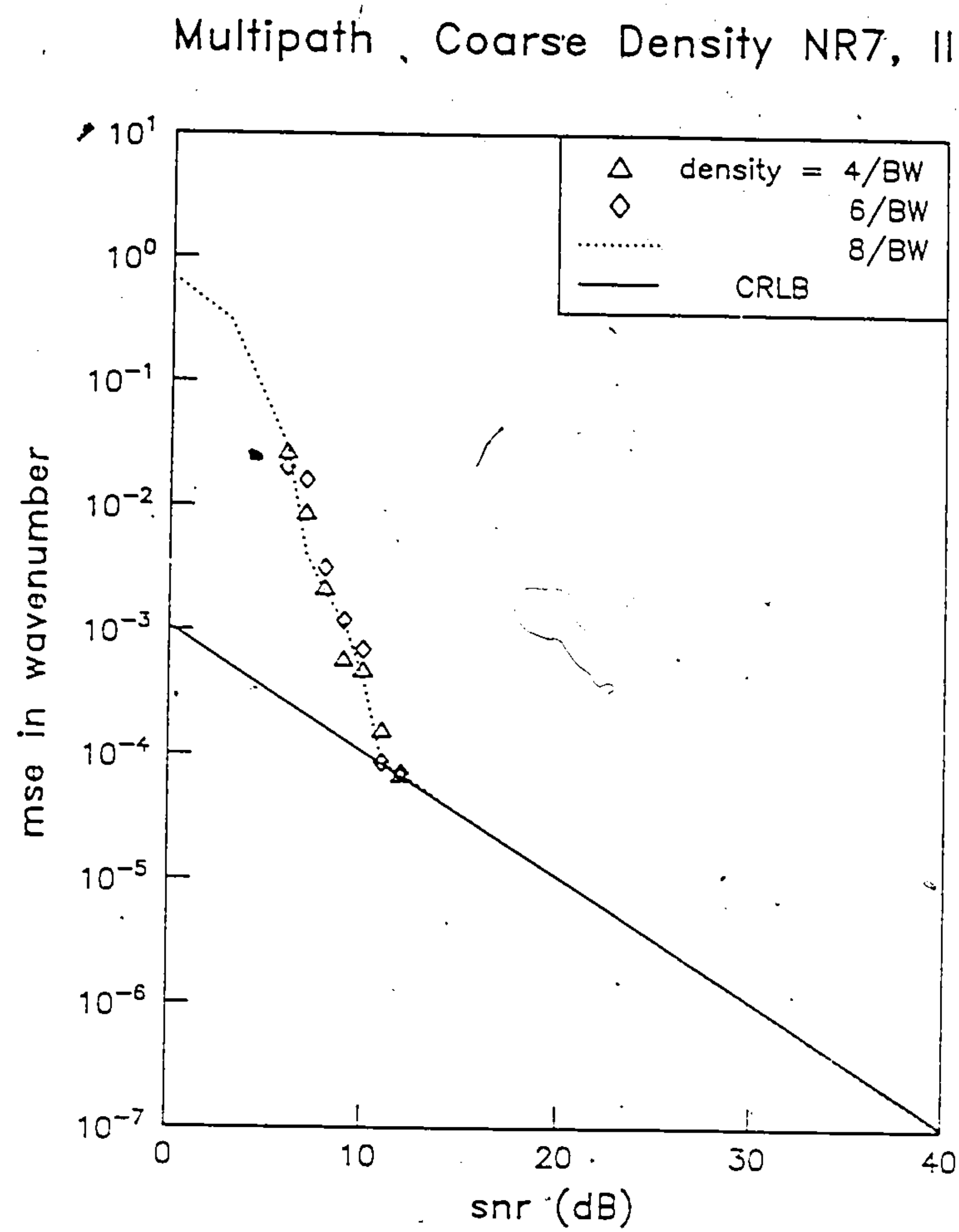

Figure 5.4: Effects of the coarse search density on the worst-case phase difference for the 7-element nonredundant array when target separation is $2\pi/4$.

trials. We find that there was little difference in performance beyond 4 points per beamwidth. Similar results were found in Chapter 4 for the single target case.

For small separations, less than a beamwidth, we find the density must be increased further. In general, we found an average of 3 points between target and image separation was adequate for the nonredundant arrays. In Figures 5.5 and 5.6 the separation is $2\pi/64$, corresponding to less than half a beamwidth of the 7-element nonredundant array. We found that for the 1° phase difference of Figure 5.6, the performance characterization required between 4 and 6 points per beamwidth, $(2\pi/25)$, for the coarse search density. Since the horizon point is known and we always begin the coarse search just on either side of it, we guarantee having coarse search samples between the target and image. As a general rule, we require a density greater than the minimum separation of target and image for which accurate position estimates are desired.

The 7-element uniform array performance is also examined for the effect of the coarse density search. Figures 5.7 and 5.8 exhibit the effect when the spacing between target and image is $2\pi/4$, with the best- and worst-phase conditions. There would appear to be nothing gained by increasing the coarse search density beyond 2 samples per beamwidth. However, for separations less than a

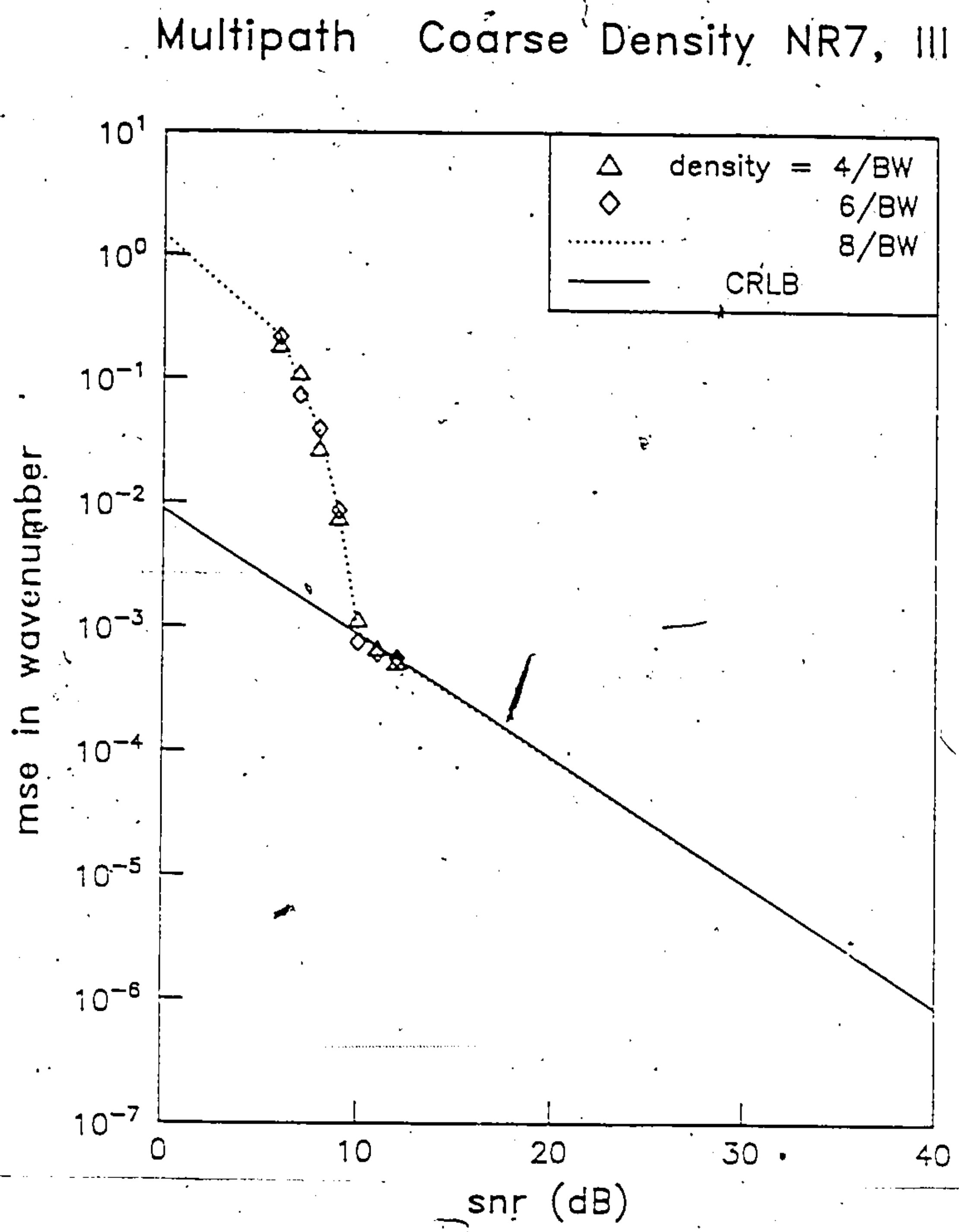

Figure 5.5: Effects of the coarse search density on the best-case phase difference for the 7-element nonredundant array when target separation is $2\pi/64$.

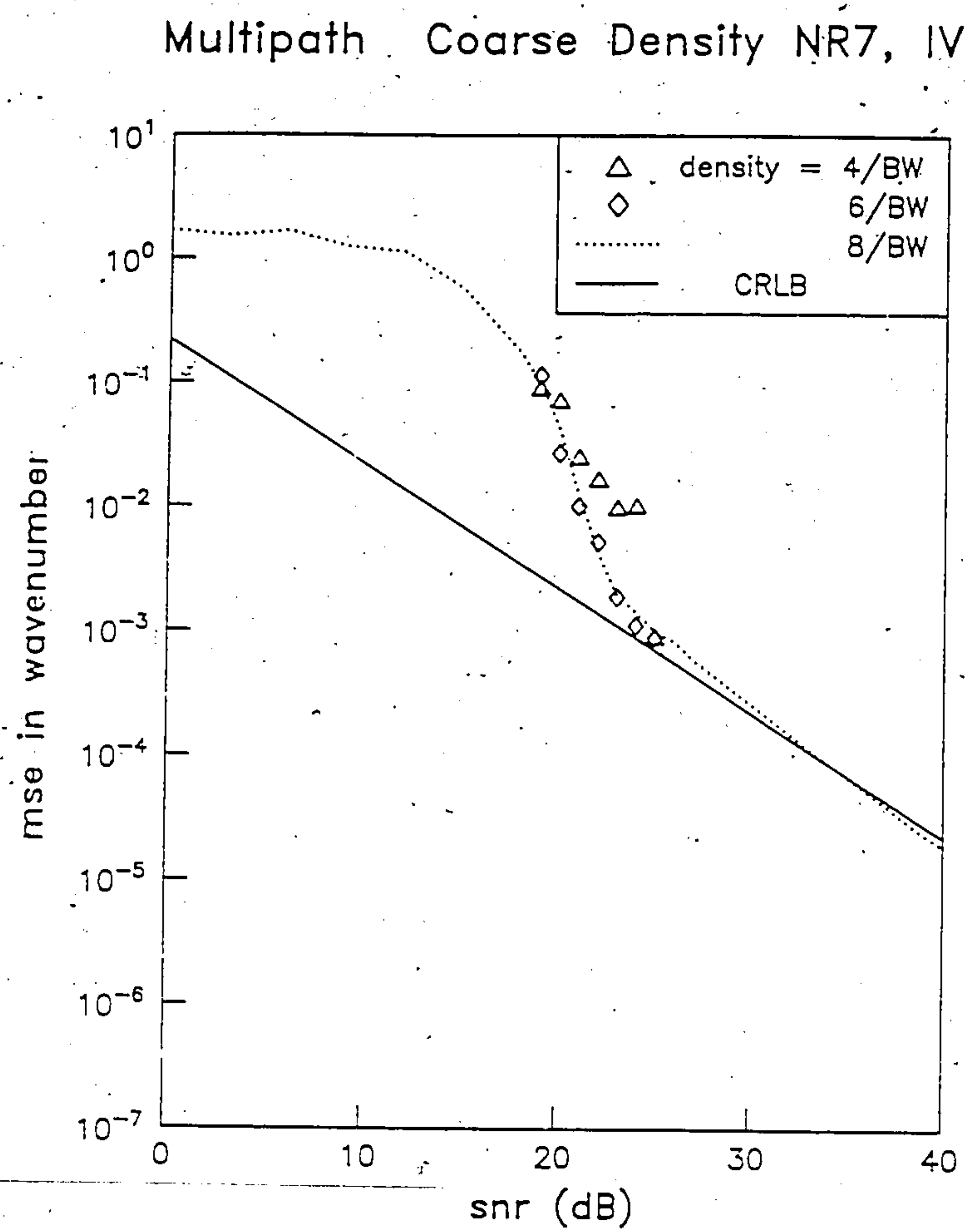

Figure 5.6: Effects of the coarse search density on the worst-case phase difference for the 7-element nonredundant array when target separation is $2\pi/64$.

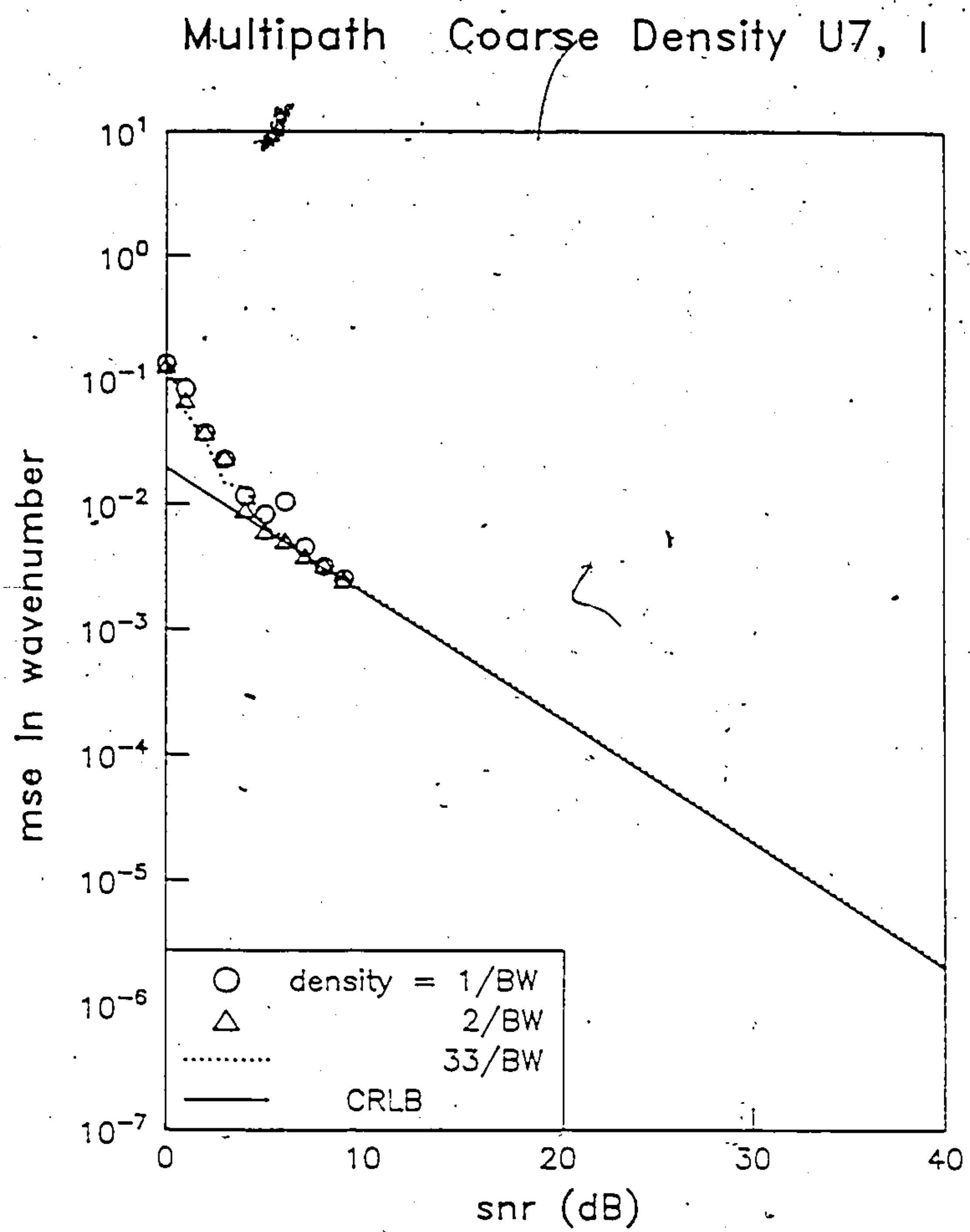

Figure 5.7: Effects of the coarse search density on the best-case phase difference for the 7-element uniform array when target separation is $2\pi/4$.

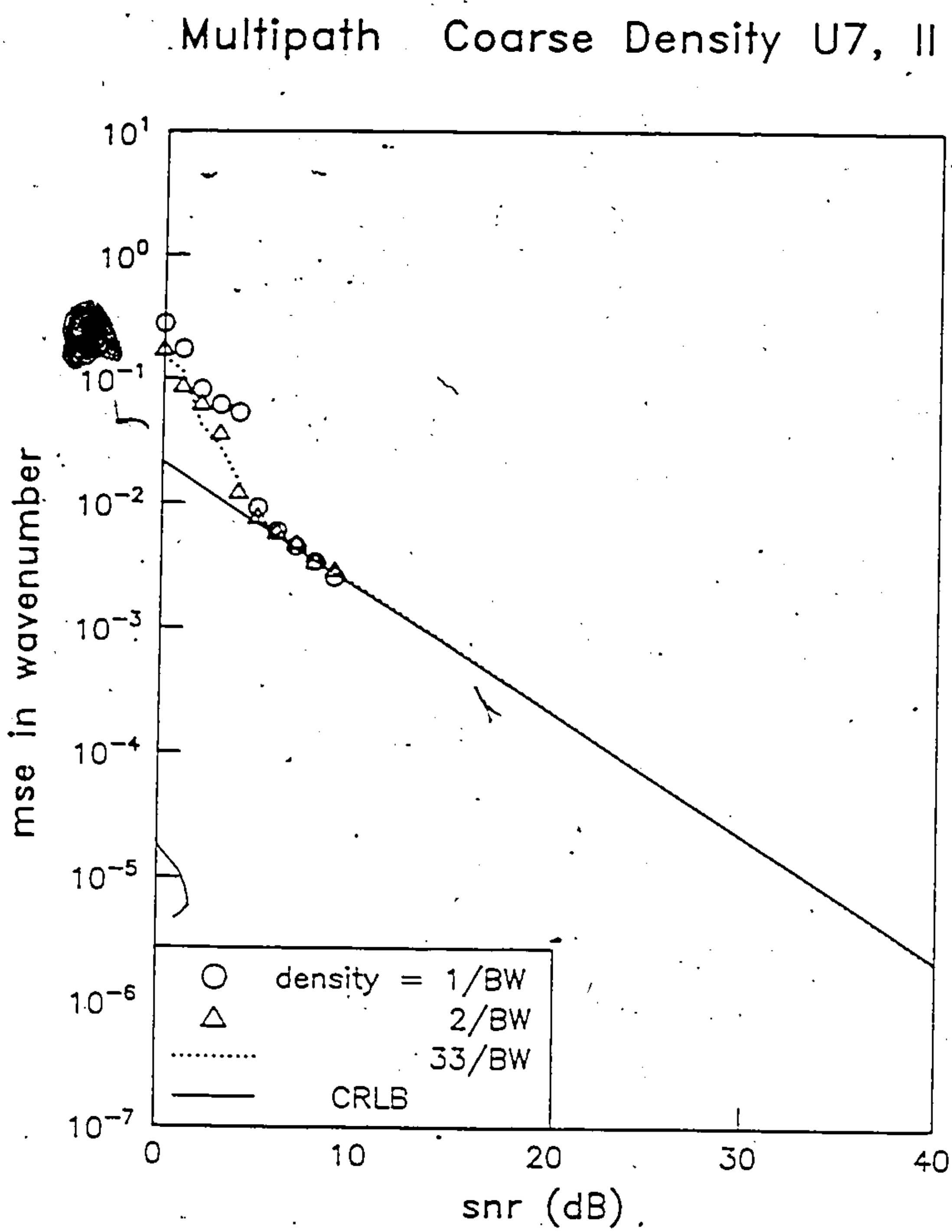

Figure 5.8: Effects of the coarse search density on the worst-case phase difference for the 7-element uniform array when target separation is $2\pi/4$.

beamwidth this is no longer true. The uniform array was applied to a target-image separation of $2\pi/32$, or slightly less than a fifth of a beamwidth, and displayed in Figures 5.9 and 5.10. The worst phase condition, Figure 5.10, clearly demonstrates the need for a greater sampling density. There was a significant improvement in going from 9 to 17 samples per beamwidth and virtually no improvement beyond this point. The use of 17 samples per beamwidth corresponds to approximately 3 samples between target and image.

From this point on, all arrays are compared with the same computational effort. We use a coarse search density of $2\pi/200$, which was adequate for, separations down to $2\pi/64$. This requires about 10,000 objective function evaluations for each simulation. The worst-case phase is demonstrated for that value of phase near 0°, and the best case phase used was the value close to 90°.

We summarize the performance for the two seven-element arrays with various separations between image and target in Figures 5.11 to 5.15. At $2\pi/4$, Figure 5.11, the separation is well over a beamwidth for both the uniform and nonredundant arrays. There is very little sensitivity in the high SNR region to phase difference. The nonredundant array provides about 13 dB of sampling gain in this region. The threshold SNR values are also not susceptible to the

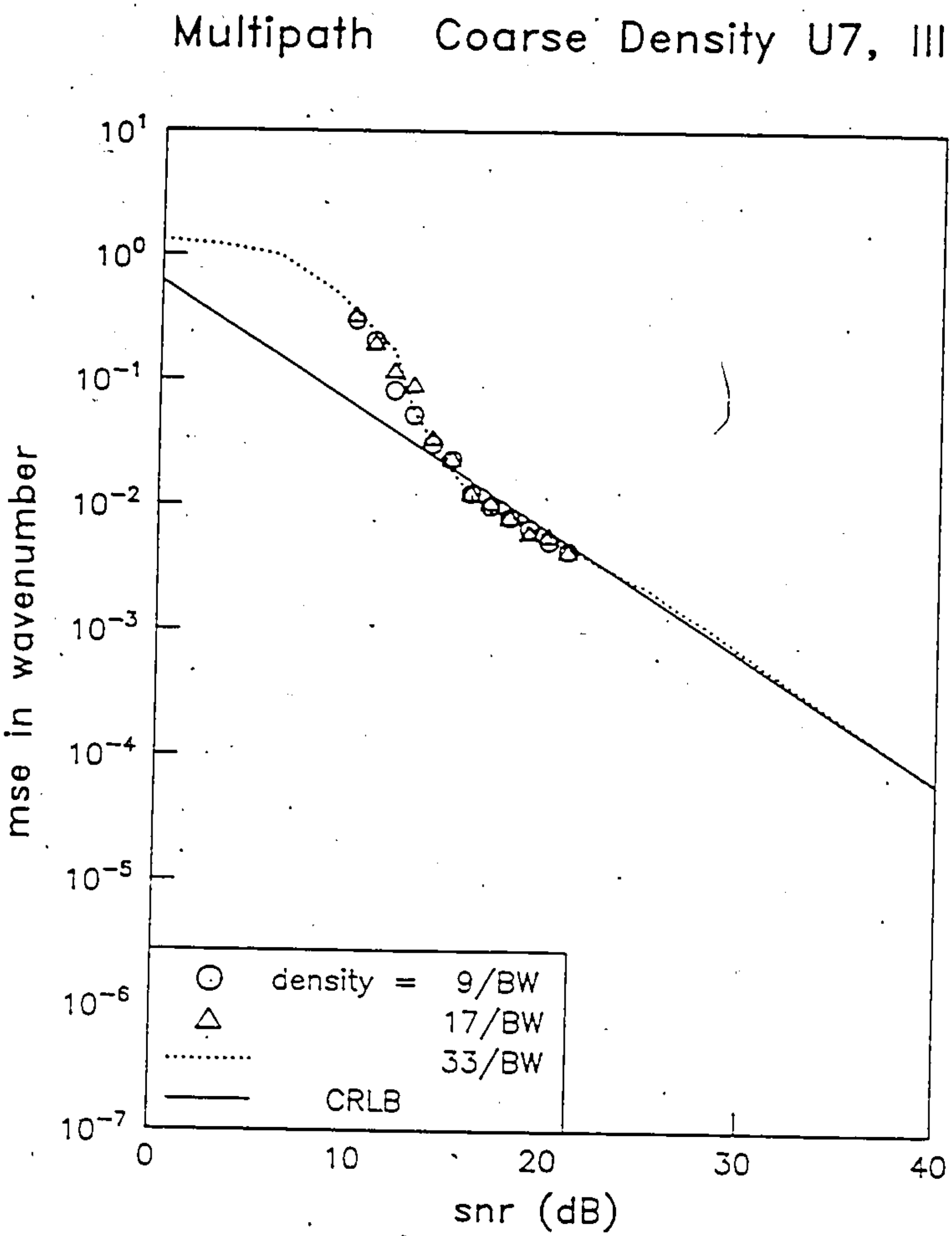

Figure 5.9: Effects of the coarse search density on the best-case phase difference for the 7-element uniform array when target separation is $2\pi/32$.

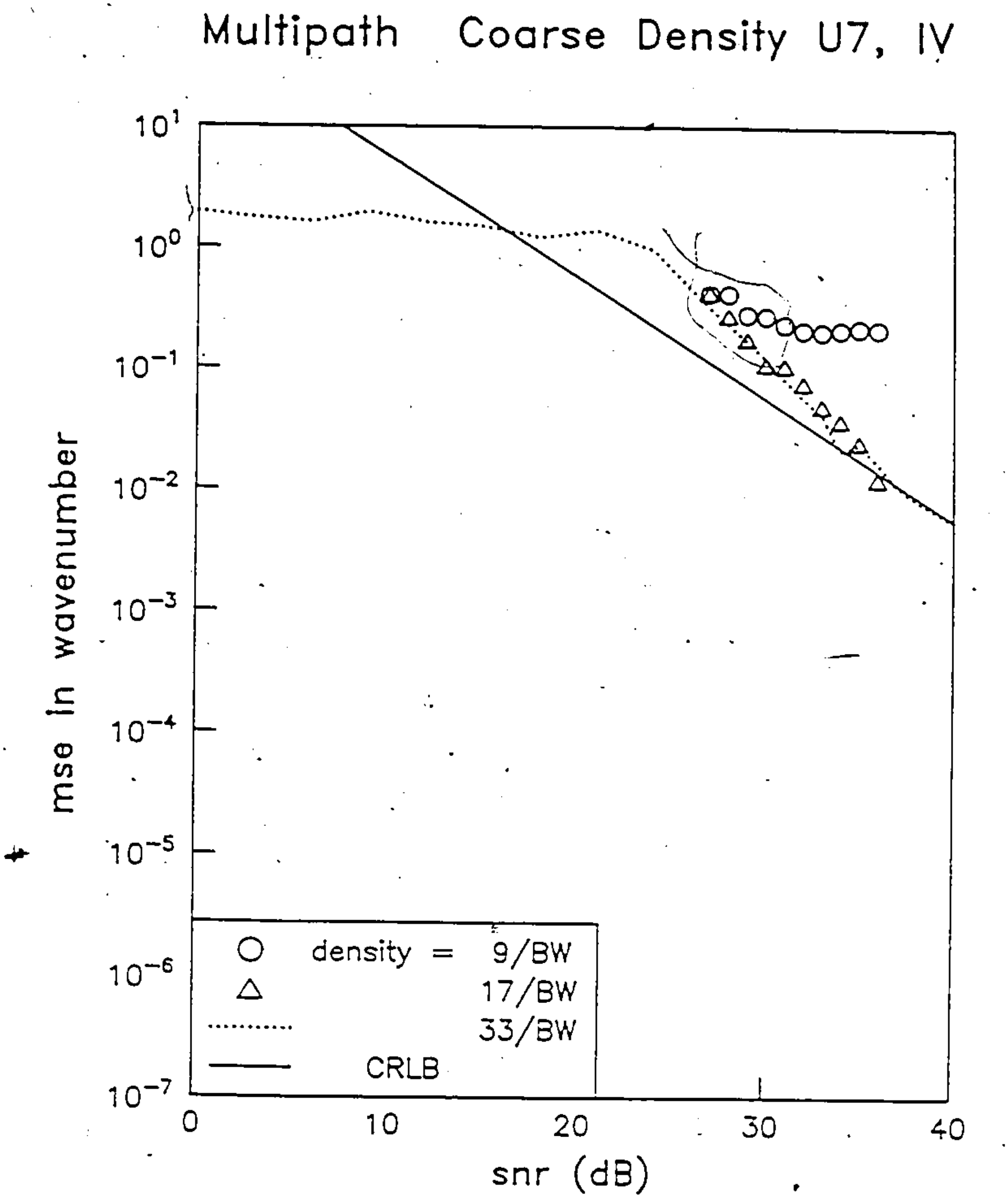

Figure 5.10: Effects of the coarse search density on the worst-case phase difference for the 7-element uniform array when target separation is $2\pi/32$.

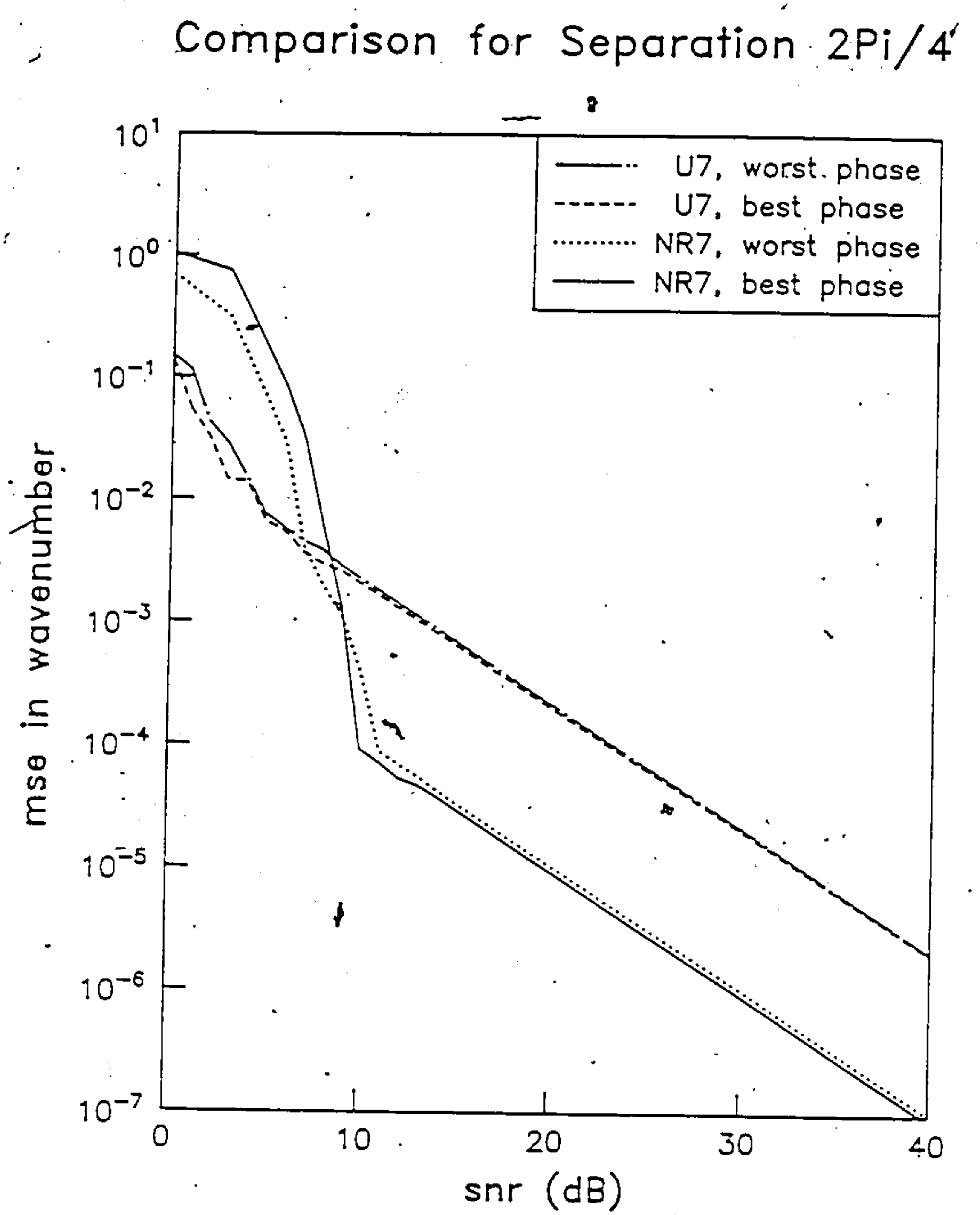

Figure 5.11: Comparison of MLE performance for 7-element uniform and nonredundant arrays with both the best- and worst-case phase difference for a target separation of $2\pi/4$.

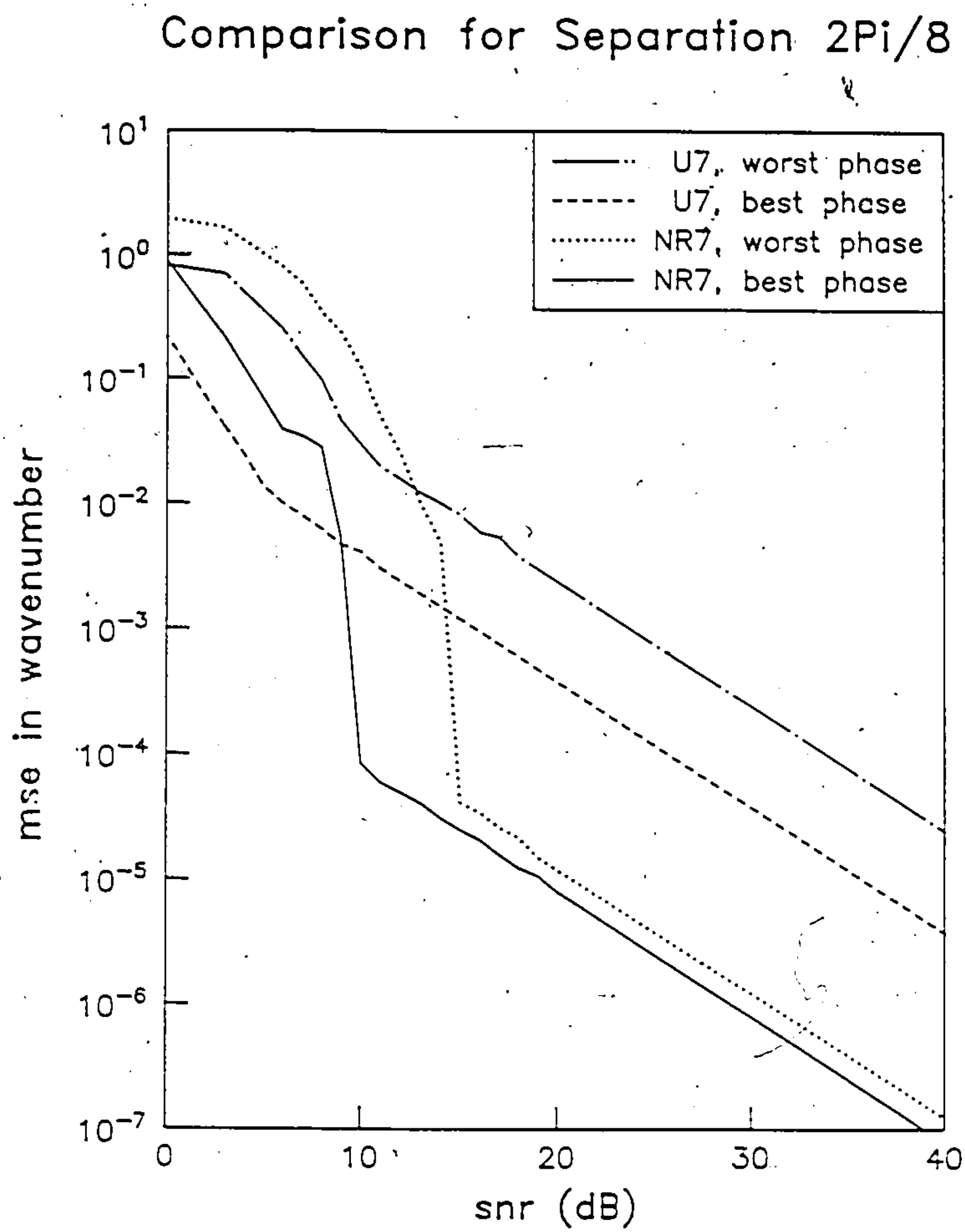

Figure 5.12: Comparison of MLE performance for 7-element uniform and nonredundant arrays with both the best- and worst-case phase difference for a target separation of $2\pi/8$.

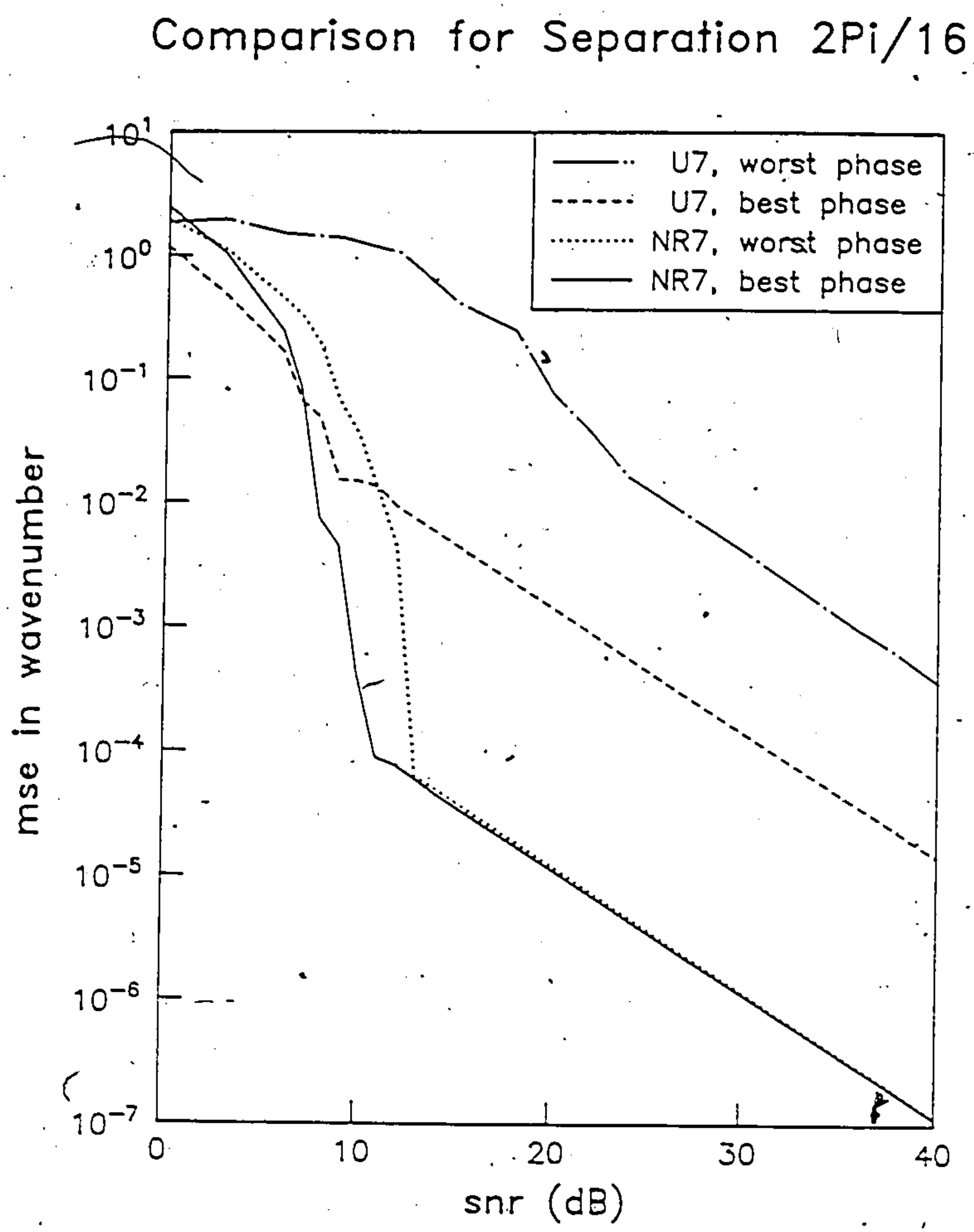

Figure 5.13: Comparison of MLE performance for 7-element uniform and nonredundant arrays with both the best- and worst-case phase difference for a target separation of $2\pi/16$.

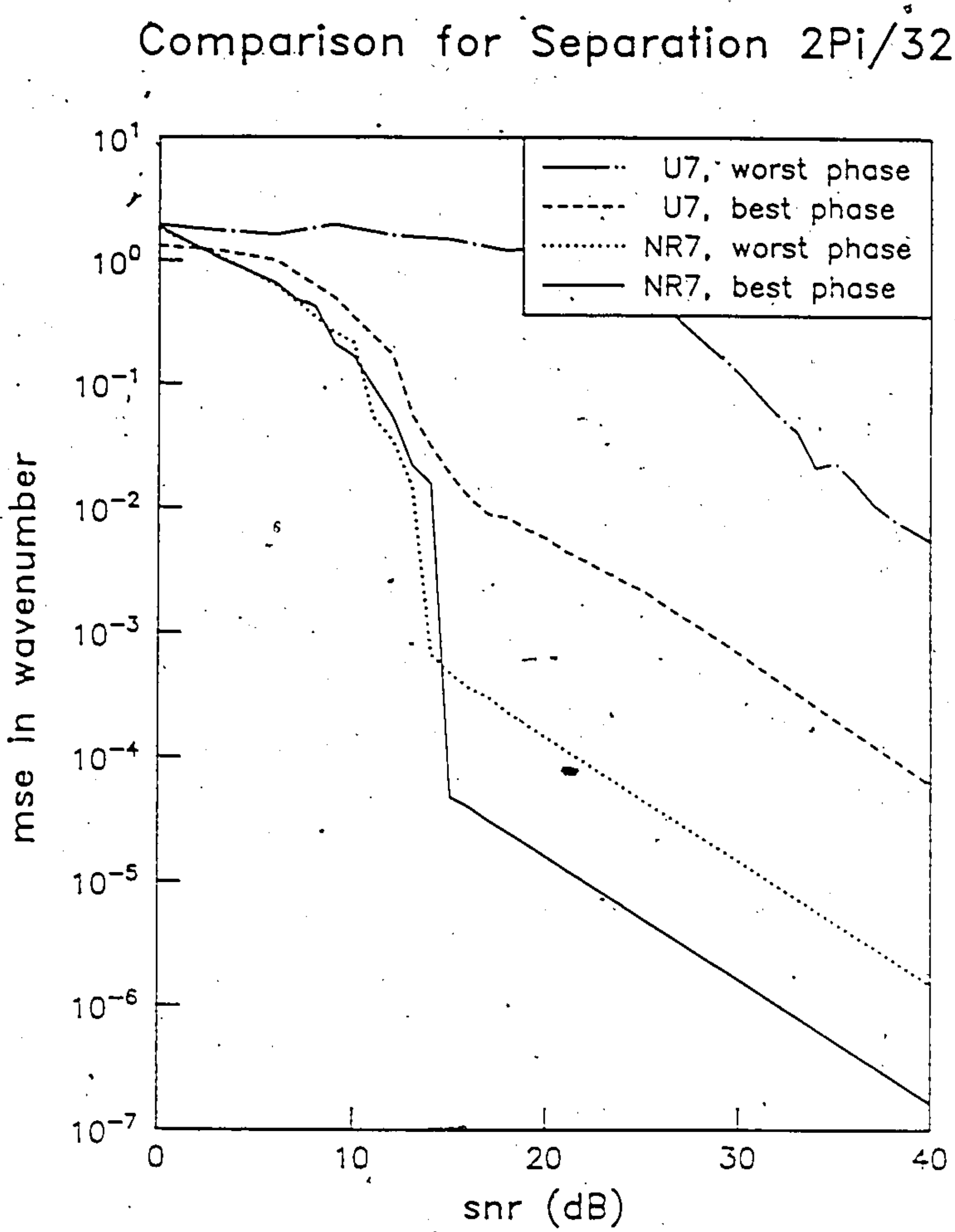

Figure 5.14: Comparison of MLE performance for 7-element uniform and nonredundant arrays with both the best- and worst-case phase difference for a target separation of $2\pi/32$.

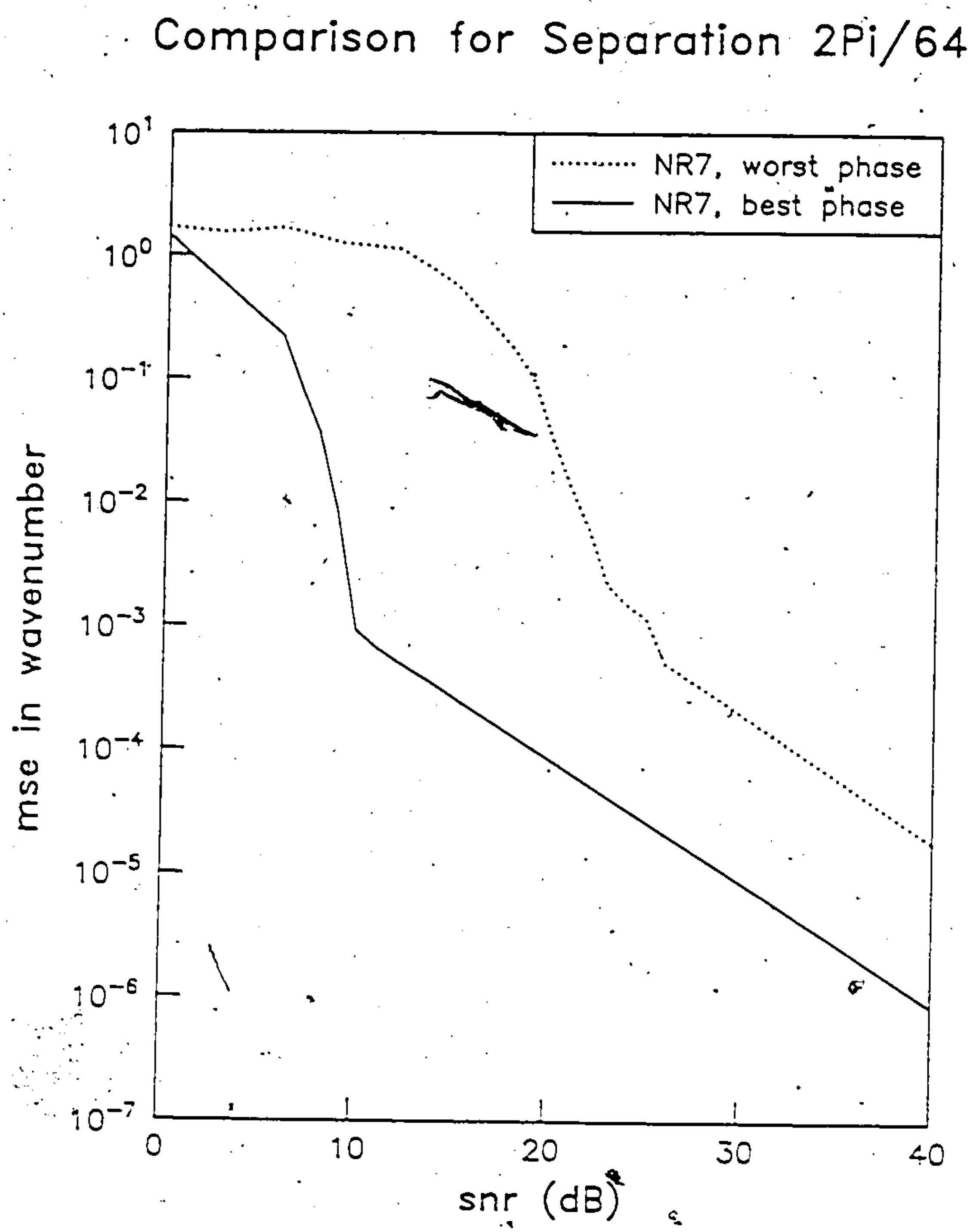

Figure 5.15: Comparison of MLE performance for 7-element uniform and nonredundant arrays with both the best- and worst-case phase difference for a target separation of $2\pi/64$.

phase difference, with the uniform value approximately 5 to 6 dB lower than that of the nonredundant array. For this large separation, we would expect the performance to parallel that of the single target cases studied in Chapter 4, which it does.

As the separation decreases to $2\pi/S$, just less than the beamwidth of the uniform array; the results change significantly as shown in Figure 5.12. The phase difference is extremely important for the uniform array structure. At high SNR, there is a difference of S dB in performance depending upon the actual phase difference at the center of the array. The nonredundant array exhibits a sensitivity of 2 dB, this particular separation is one of the worst-case sensitivities for the nonredundant structure, as seen in Figure 5.2. The nonredundant array provides 17 dB of gain when both arrays are evaluated at the optimum phase difference and 22.5 dB of sampling gain when the phase difference is the worst case for both arrays. This is a significantly larger improvement than was obtained when there was only one target present. The threshold SNR value is also sensitive to the phase difference. The worst-case threshold for the uniform array lies above the best case of the nonredundant by 1 dB and about 5 dB below the worst-case nonredundant array. The best-case phase difference is still about 4 dB below the best-case nonredundant array. The threshold SNR is therefore quite sensitive to the phase difference of the two plane waves.

Decreasing the target and image separation to $2\pi/16$, the effect of the phase difference is even more striking as presented in Figure 5.13. The high SNR sampling gain now varies from 21 dB to 34.8 dB. The lack of sensitivity to phase of the nonredundant array is as predicted by the curves of Figure 5.2 where the best and worst case CRLB almost coincide. The threshold SNR varies by approximately 2 dB for the best and worst phase conditions. The uniform array threshold is now quite sensitive to the phase difference. It is interesting to note that the threshold SNR occurs at almost the same value of MSE in both cases. In fact the threshold SNR varies from 10 dB to 24 dB, while the CRLB varies over 13.8 dB. For high SNR, the square root of the CRLB is indicative of the width of the probability density function of the wavenumber errors as described in Chapter 4. There will clearly be a problem when the width of the PDF becomes significant with the separation between target and image. For this separation of $2\pi/16$, both threshold points occur when the SNR is such that the separation is equivalent to approximately 3 standard deviations as calculated by the CRLB.

This effect is observed as the separation is decreased even further to $2\pi/32$ and demonstrated in Figure 5.14. This separation corresponds to a value just less than the beamwidth of NR-7 and approximately equal to a fifth of the U-7 beamwidth. The high SNR improvement ranges from 25.8 dB to 36.1 dB. The uniform array threshold SNR corresponds to the same MSE as it did for the $2\pi/16$ separation. The nonredundant array thresholds were not very sensitive to these phase differences and both were approximately equal to that of the best case uniform array. In these cases, the nonredundant array exhibits threshold performance as good as or better than the uniform array while providing Sampling Gains ranging from 25.8 to 36.1 dB.

Decreasing the separation further to $2\pi/64$, we obtained numerical problems with the 7-element uniform array. This separation corresponds to a tenth of a beamwidth and the 38 bit floating-point representation of the array processor was insufficient to accurately evaluate the objective function of equation (5.16). The separation is just greater than a third of the beamwidth of the nonredundant array. The simulation results are presented in Figure 5.15 where the threshold and high SNR sampling gain sensitivities are clearly displayed. The threshold SNR occurs at the point where the MSE are approximately equal. The threshold varies from 9 dB to 25 dB and the CRLB varies over 14.1 dB. The statistical nature of the threshold determination, for one or two outlier events could easily account for the small discrepancy in the two results. The MSE is less than that found in the uniform arrays of the previous two examples and corresponds to about 2 standard deviations as determined from the CRLB.

This concludes the simulation study of the arrays in the presence of multipath. We have shown that for separations between target and image wavenumber much larger than the beamwidth, the performance is qualitatively similar to that experienced in the single target simulations of Chapter 4. There is a tradeoff of about 4-6 dB in threshold performance for a Sampling Gain of 13 dB in using the 7-element nonredundant array in place of the uniform array. The nonredundant array is less sensitive to phase difference over a larger range of separations both in threshold as well as the high SNR performance. For very small separations, we find the nonredundant array may have a better threshold performance than the uniform array. Finally, the high SNR Sampling Gains may be significantly larger, for small separations, than what was determined for the single target case.

5.5 Experimental Data

This section deals with the results obtained in an experiment conducted off Tobermory, Ontario on Lake Huron.

A 32-element uniformly spaced sampled aperture was built at the Communications Research Laboratory, McMaster University, by this author in collaboration with another Ph.D. student, Mr. V. Kezys, under the supervision of Dr. Simon Haykin. A 10-dB gain horn was positioned at the top of a tower located on one side of the mouth of a bay, acting as a stationary target or beacon, effectively floodlighting the water surface. At a distance of 4.75 km the receiving array was erected, with both towers approximately 10 m from the water's edge. The data used in this thesis was collected in December of 1984. The hardware and other experiment characteristics are discussed in greater detail in Appendix C. The basic system configuration, experiment specifications, calibration procedure and accuracy limitations may be found in that section. Only the essential statistics are quoted in this chapter.

The transmitter heights were approximately 19 and 16.6 m and the center of the receiving array was located at 8.6 m. As described in Appendix C, converting all units to the normalized system of this work, for the upper transmitter we obtain the projected wavenumbers of the target and image to be 0.023 and -0.067, respectively. In terms of the elevation angles measured in physical space, they are at 0.11° and -0.33°. The lower height transmitter corresponds to a target at 0.08° and image at -0.30° of elevation angle.

Data was collected with various water roughness conditions over 3 days. We denote the different surface roughness levels as 'smooth', 'chop', and 'rough' where the respective total peak to trough waveheights were less than approximately 0.25m, 1m and 2.5m. The data spans approximately 2 seconds for which 256 snapshots were obtained.

For each snapshot an estimate of the target and image position are obtained. Using the entire array of 32 elements the average target and image wavenumber are presented in Table 5.1 for each scenario. The RMS value obtained over the time of data collection for each quantity is also provided. For the larger separation, the mean values of the estimates all differ by less than 0.012 units of normalized wavenumber from the expected values. This corresponds to an error of 0.06° of elevation angle or about $1/17^{th}$ of a beamwidth.

The smaller separation performance is much less accurate and clearly shows the breakdown of the estimation scheme setting in. Qualitatively, the mean values of the estimates are still within a beamwidth of the anticipated location, although the errors are larger than can be accounted for by sway of the receiving tower. We are led to believe that for this separation, the calibration errors are almost certainly the limiting factors.

Table 5.1

Experimental Target and Image Wavenumbers

		Target ± rms		Image ± rms	
h_t = 19.0 m		.023		-.067	
	Smooth	.011	.004	-.075	.006
	Chop	.018	.016	-.054	.018
	Rough	.011	.012	-.061	.018
h_t = 16.6 m		.017		-.062	
	Smooth	-.013	.004	-.087	.006
	Chop	.033	.005	-.104	.013
	Rough	.009	.010	-.065	.033

It should be pointed out that the MLE based upon equal additive noise powers at each sensor is not necessarily optimum in a calibration accuracy limited environment. The most general MLE, in which an accurate assessment of the calibration error statistics would be required, may be significantly more complex in terms of the implementation. Factors such as gain errors, which may not be Gaussian distributed etc., greatly complicate the final expression and the reduction which leads to the form of equation (5.16) might not be possible. Therefore, the form of the MLE implemented for the multipath problem, equation (5.16), assumed the overall effects of all the noise sources could be modelled as independent, additive and Gaussian distributed from element to element.

The larger separation, and to some degree the smaller separation, performance indicates that high accuracy estimation for sub-beamwidth separations is obtainable in a working system. It now remains to examine the nonuniform array performance. The primary question of interest is whether the nonuniform arrays can operate in a system limited by calibration errors and other limitations found in a 'real world' environment.

From the 32-element array, we can select subsets corresponding to the array configurations outlined in Chapter 2. The 7-element nonredundant array spans a total of 26 elements, and will therefore be examined as the nonuniform representative configuration. There are a total of 7 such arrays, each one obtained by 'sliding' the first subset along the length of the full array. Since the array is not symmetrical, we can identify another 7 arrays using the inverted representation. These two configurations will be referred to as NR7a and NR7b. For comparison purposes we use the 26-element uniform array which spans the same aperture as NR7 and therefore find 7 such subarrays in the 32-element set. We also compare the results obtained by using a 14-element uniform array of which there are 19.

Each estimate is compared snapshot by snapshot to the corresponding result obtained by using the 32-element uniform array at the same time instant. This ~~will~~ remove the effect of tower sway and wind loading from influencing the estimation errors. Since our primary interest is the comparison of different array structures, we wish to avoid the factors stated previously as well as the change in surface conditions etc., over the 3 days of measurement. We call the 32-element estimates, the 'true' values for a given snapshot, and determine the mean squared error for each array structure over the 256 snapshots. The arrays U26, NR7a and NR7b all have beamwidths defined as 0.25 units of normalized wavenumber. The array U14 has a beamwidth of 0.45.

Since the phase difference at the midpoint of the array under investigation may greatly influence the performance as shown in the simulations of Section 5.3, we keep each subarray separate and determine the errors independently. Figures 5.16 to 5.18 demonstrate the performance for each subarray as compared to the 32-element full array for the 3 different surface conditions. Since the combined MSE of target and image wavenumbers cover a large dynamic range, a

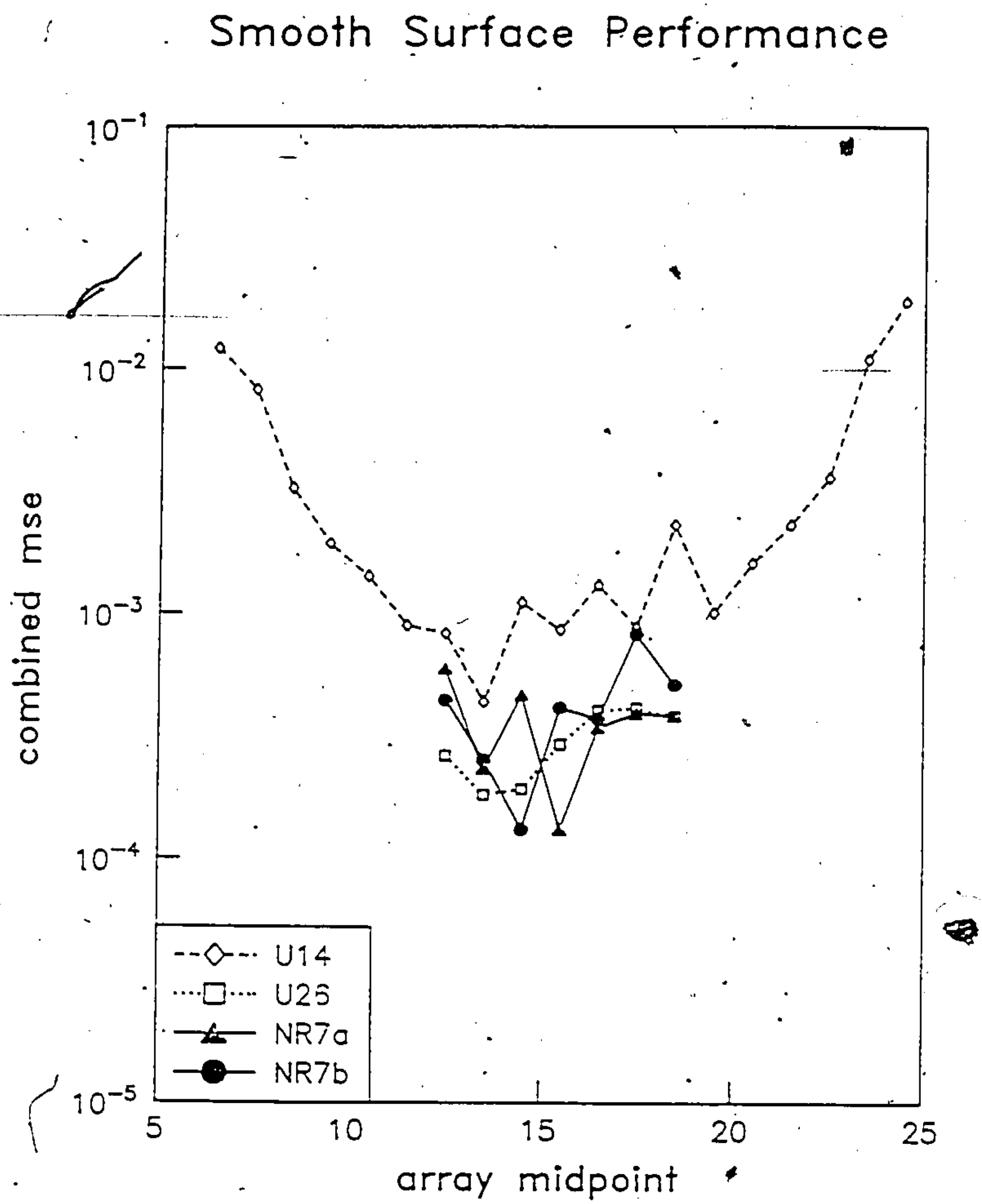

Figure 5.16: Comparison of 14- and 26-element uniform with 7-element nonredundant subarrays using the full 32-element array as a reference on the 'smooth' surface with the top transmitter.

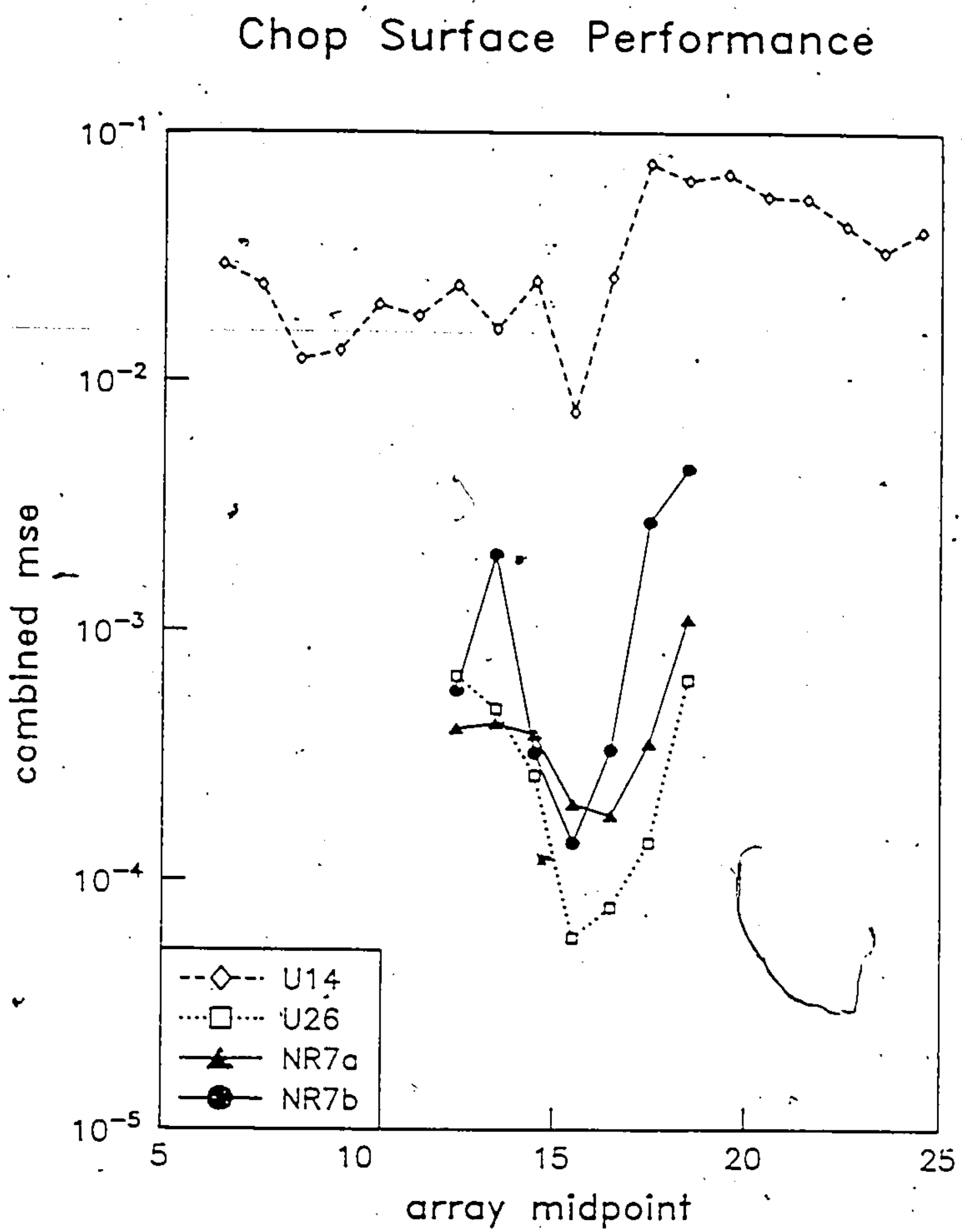

Figure 5.17: Comparison of 14- and 26-element uniform with 7-element nonredundant subarrays using the full 32-element array as a reference on the 'chop' surface with the top transmitter.

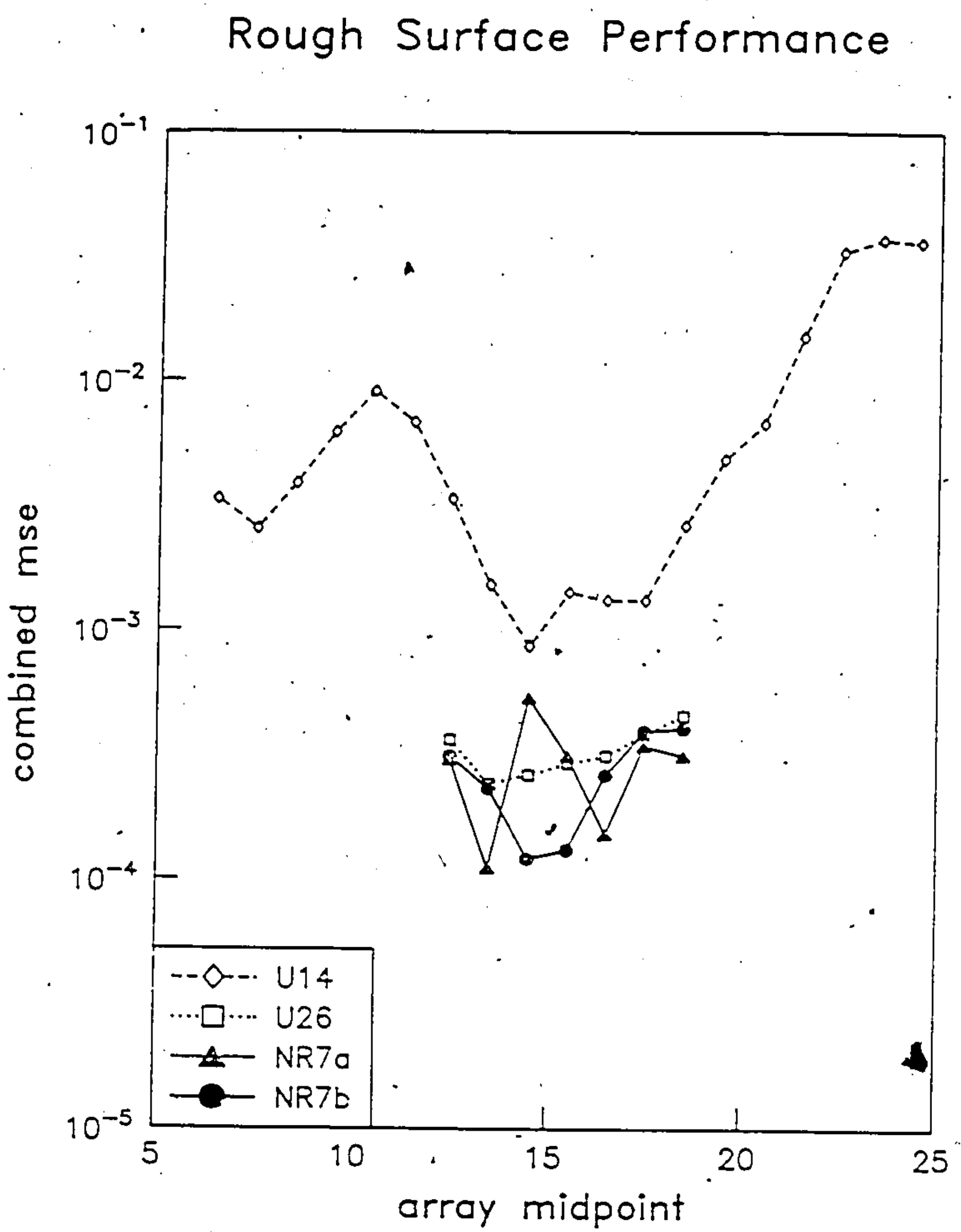

Figure 5.18: Comparison of 14- and 26-element uniform with 7-element nonredundant subarrays using the full 32-element array as a reference on the 'rough' surface with the top transmitter.

log scale was used for the presentation. The horizontal axis corresponds to the location of the midpoint of the subaperture array measured with respect to the top of the 32-element full array (whose midpoint would be 15.5 on the same axis). The figures are best appreciated by initially considering the results qualitatively. The nonredundant array performance generally oscillates about the 26-element uniform array performance for all 3 surface conditions. We found a strong null in the received amplitude in the vicinity of element 26 implying a phase difference of 180°. As shown in Section 5.3, this is the worst-case phase condition for sub-beamwidth separations. Therefore, we anticipate performance to be particularly poor for arrays centered near this point. Similarly, the phase difference is well below 90° at the other end of the array.

In all of the nonredundant subarrays considered, the performance was better than that of the 14-element uniform array when compared with the same midpoint. In 37 of the 42 comparisons the improvement was greater than 3 dB.

A comparison of the minimum MSE is presented in Table 5.2 for the uniform 14-element array and the 2 sets of nonredundant arrays. This comparison is made independent of the subarray center and we find the improvement was 5.2 dB on the smooth surface, 16.1 dB for the choppy sea state and 8.5 dB on the rough surface data.

Table 5.2

Minimum MSE Comparisons

Array	Smooth	Chop	Rough	
U14	4.3	74.0	S.5	$\times 10^{-4}$
NR7a	1.3	1.S	1.1	$\times 10^{-4}$
NR7b	1.3	1.4	1.2	$\times 10^{-4}$

For the smaller separation, the absolute performance of the 32-element array was not as accurate as for the larger separation. We can still examine the performance of the subarrays with respect to the 32-element array. This will still indicate how sensitive the different structures are to having elements missing. Figures 5.19 to 5.21 present the results of this examination. The results are similar to those observed in the previous 3 diagrams. The degradation of the 14-element uniform array is significantly larger than it was when the spacing was larger. That is, the NR7 and U26 arrays provide results which are in much closer agreement to the 32 element estimates than does U14.

The results of these experiments were not limited by the thermal noise but rather by calibration accuracy. This is the accuracy with which the relative phase and amplitude of each channel can be evaluated as well as the d.c. offsets. The calibration procedure is discussed in Appendix

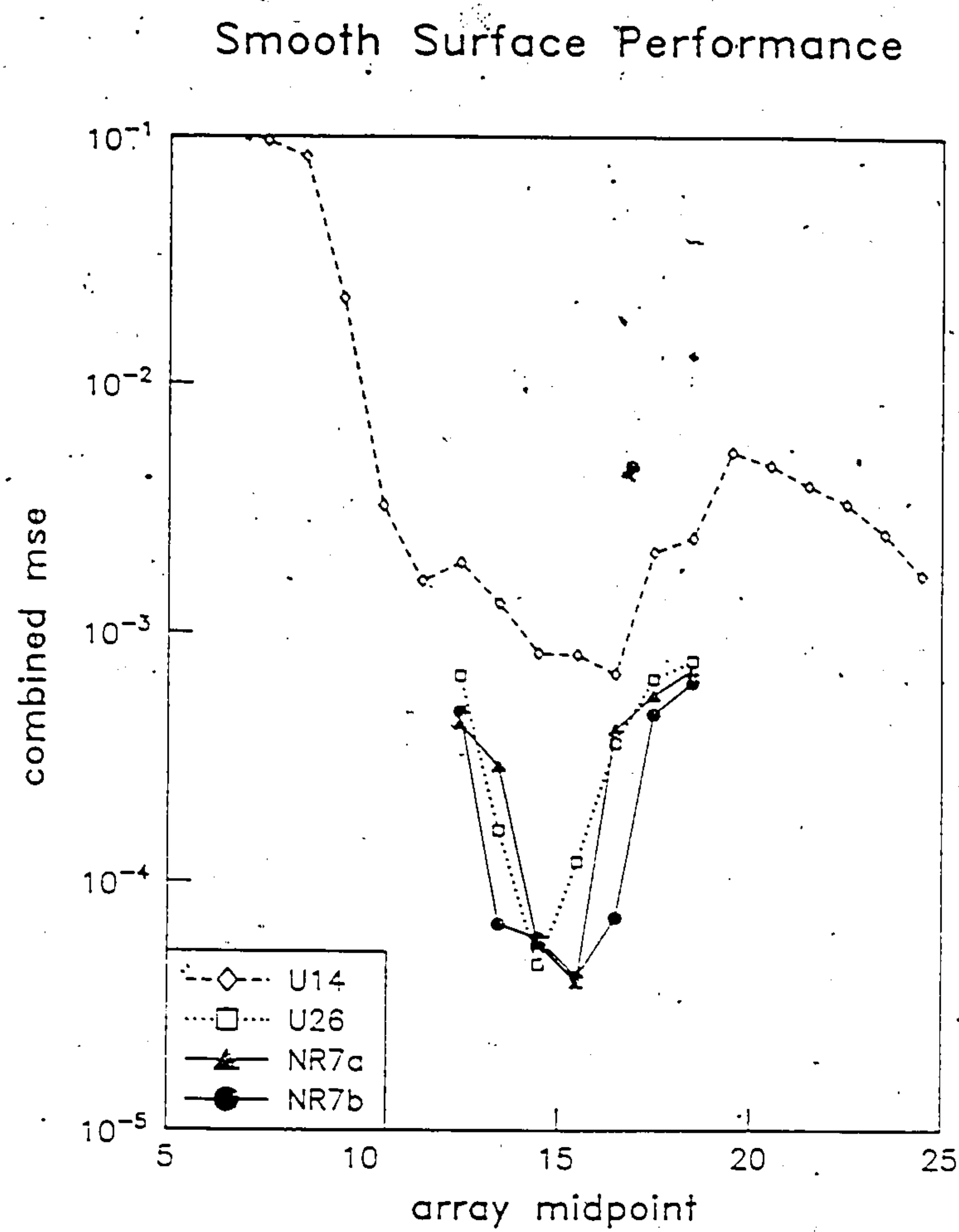

Figure 5.19: Comparison of 14- and 26-element uniform with 7-element nonredundant subarrays using the full 32-element array as a reference on the 'smooth' surface with the lower transmitter.

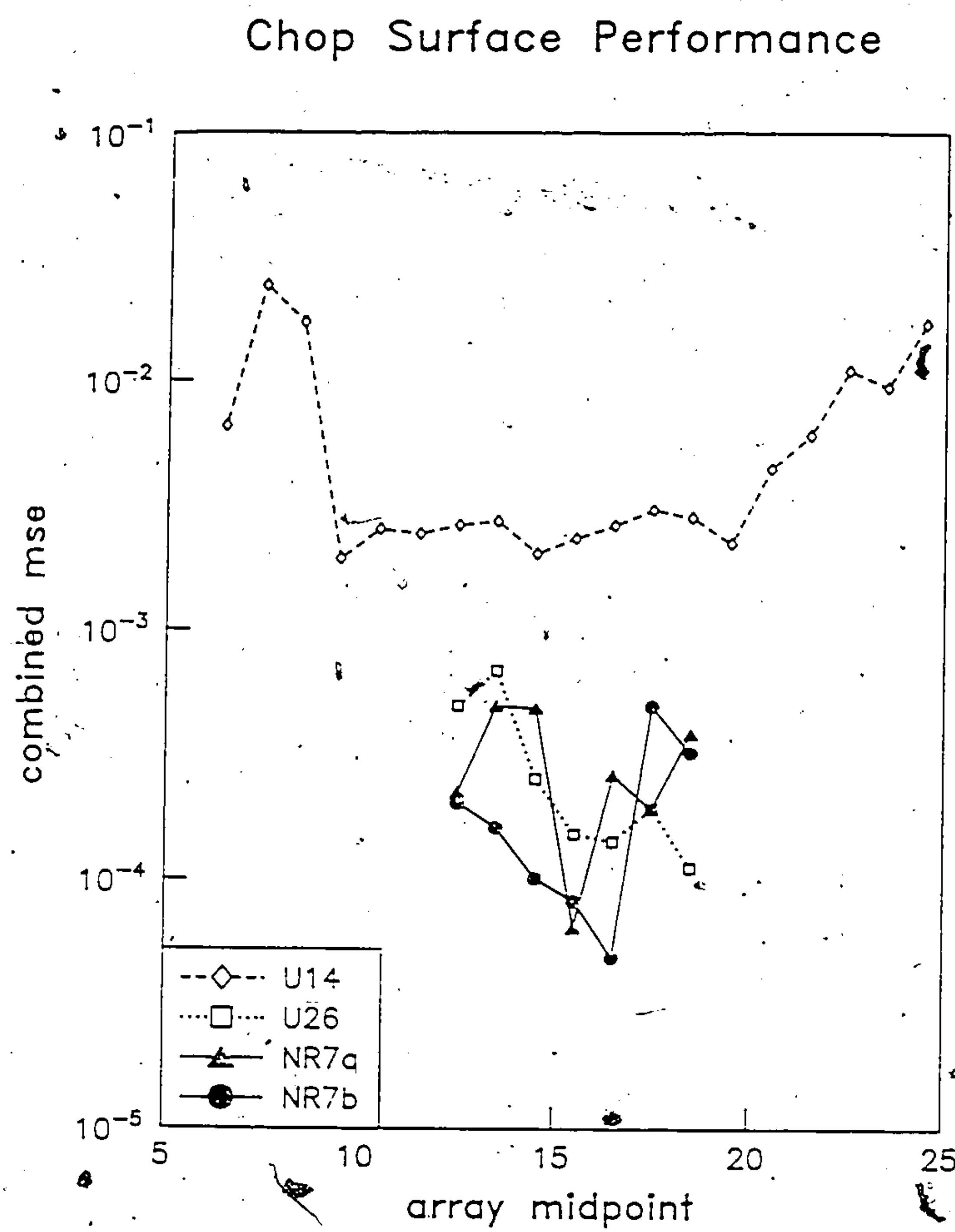

Figure 5.20: Comparison of 14- and 26-element uniform with 7-element nonredundant subarrays using the full 32-element array as a reference on the 'chop' surface with the lower transmitter.

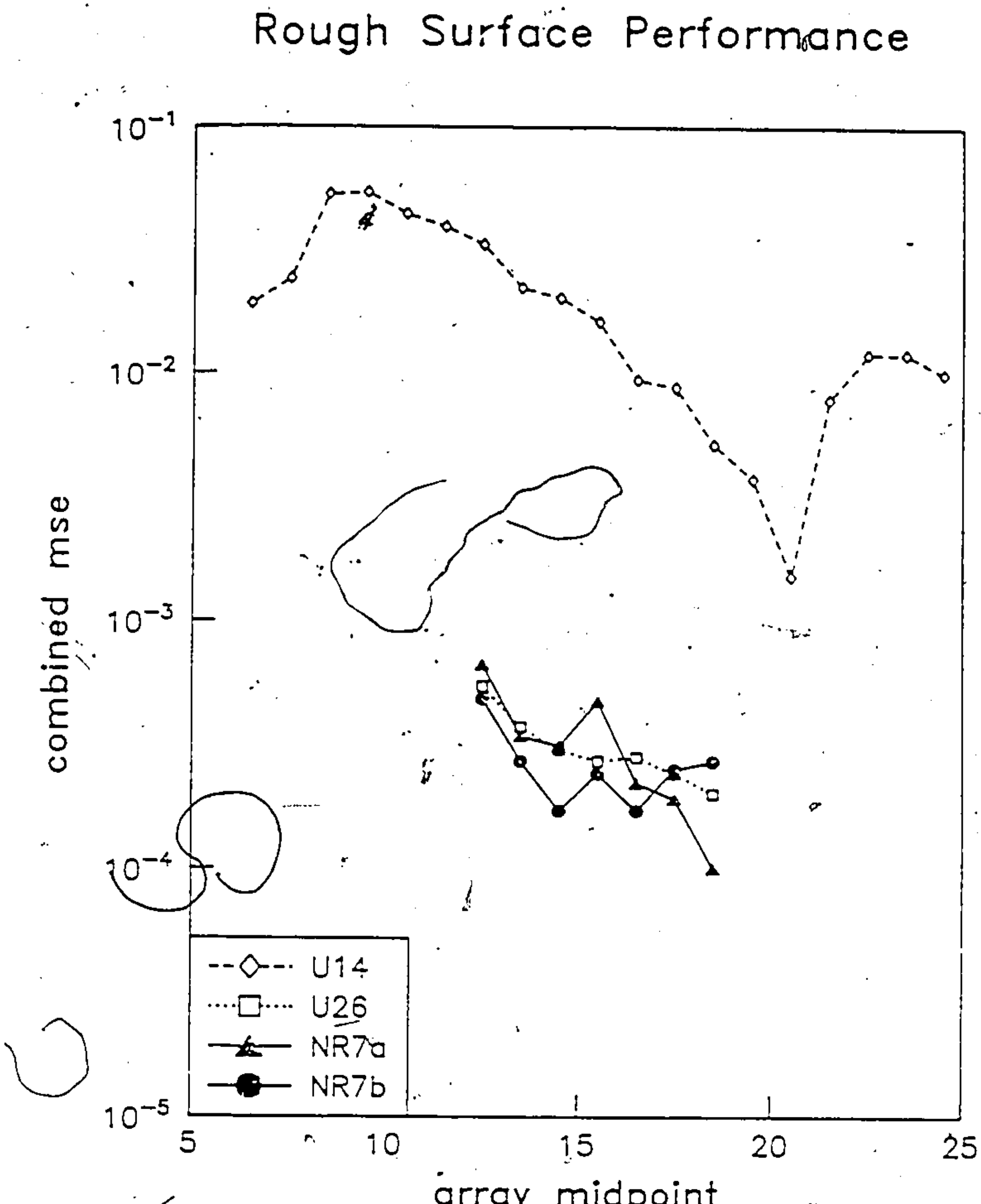

Figure 5.21: Comparison of 14- and 26-element uniform with 7-element nonredundant subarrays using the full 32-element array as a reference on the 'rough' surface with the lower transmitter.

C where some of the limitations are addressed as well as the improvements which may be made to the system. It is however clear, that for the same calibration accuracy, the nonredundant arrays perform significantly better than uniform arrays consisting of even twice as many elements.

5.6 Multipath Summary

In this chapter the effects of multipath in direction-of-arrival estimation were examined in great detail. The Cramér-Rao Lower Bound for nonrandom parameters was developed with appropriate extensions to arbitrary linear arrays. The exact maximum likelihood estimator for the multipath problem was also described and simulated.

Several important results were indicated from this portion of the study. For large SNR, the simulation results were shown to be in agreement with the CR bound for arbitrary linear arrays. Nonredundant arrays exhibit reduced sensitivity in estimation performance to the phase difference between the two plane waves compared to the uniform array consisting of the same number of elements. This is primarily due to the larger aperture and the effect is most significant for closely spaced or low flying targets.

The threshold effect observed at lower SNR values was similar to that demonstrated in Chapter 4 when the spacing between the targets was large compared to a beamwidth. For closely spaced targets the thresholds were lower for the nonredundant arrays than for the corresponding uniform arrays. In these regions, it appears the tradeoffs made in choosing an array structure are not similar to the single plane wave situation. That is, the nonredundant array provided a lower RMS error than the uniform array for all values of snr.

This chapter also provides a comparison demonstration of performance for the nonredundant and uniform arrays in a 'real world' multipath environment. The target and image were closely spaced with respect to the 32-element aperture. From the available conditions, the nonredundant arrays performed significantly better than the uniform arrays consisting of up to twice as many elements.. This addresses the question of calibration error effects on the array structures. For the calibration errors obtained in the experiment, the larger aperture of the thinned array was more significant than the more densely spaced uniform array.

The greatest limitation of the experimental data was the number of distinct scenarios that could be generated. An improved system, presently under construction, would have multifrequency capability. Even small variations of frequency would generate a large number of phase relationships between the target and image impinging on the receive aperture.

CHAPTER 6

CONCLUSIONS, CONTRIBUTIONS and FURTHER RESEARCH

In this chapter, we highlight and summarize the results of the previous chapters. The original contributions made in this work are indicated. Areas which have not been explored and may prove fruitful for thinned array applications are described in the last section of this chapter.

6.1 Conclusions and Contributions

The fundamental result obtained in this research has been the establishment of the conditions under which a thinned array may provide improved direction of arrival estimation performance. It has never been demonstrated in the literature, to the author's knowledge, that there exist tradeoff conditions under which a thinned arrays may not provide improved performance and prior to this work, a framework for this evaluation had not been established. Using the Cramer-Rao lower bound for unbiased estimation, this effect is not evident. We have been able to apply the Weiss-Weinstein lower bound which establishes the tradeoff in SNR through the threshold effect, when a given number of elements are used to estimate the direction of a single target in additive, white, Gaussian noise. The threshold SNR is lower for uniform arrays than it is for thinned arrays. The high SNR region (above the threshold,) showed the nonuniform arrays provided a significant savings in SNR.

The generalized maximum likelihood estimator was used in simulations in order to characterize the effect of array geometry. The tradeoff was identical in nature to that obtained by the WWLB. Both the MLE and the WWLB provided qualitatively similar performance indications under a variety of a priori information conditions.

An alternative view of the threshold condition, using the concept of outliers, was extended to include the performance of nonuniform arrays when exact maximum likelihood estimation is used. In this assessment of an array structure, the SNR is determined which produces a specified probability of having a 'poor' estimate occur. An empirical, asymptotic interpolation/extrapolation procedure was determined and was shown to be adequate for many practical problems. This expression could be used to determine the minimum SNR for which a specified performance level would be met. This proved to be a useful measure in discriminating between array structures as well as providing further insight on the impact of the structure on estimation performance.

The tradeoffs in a multipath environment were found to be more complex than in single target scenarios. This analysis involved simulations using an exact maximum likelihood estimator for 2 targets. For large separations between target and image, the tradeoffs were similar to those determined in the single target case. However, when the separation between target and image was within the beamwidth of the uniform array, we found the thresholds were lower for the thinned arrays than they were for the uniform structures. As such, no tradeoff exists since the RMS error was always less for the thinned arrays. The thinned arrays also indicated lower sensitivity to the phase difference between target and image than did the uniform arrays for small separations. Of course, for sufficiently large separations, neither form of array exhibited great phase sensitivity. This was also shown using the Cramer-Rao lower bound for unbiased estimators at high SNR. These relationships between thinned and full arrays have not been demonstrated in the literature.

A further question remained as to the performance of thinned arrays in a 'real world' environment. An experimental, 32-element, sampled-aperture array at X-band, was developed and brought into the field for data collection. This apparatus provided real data of an accuracy that was previously not available for the evaluation of high accuracy/high resolution estimation algorithms. The limiting source of error was calibration and electrical/mechanical tolerances as opposed to additive, white, Gaussian noise. For the set of conditions under which data was collected, the nonredundant array performed substantially better than the uniform arrays consisting of twice as many elements. The target and image were closely spaced in this experiment. We conclude that the thinned arrays had less sensitivity to calibration errors than did the uniform arrays.

Other contributions of this research provide estimates, based on a statistical analysis, of the search densities required in implementing a maximum likelihood search over the multimodal expressions developed in wavenumber estimation for both uniform and nonuniform arrays. We also illustrated the error distribution for maximum likelihood estimators is related to the classical beam pattern of the array.

6.2 Future Research

The observation of the PDF of the error distribution, coupled with the outlier analysis, indicate the possibility of improving the threshold performance of an array using windowing. The effects of windows in this type of analysis has not been documented. In addition, there is a very large selection of possibilities, see [52] for example, and the 'optimum' choice is not clear.

This work has assumed detection has occurred and the number of targets has been determined. It seems the next logical step would be to examine the detection performance of thinned versus uniform arrays. By virtue of the larger aperture obtained with a thinned array, it would seem there is promise for improved detection and determination of the number of targets present. Perhaps further tradeoffs will be encountered which will necessitate the design engineer anticipating the final operating conditions.

Recently, a determination of the number of signals which may be resolved by a uniform array has been determined, see [53]. The authors of this paper specifically state their results do not apply to nonuniform arrays. Clearly, this is an important determination which should be clarified for nonuniform arrays as well.

The inclusion of a multiple frequency capability into the experimental apparatus would allow for a significantly greater variety of experimental conditions. For a given target location, the relative phase between target and image could be varied, ideally from 0 to 2π with a small change in frequency. Further improvements in the calibration procedures and greater accountability for the receiver sway would then increase the amount of evidence from 'real world' data in determining the improvement obtained through the use of the various array structures.

Finally, much of the work in this thesis was illustrated using nonredundant arrays. These were chosen because of their lack of visibility in the literature as compared to their minimum redundancy counterparts. Of course, there exist other structures based on different constraints such as aperture limits. The concepts developed in this thesis will apply to arbitrary linear array structures and as new arrays are proposed, an identical analysis may be performed in order to make sound comparisons between different structures.

APPENDIX A

THE WEISS-WEINSTEIN LOWER BOUND

A.1 Derivation of Weiss-Weinstein Lower Bound

Let $Z = (Z_1, Z_2, \ldots, Z_N)^T$ be the N-dimensional vector of received data random variables taking on complex values, $z = (z_1, z_2, \ldots, z_N)^T$. Let $A = (A_1, A_2, \ldots, A_M)^T$ be the M-dimensional vector of random variables representing the random parameters of the estimation problem, taking on values $\alpha = (\alpha_1, \alpha_2, \ldots, \alpha_M)^T$. To save on notation, we let $p(z,\alpha)$ be $p_{Z,A}(z,\alpha)$, the joint probability density function of the N received values and the M parameters. Let $g(z)$, and $f(\alpha)$ be functions from $\mathbb{C}^N$ to $\mathbb{R}^1$ and $\mathbb{R}^M$ to $\mathbb{R}^1$, respectively. Finally, let $h = (h_1, h_2, \ldots, h_M)^T$ be any other M-tuple in $\mathbb{R}^M$ and q a real number of the open interval (0,1). We may show the identity

$$\int dz \int d\alpha \;\; f(\alpha-h)\; p^{1-q}(z,\alpha-h)\; p^q(z,\alpha)$$
$$= \int dz \int d\alpha \; f(\alpha)\; p^{1-q}(z,\alpha)\; p^q(z,\alpha+h) \qquad (A.1)$$

is true by replacing $\alpha-h$ with α on the left side. Subtracting $\int dz \int d\alpha\ f(\alpha)\ p^{1-q}(z,\alpha-h)\ p^{q}(z,\alpha)$ from both sides of (A.1), we obtain:

$$\int dz \int d\alpha\ [f(\alpha-h) - f(\alpha)]\ p^{1-q}(z,\alpha-h)\ p^{q}(z,\alpha)$$
$$= \int dz \int d\alpha\ f(\alpha) \left[p^{1-q}(z,\alpha)p^{q}(z,\alpha+h)-p^{1-q}(z,\alpha-h)p^{q}(z,\alpha)\right] \quad (A.2)$$

We can also verify the identity

$$\int dz\ g(z) \int d\alpha\ p^{q}(z,\alpha+h)\ p^{1-q}(z,\alpha)$$
$$= \int dz\ g(z) \int d\alpha\ p^{1-q}(z,\alpha-h)\ p^{q}(z,\alpha) \quad (A.3)$$

with the replacement of $\alpha+h$ by α on the left side. This result can then be summarized as

$$\int dz\ g(z) \int d\alpha\ [p^{q}(z,\alpha+h)p^{1-q}(z,\alpha)-p^{1-q}(z,\alpha-h)p^{q}(z,\alpha)] = 0 \quad (A.4)$$

Combining (A.2) and (A.4), we obtain

$$\int dz \int d\alpha\ [f(\alpha)-g(z)]\left[p^{1-q}(z,\alpha)p^{q}(z,\alpha+h)-p^{1-q}(z,\alpha-h)p^{q}(z,\alpha)\right]$$
$$= \int dz \int d\alpha\ [f(\alpha-h)-f(\alpha)]\ p^{1-q}(z,\alpha-h)p^{q}(z,\alpha) \quad (A.5)$$

Since $0 < q < 1$ we can understand the integrals of equation (A.5) to be performed over the regions where $p(z,\alpha) > 0$. This allows terms of the form $p(z,\alpha+h)/p(z,\alpha)$ to be well defined. The original paper [27] uses this fact implicitly. With this understanding, we continue by squaring equation (A.5) and applying the Schwartz Inequality as follows

$$\left[\int dz \int d\alpha \; [f(\alpha-h) - f(\alpha)] \; p^{1-q}(z,\alpha-h)p^{q}(z,\alpha)\right]^2$$
$$= \left[\int dz \int d\alpha [f(\alpha)-g(z)][p^{1-q}(z,\alpha)p^{q}(z,\alpha+h)-p^{1-q}(z,\alpha-h)p^{q}(z,\alpha)]\right]^2$$
$$\leq \left[\int dz \int d\alpha (f(\alpha)-g(z))^2 p(z,\alpha)\right] \cdot$$
$$\left[\int dz \int d\alpha \left[\frac{p^{q}(z,\alpha+h)}{p^{q}(z,\alpha)} - \frac{p^{1-q}(z,\alpha-h)}{p^{1-q}(z,\alpha)}\right]^2 p(z,\alpha)\right] \qquad \text{(A.6)}$$

We now identify the terms as expectations, and after rearranging, obtain:

$$E\{[f(\alpha)-g(z)]^2\} \geq \frac{[\; E\{[f(\alpha-h) - f(\alpha)] \; L^{1-q}(z:\alpha-h,\alpha)\} \;]^2}{E\{[L^{q}(z:\alpha+h,\alpha) \quad - \quad L^{1-q}(z:\alpha-h,\alpha)]^2\}}$$

(A.7)

where $L^{q}(z:\beta,\alpha) = p^{q}(z,\beta)/p^{q}(z,\alpha)$. We may identify $f(\alpha) = 1^{T}\alpha$ and $g(z) = 1^{T}\hat{\alpha}$ where $\hat{\alpha}$ is any estimator of α. based on received data z. 1 is an arbitrary M-dimensional vector defined on $\mathbb{R}^M$. We note that $f(\alpha-h) - f(\alpha) = -l^T h$. Equation (A.7) now reduces to

$$l^T E\{(\alpha-\hat{\alpha})(\alpha-\hat{\alpha})^T\} l \geq l^T h \, Q^{-1} h^T l \qquad \text{(A.8)}$$

where:

$$Q^{-1} = E^2\{L^{1-q}(z;\alpha-h,\alpha)\}/E\{[L^q(z;\alpha+h,\alpha)-L^{1-q}(z;\alpha-h,\alpha)]^2\} \qquad \text{(A.9)}$$

Finally, we obtain :

$$l^T \left[E\{(\alpha-\hat{\alpha})(\alpha-\hat{\alpha})^T\} - hQ^{-1}h^T \right] l \geq 0 \qquad \text{(A.10)}$$

where (A.10) holds for any l, and as pointed out in [27], this implies the internal matrix in (A.10) is nonnegative definite. This, in turn, provides a lower bound on the mean square error of any parameter estimator:

$$E\{(\alpha_i-\hat{\alpha}_i)^2\} \geq h_i^2 / Q \qquad \text{(A.11)}$$

As this expression is valid for any h and q, we obtain the tightest bound by maximizing the right side of (A.11). This maximization is on the order of an (N+1)-dimensional search.

A.2 Application of the Weiss-Weinstein Lower Bound

We now attempt to apply this bound to the direction of arrival estimation problem. We assume the wavenumber and phase of the incoming plane waves are random parameters. We also assume the amplitude is known. In this way we obtain a lower bound on the mean square estimation error as a function of signal to noise ratio. It turns out that knowledge of the amplitude does not in fact change the Cramér-Rao bound either, as was shown in Section 3.2. In any event, this is still a lower bound on mean square error performance. As in the CRLB derivation, we identify $\alpha = (\alpha_1, \alpha_2)^T$ with $(k, \theta)^T$ where k is the unknown wavenumber and θ is the unknown phase of the plane wave at the centroid of the array. In all other respects, the problem is identical to that outlined in section 3.1. The wavenumber is normalized such that the 'visible' region is within $(-\pi; \pi)$.

As we have done earlier, we drop the subscript on the probability density functions. It should be clear from the context, which density function is being employed. Therefore, $p(\alpha_1)$, $p(h_1)$ or $p(k)$ all refer to the PDF $p_{A_1}(\cdot)$ as $p(\alpha_2)$, $p(h_2)$, $p(\theta)$ all refer to the PDF $p_{A_2}(\cdot)$. Similarly by $p(z/\alpha)$, we implicitly assume $p_{Z/A}(z/\alpha)$ etc.

All terms can be reduced to the general expression

$$E\{L^{q'}(z,\alpha',\alpha)\ L^{q''}(z,\alpha'',\alpha)\}$$
$$= \int d\alpha \int dz \left[\frac{p(z,\alpha')}{p(z,\alpha)}\right]^{q'} \left[\frac{p(z,\alpha'')}{p(z,\alpha)}\right]^{q''} p(z,\alpha)$$
$$= \int d\alpha \int dz\ p^{q'}(z,\alpha')\ p^{q''}(z,\alpha'')\ p^{1-q'-q''}(z,\alpha) \quad (A.13)$$

where the integration is taken over the region for which $p(z,\alpha) > 0$. We continue by expanding the joint densities so that

$$E\{L^{q'}(z,\alpha',\alpha)\ L^{q''}(z,\alpha'',\alpha)\}$$
$$= \int d\alpha\ p^{q'}(\alpha')\ p^{q''}(\alpha'')\ p^{1-q'-q''}(\alpha)\ f(\alpha',\alpha'',\alpha)$$
$$(A.14)$$

where

$$f(\alpha',\alpha'',\alpha) = \int dz\ p^{q'}(z\backslash\alpha')\ p^{q''}(z\backslash\alpha'')\ p^{1-q'-q''}(z\backslash\alpha) \quad . \quad (A.15)$$

With

$$p(z\backslash\alpha) = \frac{1}{(2\pi\sigma^2)^N} \exp\{-\|z - s(\alpha)\|^2/\ 2\sigma^2\} .$$

Equation (A.15) becomes

$$f(\alpha',\alpha'',\alpha) = \frac{\exp\{-d(\alpha',\alpha'',\alpha)/2\sigma^2\}}{(2\pi\sigma^2)^N} \cdot$$

$$\int dz \, \exp\left[-\frac{\|z - (q's(\alpha')+q''s(\alpha'')+(1-q'-q'')s(\alpha)\|^2}{2\sigma^2}\right]$$

$$= \exp\{-d(\alpha',\alpha'',\alpha)/2\sigma^2\} \qquad (A.16)$$

where

$$\begin{aligned} d(\alpha',\alpha'',\alpha) = {} & [q'(1-q') + q''(1-q'') + (1-q'-q'')(q'+q'')]Na^2 \\ & - q'q''(s^H(\alpha')\, s(\alpha'') + s^H(\alpha'')\, s(\alpha')) \\ & - q'(1-q'-q'')(s^H(\alpha')\, s(\alpha) + s^H(\alpha)\, s(\alpha')) \\ & - q''(1-q'-q'')(s^H(\alpha'')\, s(\alpha) + s^H(\alpha)\, s(\alpha'')) \end{aligned} \qquad (A.17)$$

We denote α^H to be the complex conjugate transpose or hermitian of α. We define

$$\begin{aligned} c(h) = c(h_1,h_2) &= \sum_{i=1}^{N} \{1 - \cos(h_1 x_i + h_2)\} \\ &= N - \sum_{i=1}^{N} \cos(h_1 x_i + h_2) \end{aligned} \qquad (A.18)$$

We notice $c(h) = c(-h) \geq 0$, which will simplify calculations during implementation. Equation (A.17) simplifies to

$$d(\alpha',\alpha'',\alpha) = 2a^2\,[q'(1-q')\,c(\alpha-\alpha') + q''(1-q'')\,c(\alpha-\alpha'') - q'q''(c(\alpha-\alpha') + c(\alpha-\alpha'') - c(\alpha''-\alpha'))] \quad (A.19)$$

Since α' and α'' are of the forms $\alpha \pm h$, equation (A.19) indicates that $d(\alpha',\alpha'',\alpha)$, and hence $f(\alpha',\alpha'',\alpha)$, are independent of α. Therefore in equation (A.14) it only remains to evaluate terms consisting of the random parameter PDF. This integral contains the a priori information known about the random parameters.

We consider the wavenumber and phase to be independent parameters, and as such the a priori integral can be expanded as

$$\begin{aligned}\int d\alpha\, p^{q'}(\alpha')\, p^{q''}(\alpha'')\, p^{1-q'-q''}(\alpha) &= \left[\int d\alpha_1\, p^{q'}(\alpha_1')\, p^{q''}(\alpha_1'')\, p^{1-q'-q''}(\alpha_1)\right] \cdot \\ &\quad \left[\int d\alpha_2\, p^{q'}(\alpha_2')\, p^{q''}(\alpha_2'')\, p^{1-q'-q''}(\alpha_2)\right] \quad (A.20)\end{aligned}$$

At this point, the a priori information would be entered into the bounding formula. We begin by assuming the phase to take on any value with equal likelihood. If we set the phase density to be uniformly distributed over $[-m\pi, m\pi]$, $m \in \mathbb{Z}^+$ and take the limit as $m \to \infty$, the second integral tends to unity. As we show later, this will provide a position-independent bound.

The wavenumber is considered to be uniformly distributed over (k_n, k_x), normally taken to be a subregion of $(-\pi, \pi)$. The result of the integration then becomes:

$$\int d\alpha_1 \; p^{q'}(\alpha_1') \; p^{q''}(\alpha_1'') \; p^{1-q'-q''}(\alpha_1)$$

$$= \begin{cases} (\alpha_x - \alpha_n)/(k_x - k_n), & \alpha_n \leq \alpha_x \\ 0, & \text{elsewhere} \end{cases} \tag{A.21}$$

where

$$\alpha_x = \min\{k_x, \; k_x - (\alpha_1' - \alpha_1), \; k_x - (\alpha_1'' - \alpha_1)\}$$

$$= k_x - \max\{0, \; (\alpha_1' - \alpha_1), \; (\alpha_1'' - \alpha_1)\}, \tag{A.22.a}$$

and

$$\alpha_n = \max\{k_n, \; k_n - (\alpha_1' - \alpha_1), \; k_n - (\alpha_1'' - \alpha_1)\}$$

$$= k_n - \min\{0, \; (\alpha_1' - \alpha_1), \; (\alpha_1'' - \alpha_1)\} \tag{A.22.b}$$

We notice that it is only the range of uncertainty which governs this a priori integral. The result depends only upon $(k_x - k_n)$, and not the individual values.
The result can then be summarized as

$$E\{L^{q'}(z, \alpha', \alpha) \; L^{q''}(z, \alpha'', \alpha)\} = \frac{(\alpha_x - \alpha_n)}{k_x - k_n} \, e^{\{-d(\alpha', \alpha'', \alpha)/2\sigma^2\}}$$

(A:23)

where $d(\alpha', \alpha", \alpha)$ is defind by (A.19) and will be independent of α for the choices of α', $\alpha"$ considered and α_x, α_n defined in (A.22). Equation (A.9) is reproduced here without the inversion:

$$
\begin{aligned}
Q &= E\{[L^q(z,\alpha+h,\alpha) - L^{1-q}(z,\alpha-h,\alpha)]^2\} \,/\, E^2\{L^{1-q}(z,\alpha-h,\alpha)\} \\
&= E\{[L^{2q}(z,\alpha+h,\alpha) - 2L^q(z,\alpha+h,\alpha)\, L^{1-q}(z,\alpha-h,\alpha) \\
&\qquad + L^{2-2q}(z,\alpha-h,\alpha)]\} \,/\, E^2\{L^{1-q}(z,\alpha-h,\alpha)\}
\end{aligned} \tag{A.24}
$$

We define the function:

$$
H(h) = \begin{cases} 1 - |h|/(k_x - k_n), & |h| < (k_x - k_n) \\ 0, & \text{elsewhere} \end{cases} \tag{A.25}
$$

The denominator of (A.24) can be evaluated with $q' = 1-q$, $\alpha' = \alpha-h$, $q" = 0$, $\alpha" = \alpha'$ substituted in (A.23). The result is

$$
E\{L^{1-q}(z,\alpha-h,\alpha)\} = H(h_1)\exp\{-2\Gamma q(1-q)C(h)\} \tag{A.26}
$$

Making similar comparisons, the numerator expressions are also obtained as follows

$$E\{L^{2q}(\mathbf{z},\boldsymbol{\alpha}+\mathbf{h},\boldsymbol{\alpha})\} = H(h_1)\exp\{-2\Gamma 2q(1-2q)c(\mathbf{h})\} \qquad (A.27)$$

$$E\{L^{q}(\mathbf{z},\boldsymbol{\alpha}+\mathbf{h},\boldsymbol{\alpha})L^{1-q}(\mathbf{z},\boldsymbol{\alpha}-\mathbf{h},\boldsymbol{\alpha})\} = H(2h_1)\exp\{-2\Gamma q(1-q)c(2\mathbf{h})\} \qquad (A.28)$$

$$E\{L^{2-2q}(\mathbf{z},\boldsymbol{\alpha}-\mathbf{h},\boldsymbol{\alpha})\} = H(h_1)\exp\{-2\Gamma 2(1-q)(2q-1)c(\mathbf{h})\} \qquad (A.29)$$

Equation (A.24) now reduces to:

$$Q = \frac{H(h_1)[\exp\{-2\Gamma 2q(1-2q)c(\mathbf{h})\} + \exp\{-2\Gamma 2(1-q)(2q-1)c(\mathbf{h})\}]}{H^2(h_1)\exp\{-2\Gamma 2q(1-q)c(\mathbf{h})\}} - \frac{2H(2h_1)\exp\{-2\Gamma(q(1-q)c(2\mathbf{h})\}}{H^2(h_1)\exp\{-2\Gamma 2q(1-q)c(\mathbf{h})\}}$$

$$= \frac{H(h_1)[\exp\{4\Gamma q^2 c(\mathbf{h})\} + \exp\{4\Gamma(1-q)^2 c(\mathbf{h})\}]}{H^2(h_1)} - \frac{2H(2h_1)\exp\{2\Gamma q(1-q)(2c(\mathbf{h}) - c(2\mathbf{h}))\}}{H^2(h_1)} \qquad (A.30)$$

Finally, the bound reduces to

$$E\{(k-\hat{k})^2\} \geq h_1^2/Q \qquad (A.31)$$

where this is true for all $\mathbf{h}$ and q, as defind earlier. The "tightest bound" will result for those values of $\mathbf{h}$ and q which maximize (A.31).

A.3 The Search Implementation

The maximization of (A.31) involves a three-dimensional search, for which the regions of search need to be specified. For $|h_1| \geq (k_x-k_n)$, the value of Q is undefined. As $|h_1| \rightarrow (k_x-k_n)$, $Q \rightarrow \infty$ and hence the bound tends to zero. This limits the necessary search region. We observe that h_2 appears only as a term in $c(h)$, which [from (A.18)] can be seen to be periodic in h_2 with period 2π. Again this constrains the necessary search in h_2 to be over $(-\pi,\pi)$. The bound is also mirrored for $\pm h$. Using these results, the final search regions for h are defined below:

$$0 \leq h_1 \leq k_x-k_n \tag{A.32}$$

$$-\pi \leq h_2 \leq \pi \tag{A.33}$$

Finally, from (A.30) we observe Q has an axis of symmetry about $q = ½$. Therefore, we need only search the region [0..5] for q.

We can go further than this in determining the maximum of Q with respect to q. We examine two cases separately:

Case I	$(k_x-k_n)/2 \leq h_1 \leq k_x-k_n$	(A.34)
Case II	$0 \leq h_1 \leq k_x-k_N/2$	(A.35)

Case I

$$Q_1 = a[\exp\{bq^2\} + \exp\{b(1-q)^2\}] \tag{A.36}$$

$$\frac{dQ_1}{dq} = a[2qb \exp\{bq^2\} - 2(1-q)b \exp\{b(1-q)^2\}] \tag{A.37}$$

$$\frac{d^2Q_1}{dq^2} = a[2b \exp\{bq^2\} + 2b \exp\{b(1-q)^2\} + 4q^2b^2 \exp\{bq^2\} + 4b^2(1-q)^2 \exp\{b(1-q)^2\}] \tag{A.38}$$

where $a = 1/H(h_1)$ and $b = 4\Gamma c(h)$ are both positive quantities. From (A.38) we notice the second derivative of Q_1 is strictly greater than zero whenever $b > 0$. Equation (A.37), however, indicates that $dQ/dq = 0$ at $q = ½$. Therefore, Q must have a minimum (and the only one) at $q = ½$. This, in turn, implies the bound is a global maximum (h_1^2/Q) at $q = ½$, whenever $(k_x-k_n)/2 \leq h_1 < k_x-k_n$

Case II

$$Q_2 = Q_1 - c \exp\{-eq(1-q)\} \tag{A.39}$$

$$\frac{dQ_2}{dq} = \frac{dQ_1}{dq} + ce(1-2q) \exp\{-eq(1-q)\} \tag{A.40}$$

$$\frac{d^2Q_2}{dq^2} = \frac{d^2Q_1}{dq^2} - ce(2 + e(1-2q)^2) \exp\{-eq(1-q)\} \tag{A.41}$$

where a,b are defined as in Case I with $c = 2H(2h_1)/H^2(h_1)$ and $e = 2\Gamma(c(2h) - 2c(h))$.

Again the derivative of Q at $q = ½$ is zero. We cannot show that Q has a minimum for all h. To eliminate a search, we would need to establish this was the global minimum as well. Therefore, in this region of h_1, a grid search is performed for $0 < q \leq ½$.

Finally, this bound can be shown to be independent of the absolute location in space of the array. We will demonstrate this by showing that a shift of the array elements will still produce the same values of the bound, although they may occur at different points of the search area.

Consider the bound evaluated at a point h for a given set of array locations, $\{x_1, x_2, \ldots\}$. Now shift the array by d units such that $x_i' = x_i + d$. If $h_1' = h_1$ and $h_2' = h_2 - h_1 d$ modulo 2π, then from equation (A.18), $c(h') = c(h)$ and $c(2h') = c(2h)$. Since the only value changed is h_2, and all other terms in the bound formula are independent of h_2, the bound evaluation will provide the same result as for the previous array structure. Thus, any change in the absolute location of the array in space merely translates the surface of evaluations over the search region. This property is also evident with the Cramér-Rao lower bound.

A.4 Special Cases of WWLB

We now consider several special conditions of the WWLB. For low SNR, this implementation will be shown to be within 0.5 dB of the attainable mean square error. This may be contrasted with the CRLB, which is clearly not valid for our wavenumber estimation problem at these very low values of SNR. At high SNR, we show this form to be greater than or equal to the CRLB developed in Section 3.2.

A.4.1 Low Signal to Noise Ratios

We will now consider the special case for which the elemental SNR, Γ, is very small. Equation (A.30) then becomes

$$\lim_{\Gamma \to 0} Q = \frac{2[H(h_1)-H(2h_1)]}{H^2(h_1)} \qquad \text{(A 42)}$$

We note that (A.42) is independent of q and of h_2. To simplify the notation we replace h_1 by h and $(k_x - k_n)$ by r. Further we denote the bound in (A.31) as B. The solution is broken into two cases: Case 1 for $h < r/2$, and Case 2 with

$h > r/2$.

Case 1 : $h < r/2$ The bound becomes

$$B = \frac{h^2\,(1 - h/r)^2}{2\,h/r} \qquad (A.43)$$

After taking the first and second derivatives, we find the maximum of B occurs at $h = r/3$, and so the bound becomes

$$B_{max} = \frac{r^2}{13.5} \qquad (A.44)$$

Case 2 : $h > r/2$ The bound is determined to be

$$B = h^2\,(1 - h/r)\,/\,2 \qquad (A.45)$$

having a maximum at $h = 2r/3$, for which the bound is

$$B_{max} = \frac{r^2}{13.5} \qquad (A.46)$$

At very low SNR, the estimator which simply chooses the midpoint of the interval will have a MSE equal to $r^2/12$. Hence, this technique will provide a bound within 0.5 dB of the attainable performance at low SNR.

A.4.2 High SNR Comparison with CRLB

The last special case to be examined will be for very high SNR, Γ. To simplify the notation we will assume that the array locations are adjusted such that the centroid is zero. Since the phase is assumed unknown, the absolute location in space is arbitrary, and so this can always be done. We will show that if $h_2 = 0$, $q = \frac{1}{2}$ then a value of h_1 can be found, dependent upon Γ , such that as $\Gamma \to \infty$, the bound will approach the CRLB. Note that this only states that at high SNR the WWLB bound is at least as tight as the CRLB, and other values of the parameters may exist for which the bound is in fact larger than CRLB.

If d is a positive constant, such that d << 1, we take

$$h_1 = \left[\frac{2d}{\Gamma S}\right]^{\frac{1}{2}} \qquad \text{(A.47)}$$

where

$$\begin{aligned} S &= \sum_{i=1}^{N} (x_i - C)^2 \\ &= \sum_{i=1}^{N} x_i^2 \end{aligned} \qquad \text{(A.48)}$$

For Γ large and hence h_1 small, we approximate the function defined in (A.18) by the first term of the expansion as

$$c(\mathbf{h}) = \sum_{i=1}^{N} \{ 1 - \cos(h_1 x_i + h_2) \}$$

$$\cong \sum_{i=1}^{N} (h_1 x_i)^2/2$$

$$= h_1{}^2 S/2$$

$$= d \ / \ \Gamma \qquad (A.49)$$

and $$c(2h) \cong 4 \ d \ / \ \Gamma \qquad (A.50)$$

We now evaluate the bound, B, from (A.31):

$$B = \frac{h_1{}^2 \ (1-h_1/r)^2}{2(1-h_1/r)e^{d} - 2(1-2h_1/r)e^{-d}}$$

$$= \frac{d \ (1-h_1/r)^2 \ / \ (\Gamma S)}{(1-h_1/r)e^{d} - (1-2h_1/r)e^{-d}} \qquad (A.51)$$

As $\Gamma \to \infty$, or equivalently, $h_1 \to 0$, terms of the form $(1-h_1/r) \to 1$, and so equation (A.51) becomes

As $\Gamma \to \infty$, $$B \cong \frac{d \ / \ (\Gamma S)}{e^{d} - e^{-d}} \qquad (A.52)$$

If $d \ll 1$ then, (A.52) can in addition be approximated as

$$B \cong (2\Gamma S)^{-1} \qquad (A.53)$$

Here we have shown that this version of the WWLB has the original CRLB as a special case at high SNR. Of course, it may turn out that the bound is always much larger than this value, depending upon other parameters such as the amount of a priori knowledge.

APPENDIX B

STATISTICAL ANALYSIS OF PROBABILITY OF OUTLIER

Determining the probability of outlier, p, is essentially a counting problem. We keep track of the number of times the error falls outside the beamwidth of the array, say N_p of N_t trials. The estimate of p is then given by p_o as

$$p_o = N_p / N_t \tag{B.1}$$

with

$$\sigma_p^2 = N_p / N_t^2$$

$$= p_o^2 / N_p \tag{B.2}$$

Provided N_p is large and p_o is small, the mean square error in the estimate of p_o is given by (B.2). For each value of SNR, Γ_i, an estimate of the probability of outlier is determined, p_i, having an estimated standard deviation, σ_{p_i}.

To characterize the probability of outlier as a function of SNR, a least squares fit must be performed. We follow the procedure of [47], using orthogonal polynomials to fit the ln(p) to a linear curve by minimizing the chi-squared with respect to the free parameters. The formats of the terms are:

$$\ln(p) = a + b(\Gamma-\beta) \tag{B.3a}$$

$$\sigma_i^2 \equiv \sigma^2_{\ln(p_i)}$$

$$= 1/N_{p_i} \tag{B.3b}$$

The coefficients are found from the following expressions

$$\beta = \sum_i (\Gamma_i/\sigma_i^2) \;/\; \Delta \tag{B.4a}$$

$$a = \sum_i (\ \ln(p_i)/\sigma_i^2\ ) \;/\; \Delta \tag{B.4b}$$

$$b = \frac{\Sigma_i(\ (\Gamma_i-\beta)\ln(p_i)/\sigma_i^2\ )}{\sum_i (\ (\Gamma_i-\beta)^2/\sigma_i^2\ )} \tag{B.4c}$$

$$\Delta = \sum_i (\ 1/\sigma_i^2\ ) \tag{B.4d}$$

The choice of β, in equation (B.4a), provides us with independent coefficients a and b. We may estimate the respective variances of these two parameters as follows

$$\sigma_a^2 = 1 \;/\; \Delta \tag{B.5a}$$

and

$$\sigma_b^2 = 1 \;/\; \sum_i (\ (\Gamma_i-\beta)^2/\sigma_i^2\ ) \tag{B.5b}$$

For comparison purposes, it is convenient to determine the simplified model

$$\ln(p) = c + b\Gamma \tag{B.6}$$

where the coefficient c is given by

$$c = a - b\beta \tag{B.7a}$$

with it's variance given by

$$\sigma_c^2 = \sigma_a^2 + \beta^2\sigma_b^2 \tag{B.7b}$$

However, the coefficient c is not independent of b, and any error analysis should use the format of equation (B.2).

We can invert equation (B.2) to obtain the expected SNR for a given probability of outlier, and also estimate the error of this calculation (which may be an interpolation or extrapolation). The inverse function is given by

$$\Gamma = \beta - (\ \ln(p) - a\ )/b \tag{B.8}$$

with variance $$\sigma_\Gamma^2 = \frac{(\ln(p)-a)^2}{b^4}\,\sigma_b^2 + \frac{1}{b^2}\,\sigma_a^2 \tag{B.9}$$

The above procedure for fitting was based upon the approximate analysis of Rife and Boorstyn, [38], in the limit of high SNR, the probability of outlier occurrence varied as a single exponential. In this respect, the fitting of the data to a straight line must be considered an empirical result. Therefore, we also include an estimate of the goodness of fit of the data.

We will use the chi-squared value as a parameter for the goodness of fit: It may be obtained from

$$\chi^2 = \sum_i \frac{[\ln(p_i) - a - b(\Gamma_i - \beta)]^2}{\sigma_i^2} \tag{B.10}$$

With N_Γ data points, the reduced chi-squared is

$$\chi_\nu^2 = \chi^2/(N_\Gamma - 2) \tag{B.11}$$

If the fit is justified and the error analysis is correct, the reduced chi-squared should be approximately equal to 1. The probability that chi-squared exceeds the determined value for a given number of degrees of freedom has been tabulated in [47]. This quantity should be approximately equal to 0.5. Using these figures, we can usually determine whether or not the fit is adequate. The probability is usually either close to 0.5, indicating a reasonable fit, or it is very small, indicating a poor fit within the 'experimental' accuracy.

APPENDIX C

MULTIPATH DATA COLLECTION

C.1 Overview

This appendix provides the specifications and discusses the accuracy limitations of the experimental sampled array constructed at the Communications Research Laboratory, McMaster University. The experiment was conceived, constructed and field tested in collaboration with another Ph.D. candidate, Mr. V. Kezys also under the supervision of Dr. S. Haykin. The objective was to collect multipath data representative of a low elevation target, located over water, which would allow the evaluation of high resolution direction of arrival estimation procedures. Our goal was to develop a larger array (32 elements), providing greater accuracy and operating over a wider variety of surface roughness than existing systems and would be sufficient for the evaluation of high accuracy/high resolution estimation algorithms. The design effort was started in 1981 with the first phase of data collection completed in December of 1984. It is this data which is used to evaluate the array structures studied in Chapter 5. To ensure the system design specifications and parameters would be applicable to real world, practical problems, meetings were held during the development period with individuals at the Communications Research Center in Ottawa.

The first section describes the hardware at the block diagram level. The specifications and tolerances are described as well as the operating conditions. Section C.2 provides an explanation of the calibration procedures. The third section covers the actual experiment logistics, including the geometry and ground-truthing.

From these original data sets, modifications and improvements are being made to the existing hardware to create a data base providing both greater accuracy and covering a wider range of scenarios. These changes are discussed in the final section of this appendix.

C.2 Hardware Description

The operational frequency was 9.81 GHz, providing a free space wavelength of approximately 3.05 cm. The transmitter is blocked in Figure C.1. It consists of a free running 5 MHz double-oven, crystal oscillator which is phase locked up to 9.81 GHz. The signal is amplified to approximately 10 Watts out of a TWTA and transmitted through

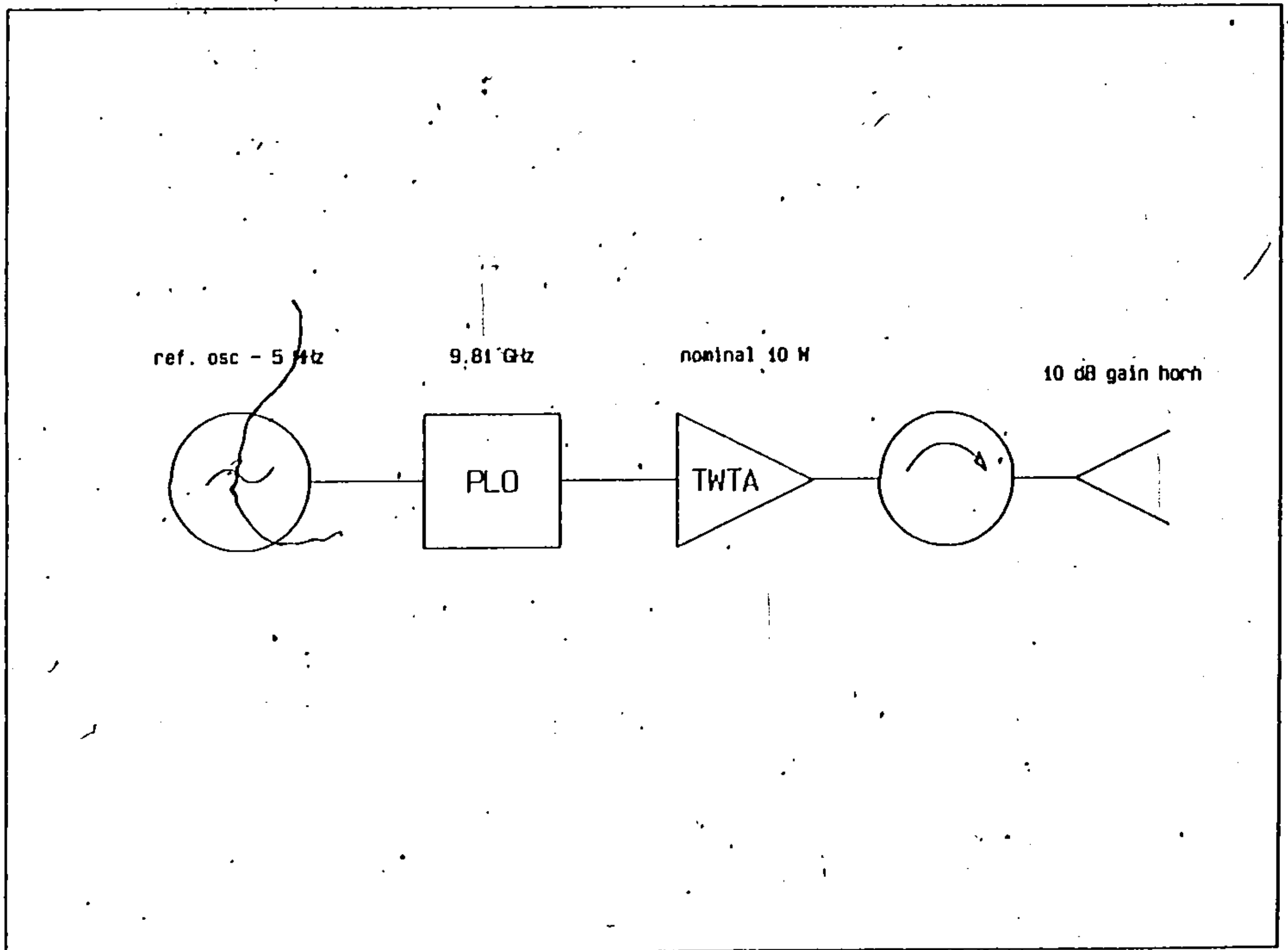

Figure C.1 Block diagram of the transmitter.

a 10 dB gain horn.

The 5 MHz crystal oscillator, also found in the receiver, provides very low phase noise. The short term phase noise was characterized by an Allan variance of 5×10^{-12} in one second. After a 24 hour burn in, the long term drift was quoted to be is less than 3 parts in 10^{10} per day. Since there was no hydroelectric power available at the experiment sites and generators were used during data collection, a 48 hour rechargeable battery backup system powered the 5 MHz ovens to maintain these specifications.

The receiver consists of a 32-element sampled aperture, with a single channel presented in Figure C.2. Each channel consists of a 10 dB gain horn followed by a 10 dB directional coupler. A test signal may be injected to the system through this coupler when the transmitter is shut down and can be used for calibrating most of the electronics. The signal is then mixed down to approximately 45 MHz and amplified. The path is split and mixed down to 'inphase' and 'quadrature baseband' signals having frequencies of 15.625 Hz. After further amplification and low pass filtering (cutoff at 31.25 Hz), it is sampled at 125 Hz, or 8 samples per cycle.

The low frequency signals were all digitally generated, synchronous with the S-100 computer system clock, including the switched-capacitor filter signals and the sample and

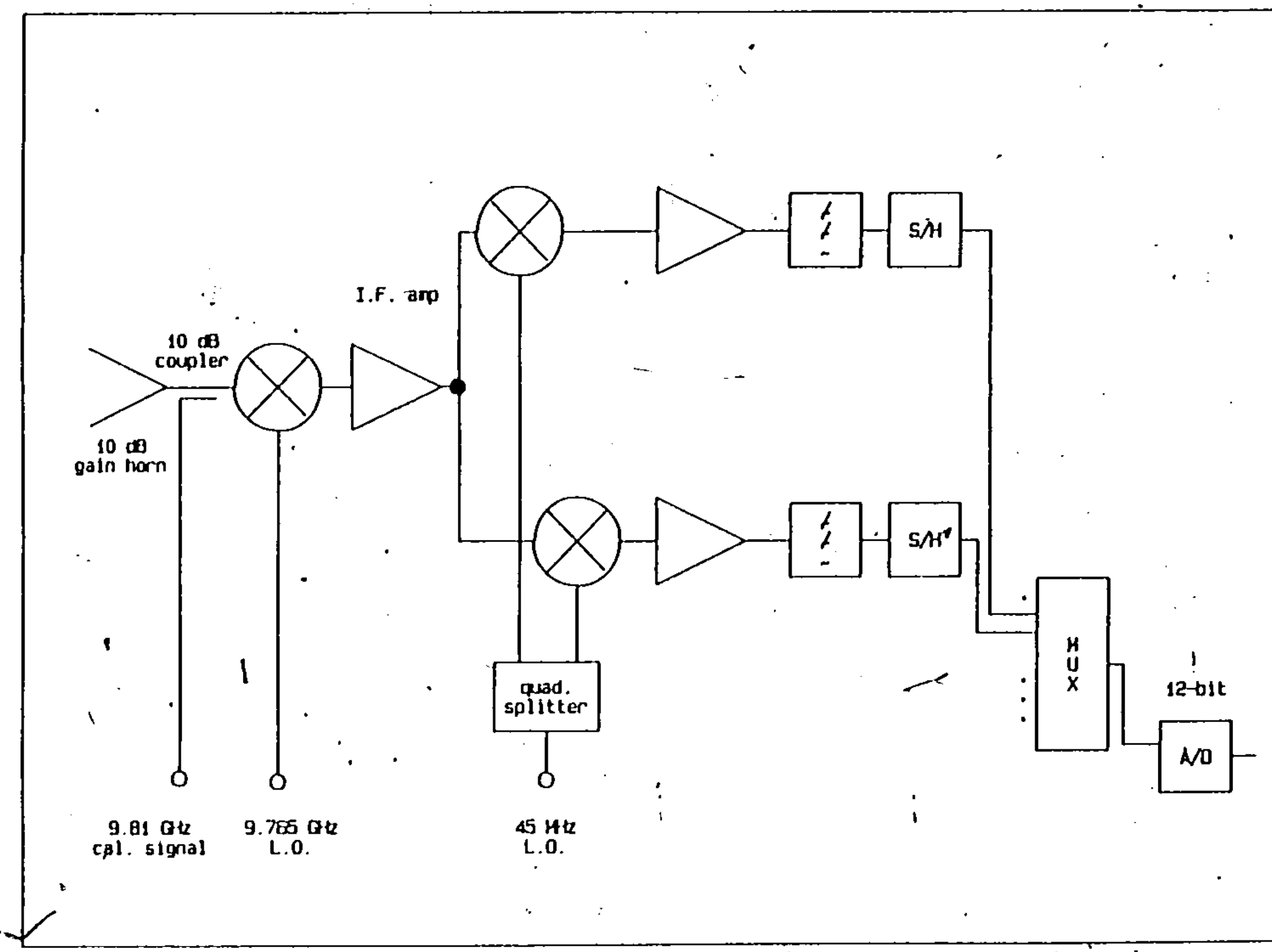

Figure C.2 Block diagram of one of 32 channels.

hold timing generation. The baseband frequency, filter bandwidths and sampling signals are all under computer control and could be varied as experimental conditions required. The IF amplification was also varied through software control.

Prior to data collection, with the transmitter on, the 5 MHz oscillator at the receiver was fine tuned such that the receiver was operating within 0.1 Hz of the transmitted signal at X-band. Because of the specifications described earlier, (and borne out in our own laboratory testing), we may describe the receiver as coherent for the duration of the data collection, usually less than 10 seconds. For long term data collection, provision was made for continuous adjustment of the 5 MHz oscillator. When the test signal is applied instead, the system is truly coherent. Since the electronic gain and phase shift will vary slightly with frequency, we wish to operate the system at the identical frequencies for which it is calibrated. While not studied in this work, the coherence allows for extremely fine doppler measurements due to the motion of the water surface.

The vertical linear array consists of 32, 10dB gain horns oriented for horizontal polarization. The structure is machined such that the spacing between horns is 5.715 ± 0.010 cm. A similar tolerance is used for the remaining two horizontal dimensions. The electrical phase error with respect to neighboring elements is less than 1°. Since the spacing is larger than $\lambda/2$, the unambiguous field of view does not extend over $\pm$ 90°. The unambiguous field of view is approximately $\pm$ 15.5°. In terms of the normalized parameters, where the spacing between elements is considered equal to 1 unit, the span of wavenumber is $\pm$ π, with $+\pi$ corresponding to a physical elevation angle of 15.5°. Since the aperture is 1.77 m the beamwidth in physical angle is approximately 1°.

Transmission lines at X-band are all cut to equal lengths within the same 0.01 cm specification, and all connectors are tightened with a torque wrench. These precautions are taken to ensure that different channels will react in similar ways to environmental changes. While the connectors and cables are not guaranteed to 1° tolerances, we only require that the relative variations over several minutes do not to exceed this specification. For example, cutting the cables to this accuracy will help ensure that temperature fluctuations change the cables of neighboring elements by identical amounts. The actual channel characteristics are determined from several calibration techniques.

C.3 Calibration

Immediately before and after a set of data is collected, an electronic calibration is performed. This consists of turning off the transmitter through the radio link, and turning on the test signal. We obtain 256 samples of the test signal, at 8 samples per baseband cycle. From this signal we characterize the gain and phase of each channel due to the electronics following the directional couplers. In this experiment only the relative amplitudes and phases of the channels are required. The electronic calibration allows us to determine the change in the relative parameters which we anticipate to be most sensitive to temperature and vary most with time.

The total time from initial electronic calibration, data collection and final calibration was usually less than 30 minutes. The two calibrations allow us to determine whether any significant changes occurred in any of the relative channel characteristics over the time period of the data collection. The system operates under virtually the same conditions during electronic calibration as during the experiment.

To accurately characterize the 'front end' components not covered by the electronic calibration we use a different technique. We place a horn 0.4 m above the water surface, 4.75 km distant, and model the return as a single plane wave. Although the multipath exists, the separation between target and image is smaller than we hope to be able to resolve. By knowing the geometry, we can 'focus' the array on this target. As in all measurements, the data is collected along with electronic calibration measurements.

By using the electronic cal at the time of the focussing experiment and using the electronic cals made when multipath data was collected, we can determine the relative changes in the system parameters. Figure C.3 shows the channel model we used for calibration. The d.c. offsets must be determined for each channel. The 90° splitter providing the Q channel has a typical error of 2° - 4° and the different filters may also provide various phase shifts. This quadrature error is labelled ϕ in the figure. There will be a gain imbalance, g, from the different amplifiers and splitters in each branch. These parameters may be immediately determined from the electronic calibration. The values of A and θ represent the variation in amplitude and phase from channel to channel and are determined by the focus experiment in conjunction with the electronic calibration.

C.4 Site Description

The experiment was performed on the mouth of Dorcas Bay

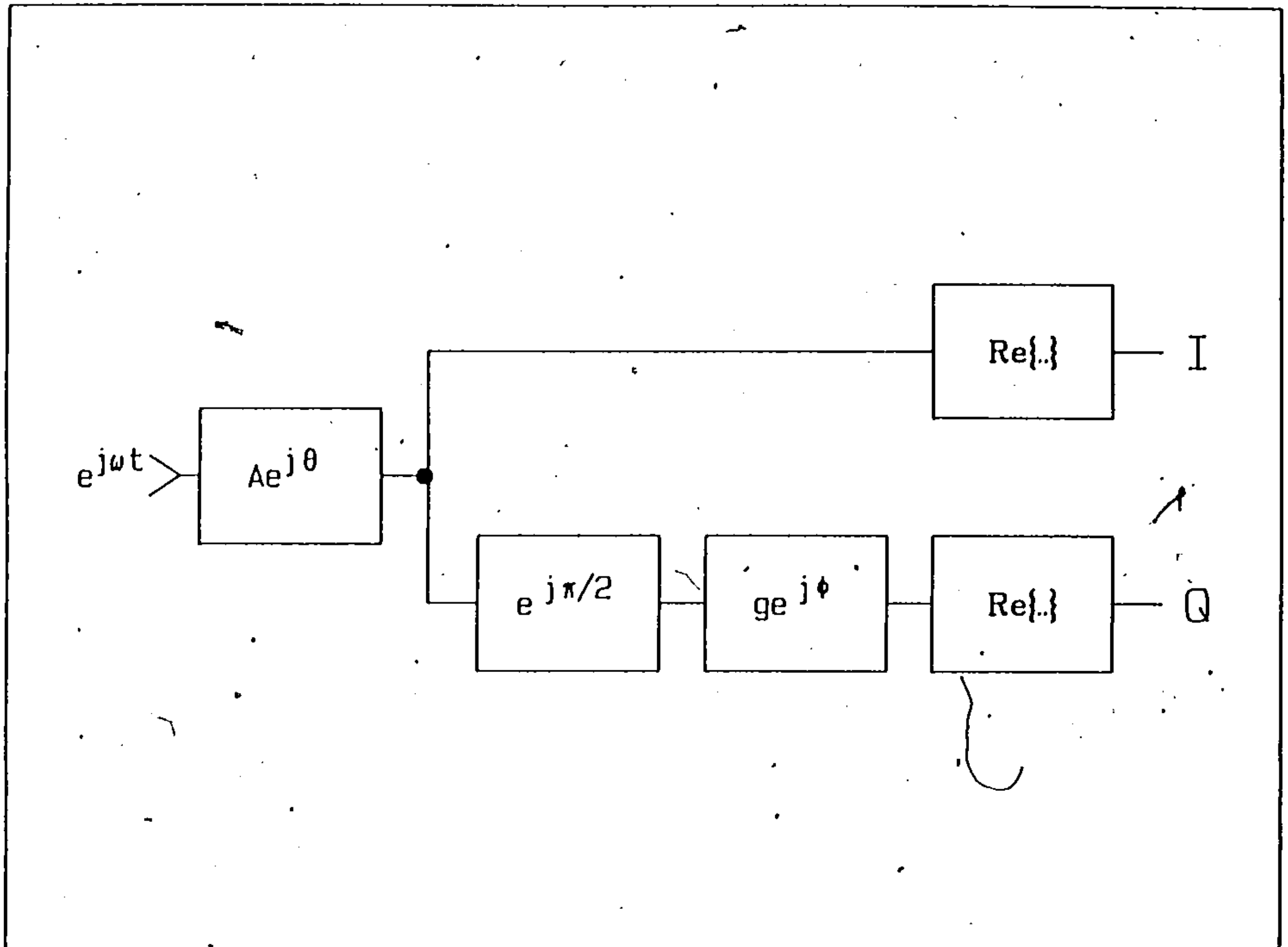

Figure C.3 Channel model used for 'I/Q calibration' showing the model parameters.

which opens onto the eastern end of Lake Huron. The transmitter was situated at a distance of 4.75 km from the receiver, both being within 10 m of the water's edge, (and occasionally, during storms, within the bay when the water level rose). The site is described in Figure C.4 showing the alternative transmitter heights which were selectable through the radio link. The center of the receiving array was at 8.6 m above the water surface. The effective normalized wavenumbers for the target and specular reflection point are provided in Table 5.1 using curved earth calculations as found in [54]. In all calculations we assume a spherical earth and use $4R_e/3$ for the radius of curvature.

A tiltmeter was located inside the array which would allow absolute angle measurements from gravitational vertical. The measurements were accurate to 2 seconds of arc and were provided approximately every ½ second. This translates to approximately 0.0001 units of normalized wavenumber or 1/2000 of the full array beamwidth. The array could be easily hoisted and secured to the tower and there was a provision for adjusting the orientation. On certain days, there was a significant amount of sway in the tower, with deviations up to 0.1° from the nominal position. This quantity is significant because of the accuracies involved in this experiment. Generally the sway was restricted to

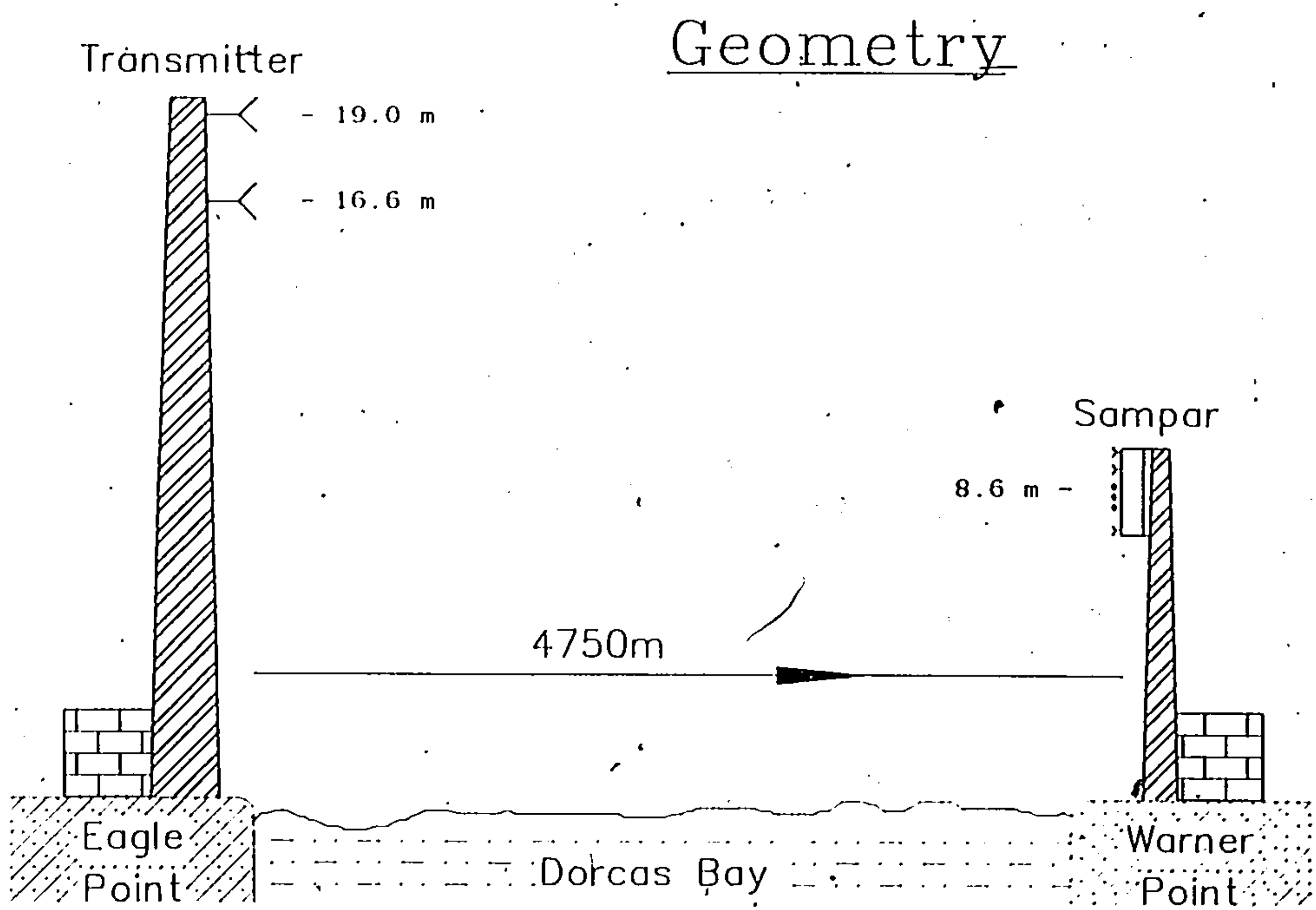

Figure C.4 Experimental site description (not to scale).

$\pm$ 200 seconds of arc or $\pm$ 0.011 units of normalized wavenumber.

C.5 Limitations and Modifications

After careful study of the data, we found it was possible to isolate the factors which most limit the final accuracy. Calibration is always a difficult area and is generally recognized as a limiting condition when attempting to obtain sub-beamwidth estimation accuracy. In the laboratory environment we found the d.c. offset was easily measured and therefore removed. In the field, for which we were exposed to sub-zero temperatures, we found the d.c. offset drift over time/temperature was slightly larger than anticipated. This was probably due to temperature fluctuations and the time required to reach thermal equilibrium inside the baseband boards.

It appears that there may have been a second reflection off of a natural breakwall in front of the array, entering through one of the grating lobes. The initial indication is that it is approximately 20 dB down in power from the direct and specular reflection signals, putting it just on the observable limit. For situations in which a 25 dB null is observed, this near field reflection is most dominant in the region of the elements near the null.

The next phase of measurements, expected to be completed in 1987, will address these two sources of errors. Because of the attainable estimation accuracy which has been demonstrated in Chapter 5, we are required to account for the sway in the tower. This requires measurements of the antenna orientation be obtained more often than once every ½ second. In this way the sway may be compensated during the estimation procedure. Finally, the greatest limitation of the data sets is the variety of the scenarios obtained. To provide a third dimension to the data base, the new system will be multi-frequency. The use of frequencies from S to 12 GHz will result in a variety of phase differences between the specular and direct signals.

Because of the small bandwidth required, 31.25 Hz, and since the system was bistatic, the thermal noise is not a limiting concern. With the aforementioned additions, the next data base should provide increased accuracy over a broader range of scenarios and will certainly increase the confidence with which we may discriminate between various estimation procedures and array configurations.

REFERENCES

[1] S. Haykin, Communication Systems, New York, John Wiley and Sons, 1978.

[2] A. Ishimaru, Y-S. Chen, "Thinning and Broadbanding Antenna Arrays by Unequal Spacings," in IEEE Trans. Antennas Propagation, vol. AP-13, pp. 34-42, Jan. 1965.

[3] Y.L. Chow, "On Grating Plateaux of Nonuniformly Spaced Arrays," in IEEE Trans. Antennas Propagation, vol. AP-13, pp. 208-215, Mar. 1965.

[4] Y.T. Lo, S.W. Lee, "A Study of Space-Tapered Arrays," in IEEE Trans. Antennas Propagation, vol. AP-14, no. 1, pp. 22-30, Jan. 1966.

[5] V.D. Agrawal, Y.T. Lo, "Mutual Coupling in Phased Arrays of Randomly Spaced Antennas," in IEEE Trans. Antennas Propagation, vol. AP-20, no. 3, pp. 288-295, May 1972.

[6] B.D. Steinberg, "Comparison Between the Peak Sidelobe of the Random Array and Algorithmically Designed Aperiodic Arrays," in IEEE Trans. Antennas

Propagation, pp. 366-370, May 1973.

[7] W.L. Stutzman, "Shaped-Beam Synthesis of Nonuniformly Spaced Linear Arrays," in IEEE Trans. Antennas Propagation, pp. 499-501, Jul. 1972.

[8] R.W. Redlich, "Iterative Least-Squares Synthesis of Nonuniformly Spaced Linear Arrays," in IEEE Trans. Antennas Propagation, pp. 106-108, Jan. 1973.

[9] H. Schjaer-Jacobsen, K. Madsen, "Synthesis of Nonuniformly Spaced Arrays Using a General Nonlinear Minimax Optimization Method," in IEEE Trans. Antennas Propagation, pp. 501-506, Jul. 1976.

[10] F. Hodjat, S.A. Hovanessian, "Nonuniformly Spaced Linear and Planar Array Antennas for Sidelobe Reduction," in IEEE Trans. Antennas Propagation, vol. AP-26, no. 2, pp. 198-204, Mar. 1978.

[11] S.C. Dutta-Roy, "Simplified Analytical Procedure for Four-Element Nonuniformly Spaced Arrays," in IEEE Trans. Antennas Propagation, vol. AP-28, no. 2, pp. 289-291, Mar. 1980.

[12] N.J. Malloy, "Non-Uniform Sampling for High Resolution Spectrum Analysis," in Proc. ICASSP 1984, pp. 6.8.1-6.8.4, Mar. 1984.

[13] A.T. Moffet, "Minimum-Redundancy Linear Arrays," in IEEE Trans. Antennas Propagation, vol. AP-16, no. 2, pp. 172-175, Mar. 1968.

[14] J. Leech, "On the Representation of 1, 2, ...,n by Differences," in J. Lond. Math. Soc., vol. 31, pp. 160-169, 1956.

[15] M. Ishiguro, "Minimum Redundancy Linear Arrays for a Large Number of Antennas," in Radio Science, vol. 15, no. 6, pp 1163-1170, Nov./Dec. 1980.

[16] S. Unnikrishna Pillai, Y. Bar-Ness, F. Haber, "A New Approach to Array Geometry for Improved Spatial Spectrum Estimation," in Proc. IEEE, vol. 73, no. 10, pp. 1522-1524, Oct. 1985.

[17] S.D. Bedrosian, "Nonuniform Linear Arrays: Graph-Theoretic Approach to Minimum Redundancy," in Proceedings of the IEEE, vol. 74, no. 7, pp. 1040-1043, July 1986.

[18] W.K. Klemperer, "Non-Redundant Phased-Array Radar," in IEE (London) Conf. on Radar - Present and Future, conf. pub. no. 105, pp. 74-80, Oct. 1973.

[19] K.S. Han, G.J. Berzins, D.S. Mason, D.G. Langer, "Digital Deconvolution of a Coded Image Obtained with a Nonredundant Pinhole Array," in Applied Optics, vol. 16, no. 5, pp. 1260-1262, May 1977.

[20] T.M. Brown, "Reconstruction of Turbulence-Degraded Images using Non-Redundant Aperture Arrays," in J. Opt. Soc. Am., vol. 68, no. 7, pp. 883-889, July 1978.

[21] J.T. Mayhan, "Thinned Array Configurations for Use with Satellite-Based Adaptive Antennas," in IEEE Trans. Antennas Propagation, vol. AP-28, no. 6, pp. 846-856, Nov. 1980.

[22] R.L. Johnson, G.E. Miner, "Comparison of Superresolution Algorithms for Radio Direction Finding," in IEEE Trans. Aerospace Elec. Syst., vol. AES-22, no. 4, pp. 432-442, July 1986.

[23] S.W. Lang, G.L. Duckworth, J.H. McClellan, "Array design for MEM and MLM array processing," in Proc. of IEEE ICASSP'81, vol. 1, pp. 145-148, Mar. 1981.

[24] G.C. Carter, "Variance Bounds for Passively Locating an Acoustic Source with a Symmetric Line Array," in J. Acoust. Soc. Am., vol. 62, no 4, pp. 922-926, Oct. 1977.

[25] L.P. Seidman, "Performance Limitations and Error Calculations for Parameter Estimation," in Proc. IEEE, vol. 58, no. 5, pp. 644-652, May 1970.

[26] L.P. Seidman, "Bearing estimation error with a linear array," in IEEE Trans. Audio Electroacoustics, vol. AU-19, no. 2, pp. 147-157, June 1971.

[27] A.J. Weiss, E. Weinstein, "A Lower Bound on the Mean-Square Error in Random Parameter Estimation," in IEEE Trans. Information Theory, vol. IT-31, no. 5, pp. 680-682, Sept. 1985.

[28] S.M. Kay, S.L. Marple, "Spectrum analysis - A modern perspective," Proc. IEEE, vol. 69, pp. 1380-1419, 1981.

[29] A.H. Nuttall, G.C. Carter, E.M. Montavon, "Estimation of the Two-Dimensional Spectrum of the Space-Time Noise Field for a Sparse Line Array," in J. Acoust. Soc. Am., vol. 55, no 5, pp. 1034-1041, May 1974.

[30] C.R. Greene, R.C. Wood, "Sparse Array Performance," in J. Acoust, Soc. Am., vol. 63, no 6, pp. 1866-1872, June 1978.

[31] M.J. Earwicker, "Signal-to-Noise Ratio Gain of Sparse Array Processors," in J. Acoust. Soc. Am., vol. 68, no 4, pp. 1129-1134, Oct. 1980.

[32] L.N. Danilevskiy, Y.A. Domanov, O.V. Korobko, B.I. Tauroginskiy, "Investigation of Some Characteristics of Well-Spaced Antenna Arrays in the Case of Digital Processing of Signals," in Telecomm. Radio Eng., vol. 37/38, english translation pp. 110-113, Nov. 1983.

[33] D.H. Johnson, "The application of spectral estimation methods to bearing estimation problems," in Proc. IEEE, vol. 70, no. 9, pp. 1018-1028, Sep. 1982.

[34] E. Vertatschitsch, S. Haykin, K.M. Wong, "Optimum Nonredundant Arrays in Beamforming," in 1983 Int. Electrical Electronics Conf., Tor., vol. 1, pp. 144-147, 1983.

[35] E. Vertatschitsch, S. Haykin, "Nonredundant Arrays," in Proc. of the IEEE, vol. 74, no. 1, p. 217, 1986.

[36] A.K. Dewdney, "Computer Recreations: The search for an invisible ruler that will help radio astronomers to measure the earth," in Scientific American, pp. 16-26, Dec. 1985.

[37] A.K. Dewdney, "Computer Recreations," in Scientific American, pp. 14-21, Feb. 1986.

[38] D.C. Rife, R.R. Boorstyn, "Single-Tone Parameter Estimation from Discrete-Time Observations," in IEEE Trans. Information Theory, vol. IT-20, no. 5, pp. 591-598, Sept. 1974.

[39] N.L. Owsley, "Sonar Array Processing," in the book entitled, <u>Array Signal Processing</u>, edited by S. Haykin, Englewood Cliffs, New Jersey, Prentice-Hall, 1985.

[40] H. Taylor, S.W. Golomb, <u>Rulers Part 1</u>, Univ. S. Cal. CSI Technical Report #85-05-01, May 1985.

[41] D.S. Robertson, private communication, July, 1986.

[42] V. Kezys, E. Vertatschitsch, T. Greenlay, S. Haykin, "High-Resolution Techniques for Angle-of-Arrival Estimation," in 1986 IEEE Mil. Comm. Conf. Milcom '86, vol. 3, pp. 41.3.1-41.3.6, Oct. 1986.

[43] R.O. Schmidt, "A Signal Subspace Approach to Multiple Emitter Location and Spectral Estimation," Ph.D.

Dissertation. Stanford University. Nov. 1981.

[44] H.L. Van Trees. Detection, Estimation, and Modulation Theory, Part 1. New York. John Wiley and Sons. 1968.

[45] M. Zoltowski. F. Haber. "A vector space approach to direction finding in a coherent multipath environment." in IEEE Trans. Antennas Propagation. vol. AP-34. no. 9. pp. 1069-1079. Sep. 1986.

[46] G. Strang. Linear Algebra and its Applications. second ed.. New York. Academic Press. 1980.

[47] P.R. Bevington. Data Reduction and Error Analysis for the Physical Sciences. New York. McGraw-Hill. 1969.

[48] D.C. Rife. R.R. Boorstyn. "Multiple tone parameter estimation from discrete-time observations." in Bell Syst. Tech. Journ.. pp. 1389-1410. Nov. 1976.

[49] D.W. Tufts. R. Kumaresan. "Estimation of frequencies of multiple sinusoids: Making linear prediction perform like maximum likelihood." in Proc. IEEE. vol. 70. no. 9. pp. 975-989. Sep. 1982.

[50] Y. Bresler. A. Macovski. "Exact Maximum Likelihood Parameter Estimation of Superimposed Exponential Signals in Noise." in Trans. Acoust. Speech & Sign. Proc.. vol. 34. no. 5. pp. 1081-1089. Oct. 1986.

[51] J.R. Sklar. F.C. Schweppe. "On the Angular Resolution of Multiple Targets." in Proceedings of the IEEE. vol. 52. pp.1044-1045. Sep. 1964.

[52] F.J. Harris. "On the Use of Windows for Harmonic

Analysis with the Discrete Fourier Transform," in Proceedings of the IEEE, vol. 66, no. 1, pp. 51-83, Jan. 1978.

[53] Y. Bresler, A. Macovski, "On the Number of Signals Resolvable by a Uniform Linear Array," in Trans. Acoust. Speech & Sign. Proc., vol. 34, no. 6, pp. 1361-1375, Dec. 1986.

[54] L.V. Blake, Radar Range Performance Analysis, Lexington, Mass., Lexington Books, 1980.

[55] S. Haykin, J.P. Reilly, "Maximum-likelihood Receiver for Low-Angle Tracking Radar," in Proc. IEE (London), Pt. I, vol. 129, pp. 261-272, Aug. 1982.

[56] J.P. Reilly, S. Haykin, "Maximum-likelihood Receiver for Low-Angle Tracking Radar," in Proc. IEE (London), Pt. II, vol. 129, pp. 331-340, Oct. 1982.